PHOSPHORS FOR BIOMEDICAL AND ENVIRONMENTAL SENSING TECHNOLOGY

SOOK VOON YAP

A thesis submitted in partial fulfilment of the
requirements of Nottingham Trent University
for the degree of Doctor of Philosophy

May 2009

Copyright statement

Abstract

Temperature measurement in an electromagnetically hostile environment, such as a magnetic resonance imaging (MRI) scanner, is challenging. The monitoring of a patient's temperature within an MRI is necessary to ensure the patient is in a comfortable condition due to the following problem. Unfortunately, the radio frequency (RF) radiation in the imaging cavity of an MRI will induce heat into both the body tissue of a patient as well as into metallic elements of any sensors.

This thesis presents a feasibility study on the production of an optical phosphor-based sensor for temperature monitoring within such a hostile environment. The concept of a desired optical sensor is based on the thermal dependence of phosphor luminescence. A pulsed ultraviolet light source is used to excite phosphors coated on a thin membrane which is in contact with the patient's skin. The skin temperature (over 27-37 °C) can then be determined by calculating the exponential decay of luminescence intensity with time after the excitation pulse has ceased. In this research, two thermographic phosphors have been investigated, namely europium doped lanthanum oxysulphide (La_2O_2S: Eu) and terbium doped lanthanum oxysulphide (La_2O_2S: Tb).

A wide range of dopant concentrations, 0.005-15 mol% for La_2O_2S: Eu and 0.005-50 for mol% La_2O_2S: Tb, have been characterised in terms of photoluminescent emission, decay time and crystallinity in determining their temperature dependent characteristics. Both phosphors have shown a dependency to dopant concentration through variance of peak intensity and decay time measurements over a low temperature range of 5 to 60 °C. Although maximum brightness of the temperature dependent lines is achieved at dopant concentrations of 1 and 10 mol% for La_2O_2S: Eu and La_2O_2S: Tb respectively, results have shown that optimum temperature dependency is at a lower mol % of 0.1 for La_2O_2S: Eu with a high quenching rate of 24.03 $m°C^{-1}$. Therefore, 0.1 mol% La_2O_2S: Eu appears to be an ideal candidate for use within an optical sensor.

A key aspect of this research is that in comparison to conventional phosphor temperature dependent characteristic, it has been shown for the first time that La_2O_2S: Tb has an increase in decay time with respect to temperature for concentrations above 2 mol%. A hypothesis of this discovery based on the differences in energy transfer pathways is described. X-ray diffraction (XRD) analysis has demonstrated a linear relationship between the *c*-axis lattice parameter of a unit cell of the phosphors with dopant concentration. As dopancy increases, the (100) and (002) reflections merge and there is a reduction in the *c*-axis parameter as well as the crystallite size. In addition, a positive thermal expansion behaviour is observed for *a* and *c* parameters as well as the volume of the unit cell over the temperature range of interest.

Acknowledgements

First and foremost, I would like to extend my heartfelt appreciation and gratitude to my director of studies, Dr. Robert Ranson, for giving me the opportunity to undertake this project. His invaluable advice, patience and encouragement from the preliminary to the concluding level enabled me to develop an understanding of the subject. This dissertation would not have come into existence without his assistance and guidance.

Special gratitude is extended to my supervisors, Professor Wayne Cranton and Dr. Demosthenes Koutsogeorgis for their amazing support and input in this research. I would also like to express my gratitude to Professor Clive Thomas for his fruitful suggestions in all fronts and for his scholarly and entertaining lectures. I am grateful to Dr. Costas Tsakonas for the interesting discussions we had.

I am deeply indebted to Dr. Gary Hix for his unstinting assistance and advice on x-ray diffraction analysis, also not forgetting his kind help with the equipment set-up. Special thanks go to Professor Jack Silver and Dr Paul Morgan for sharing their expertise in scientific matters. I thank Dr. Kafing Keita for the use of optics and her help with Matlab software. My sincere thanks are also given to all technicians in the School of Science and Technology for their technical support, in particular Steve Burton.

Many thanks go to my colleagues: Sharron Wilson, Thomas Miller, Gabriel Boutaud and Carly Farrow who continue to provide a rich and fun environment in which to work, thank you for sharing the ups and downs of PhD student life. Some debts are hard to put into words, my good friends Ariel Tang, YuSan Chan, JerWang Chan and their adorable daughter Yili, all know why their names are here. Also, I wish to express my love and gratitude to my beloved families and my fiancé Sean Ng, for their understanding, relentless support and love throughout the duration of my studies.

Finally, I gratefully acknowledge the financial support from engineering and physical sciences research council (EPSRC).

List of Publications

1) S. V. Yap, R. M. Ranson, W. M. Cranton, and D. Koutsogeorgis, "*Decay time characteristics of* La_2O_2S*:Eu and* La_2O_2S*:Tb for use within an optical sensor for human skin temperature measurement,*" Applied Optics, Vol. 47, Issue 27, pp. 4895-4899, September 2008

   The above paper has also been reviewed and selected by the editor-in-chief of Optical Society of America (OSA) Publications, Dr. Gregory Faris, for publication in the Virtual Journal for Biomedical Optics (VJBO-http://vjbo.osa.org/virtual_issue.cfm):

   S. V. Yap, R. M. Ranson, W. M. Cranton, and D. Koutsogeorgis, "*Decay time characteristics of* La_2O_2S*:Eu and* La_2O_2S*:Tb for use within an optical sensor for human skin temperature measurement,*" The Virtual Journal for Biomedical Optics, Vol. 3, Issue 11, October 2008

2) S. V. Yap, R. M. Ranson, W. M. Cranton, D. Koutsogeorgis and G. B. Hix," *Temperature dependent characteristics of* La_2O_2S*: Ln [Ln= Eu, Tb] with various Ln concentrations over 5–60 °C,*" Journal of Luminescence, Volume 129, Issue 5, pp. 416-422, 2009

Table of Contents

List of Abbreviations

Å	Angstroms (1×10^{-10} metres)
ADC	Analogue-to-digital converter
Ag	Silver
Al_2O_3	Aluminium oxide
a/o	Atomic percent
a.u.	Arbitrary units
BaCIF	Barium chlorofluoride
$BaMgAl_{10}O_{17}$	Barium magnesium aluminate
Cd	Cadmium
$CdWO_4$	Cadmium tungstate
CL	Cathodoluminescent
cm	Centimetre
CuOEP	Copper octaethyl porphyrin
Cr	Chromium
CRT	Cathode ray tube
CTS	Charge transfer state
e	Exponential
˚C	Degree Celsius
Dy	Dysprosium
EL	Electroluminescent
EPSRC	Engineering and Physical Sciences Research Council
Eu	Europium
EuTTA	Europium (III) thenoyltrifluoroacetonate
eV	Electron volt
F	Fahrenheit
FWHM	Full width at half maximum
Gd_2O_2S	Gadolinium oxysulphide
GEC	General Electric Company
Hz	Hertz
k	Boltzmann constant
K	Kelvin

kV	Kilovolt
La_0F_3	Lanthanum fluoride
La_2O_2S	Lanthanum oxysulphide
LED	Light emitting diode
mA	Milliampere
MHz	Megahertz
Mg_4FGeO_6	Magnesium fluorogermanate
Mn	Manganese
m/o	Mole percent
ms	Millisecond
MRI	Magnetic resonance imaging
µm	Micrometre (1×10^{-6} metres)
µs	Microsecond
mW	Milliwatt
N_2	Nitrogen
$Na_2W_2O_7$	Sodium tungsten oxide
Nd	Neodymium
Ni	Nickel
NTU	Nottingham Trent University
nm	Nanometre (1×10^{-9} metres)
NR	Non-radiative
ns	Nanosecond
OOI	Ocean Optics Incorporation
RAC	Radio Corporation of America
RF	Radio frequency
RTD	Resistance temperature detectors
RL	Radioluminescent
PL	Photoluminescent
PMT	Photomultiplier tube
PT	Phosphor thermography
R	Radiative
Sm	Samarium
$Sr_4Al_{14}O_{25}$	Strontium aluminate
T	Tesla

Tb	Terbium
TFEL	Thin film electroluminescent
UV	Ultraviolet
XRD	X-ray diffraction
$Y_3Al_5O_{12}$ (YAG)	Yttrium aluminium garnet
Y_2O_3	Yttrium oxide
Y_2O_2S	Yttrium oxysulphide
YVO_4	Yttrium vanadate oxide
Zn	Zinc
$Zn_3(PO_4)_2$	Zinc phosphate
ZnS	Zinc sulphide
$ZnMoO_4$	Zinc molybdate
Zn_2SiO_4	Zinc silicate

List of Symbols

c	Speed of light ($c = 3\times10^{8} m.s^{-1}$)
d	Spacing between diffracting planes
E_n	The *n*th energy level
ΔE	Thermal activation energy (energy difference)
v	Frequency
γ	Gamma
h	Planck constant ($4.136\times10^{-15} eV.s$)
θ	Incident angle
I_0	Initial intensity at time 0
I_C	Constant intensity of a reference peak
I(t)	Intensity at time t
I_{Vn}	Decreasing/ Increasing peak intensities
k	Boltzmann constant ($1.380 \times10^{-23} JK^{-1}$)
λ	Wavelength
n	Any integer
$N_e(0)$	Initial excited population
$N_e(t)$	The number of luminescent ions in the excited state after an excitation pulse at a given time
P_{eg}	The probability for spontaneous emission from the excited state to the ground state
Q	Quenching rate
R	Radiative
s	Frequency factor
t	At time (t)
T	Temperature of a component
τ_d	Decay time or decay constant
τ_q	Decay time at the quenching point
V	Volume of a unit cell
W_{NR}	Probability of non-radiative transition
W_R	Probability of radiative transition

List of Figures

List of Tables

Chapter 1 Introduction

1.1 Background

The growing interest in the field of optical sensors, has highlighted the need for research to develop optical sensor technology with adequate sensing capabilities to meet specific needs. The accelerating profile of optical temperature sensing technology is mainly due to the immunity of optical signals to electromagnetic interference[1, 2] and is of special value for use in the remote temperature measurements of a rotating component[3]. Numerous applications take advantage of this attribute within the field of engineering, aerospace and security. More recently there has been an increase in interest from the world of medicine, such an example would include the monitoring of a patient's body temperature when within a magnetic resonance imaging (MRI) system, particularly for someone who suffers from hypothermia or hyperthermia, as a patient's temperature may decrease following induction of general anaesthesia[4]. It is therefore important to monitor patient's temperature while he/ she is undergoing the scan to prevent hypothermia and aid the recovery from anaesthesia.

A survey concerning the practice of monitoring a patient's temperature within an MRI was conducted at the preliminary stage of this research. The collated information has suggested that monitoring temperature of a patient is typically standard practice outside the MRI scanner. The specialists from Queens Medical Centre (QMC) in Nottingham have stressed that there is no temperature measurement devices used within their MRI scanners, implying that no temperature measurement is performed while a MRI examination is undertaken. They will only measure a patient's temperature using a normal device after the scan is completed. This has helped to stress and emphasise the importance and practicalities of an optical temperature sensor to fill a gap for monitoring the skin temperature of a patient during a MRI scan.

To make temperature measurement of a patient in such an electromagnetically hostile environment is very challenging, as a desired diagnostic tool should not jeopardise the safety of a patient or the image quality. For instance, the electrically-conducting metallic elements of the conventional temperature measurement devices such as thermocouple, resistance temperature detectors (RTD) or thermistors[2, 5] could be problematic as they would perturb the homogeneity of the magnetic fields and thus affect the image quality. In addition, the thermal conductivity of the metal can also lead to interference of the temperature being measured. As a result, problems associated with temperature monitoring within a MRI scanner has provided an impetus for the development of a phosphor-based optical sensor for human skin temperature sensing (27- 37 °C[6, 7]) within such an environment. The concept of a phosphor-based optical sensor is to utilise a pulsed ultraviolet (UV) light source to excite the phosphor on the end of the probe and the resulting luminescence is monitored. The temperature is subsequently determined by measuring the temperature dependent rate at which the phosphorescence intensity decreases with time after the excitation pulse has ceased.

The use of phosphors within an optical sensor for surface temperature measurement may enable the above mentioned problems to be overcome because this sensing technique is purely optical and it has the ability to be employed in high levels of electric and magnetic fields due to its electrically non-conducting nature. It is well known that certain luminescent materials which consist of a ceramic host lattice doped with rare-earth ions, referred to as thermographic phosphors, have luminescence characteristics that are temperature sensitive. This has led to thermographic phosphors having been extensively explored for optical temperature sensing measurement over the past several decades. This is attributed to their accurate sensing capability over a wide range of temperatures, as well as their ability to withstand a harsh environment. For example, europium doped yttrium oxide (Y_2O_3: Eu) has been utilised for high temperature sensing within a rotating gas turbine[8, 9] and magnesium fluorogermanate doped with manganese ($Mg_4(F)GeO_6$: Mn) has been explored for thermal mapping of hot spots on the walls of a cryogenic fuel tank[10].

Typically, the temperature dependent properties of thermographic phosphors can usually be measured by determining their physical variables such as intensity, decay / rise time, or line shift of the selected spectral lines, depending on the choice of phosphors as well as the given application. When a phosphor is excited by an ultraviolet light source, the excited energy is absorbed by the material which results in promoting the electrons to higher energy states within its crystal structure. These electrons will subsequently return to lower energy states by releasing energy in the form of light (photon) or heat (phonon). The emitted photons which form the emission spectrum of the material are observed, but compete with a phonon quenching process which becomes increasingly dominant due to its greater sensitivity as a function of temperature, thus provides an optical method for monitoring temperature.

The intensity based temperature measurement has been ruled out due to the restrictions in terms of performance and the difficulties associated with maintaining calibration as the experimental arrangement requires electrical, mechanical and environmental stability[2]. Even if the signal is normalised to a temperature-independent optical signal at another emission wavelength, the chromatic differences of optical elements will make changes in element positions and thermal expansion, that will lead to a significant error of misinterpreting the changes in the signal correlated to temperature dependency[1].

As a consequence, decay time method (deduced from the time constant of the exponential decay in emission which occurs after a pulsed excitation has ceased) is adapted in this research as it is independent of excitation intensity, optical configuration and ambient light. The decay rates are measured in terms of frequency and time, and this method therefore offers relatively less uncertainty since these quantities can generally be determined with greater accuracy than optical intensities[1, 11].

Other optical techniques for temperature measurement include infrared radiometry and optical pyrometers, however, both techniques have disadvantages[12-15]. For example, the infrared techniques are not absolute in that the emissivity of the emitting material has be to known accurately in order to convert the radiometric measurements into true temperature readings. Optical pyrometers are only used for very hot sources which exhibit visible radiation but this technique also suffers from the same problem as infrared radiometers where absolute measurements are required[15]. As a result, these optical temperature sensing techniques are not suitable to be adapted for this investigation.

The presented work describes an investigation into the temperature dependent characteristics of two selected phosphors, namely europium doped lanthanum oxysulphide (La_2O_2S: Eu) and terbium doped lanthanum oxysulphide (La_2O_2S: Tb). Various dopant concentrations of both phosphors have been characterised in terms of photoluminescence (PL), decay time and X-ray diffraction (XRD). Results indicate that these phosphors are sensitive over the temperature range of 5-60 °C with an accuracy of ± 0.5 °C. Of these chosen phosphors which are strongly dependent on the required temperature range, La_2O_2S: Eu at 0.1 mol% (m/o, mole percent is defined as the ratio of the number of moles of the dopant to the total number of moles within the host lattice as a percentage[16]) is particularly favoured for use within an optical sensor head due to its high sensitivity to temperature variance. In addition, an unprecedented decay time characteristic has been discovered in this work, namely, the decay time for La_2O_2S: Tb at higher dopant concentrations (>2 m/o) increases as a function of temperature, compared to the standard decrease with temperature.

1.2 Historical context

Previous research carried out by The Optoelectronics and Phosphor Thermographic Group at NTU helped to develop a remote temperature sensing technique utilising the widely investigated rare-earth phosphor, europium doped yttrium oxide ($Y_2 O_3$: Eu) over a relatively high temperature range of 600-1200 °C, for application within turbine engines[17].

The investigation into the temperature sensing capabilities of Y_2O_3: Eu was carried out using decay time technique. The experimental results presented proof that Y_2O_3: Eu was a temperature-sensitive phosphor for the temperature range of 600-1200 °C. During the research, a new novel approach to temperature dependence was discovered, the 'rise-time' characterisation which has become an important aspect to measure the temperature dependent characteristics of some thermographic phosphors[8, 9, 18]. Of more importance and relevant to this research, the temperature dependence of Y_2O_3: Eu was also found to be dependent on the phosphor dopant concentration and the excitation wavelength.

1.3 Project aim

The aim of the present study is to further elucidate the experience and knowledge gained during the previous engineering and physical sciences research council (EPSRC) project at NTU, but focusing on the new area of biomedical and environmental sensing technology. This EPSRC studentship (GR/T27792/01) is aimed to investigate the sensing capabilities of various phosphor materials for use within an optical sensor to monitor the skin temperature of a human body, for instance within a MRI scanner where metallic temperature measurement tools are undesirable as metal absorbs the magnetic field creating extra heat and thus temperature fluctuations.

1.4 Project objectives

The objectives of this project are:

i. Perform literature survey, including consultation with the supplier-Phosphor Technology Ltd, to identify suitable phosphors which are sensitive to the temperature range of human skin.

ii. Carry out a study on the luminescent properties of the selected phosphors, in the form of a powder, to optimise both the luminescent efficiency and temperature sensitivity via dopant concentration.

iii. Investigate the temperature dependent characteristics of the identified phosphors at various dopant concentrations in terms of photoluminescent, decay time and crystallinity.

iv. Carry out a feasibility study of the design of an optical sensor prototype using the optimum phosphor.

1.5 Structures of the thesis

The remaining chapters of the thesis are as follows:-

- **Chapter 2 Literature review**

This chapter discusses the fundamentals of an optical sensing technology, phosphor thermography, in particular for measuring human skin temperature within an electromagnetic hostile environment. The chapter begins with a discussion of temperature range of human skin and an overview of human skin temperature sensing methods. Following this, historical background that outlines the nature of phosphors is described. The mechanisms of luminescence and various luminescence phenomena in certain phosphor materials, including the influence of dopant concentration on the luminescence process, are explained. Further in this chapter includes discussions of various optical temperature sensing characterisations such as two-peak ratio and decay time technique. Finally, a look-up table of a selection of phosphors is presented for comparison purposes, along with a discussion of selecting the suitable phosphors for this research.

- **Chapter 3 Experimental techniques**

This chapter details the experimental arrangements and equipment utilised to carry out this investigation. The chapter starts with a description of the process of creating a phosphor pellet and subsequently a discussion on the controlled temperature environment for phosphor characterisation. It then describes the characterisation equipment and data analysis process, including photoluminescent, decay time system and XRD.

- **Chapter 4 Europium doped lanthanum oxysulphide**

The result and discussion chapter discusses the luminescent properties of europium doped lanthanum oxysulphide. The results of XRD, photoluminescent and decay time at various europium concentrations are reported, suggesting the phosphor is strongly temperature dependent over 5- 60 °C. The optimum concentration of the phosphor has been identified.

- **Chapter 5 Terbium doped lanthanum oxysulphide**

Similar to chapter 4, the luminescent properties of terbium doped lanthanum oxysulphide and the characterisations of XRD, photoluminescent and decay time are contained within this chapter. An unprecedented decay time characteristic has been discovered, the decay time of the phosphor at higher dopant concentrations (>2 m/o) increases as a function of temperature.

- **Chapter 6 Feasibility study of an optical sensor head**

This chapter consists of a feasibility study of various potential approaches for producing an optical sensor head using the optimum phosphor. It also includes the problems and limitation factors encountered in several attempts to create a prototype optical sensor head.

- **Chapter 7 Conclusions and future work**

The conclusion chapter summarises the achievements obtained during this research and suggests future work for further development of optical temperature sensing technology.

Chapter 2 Literature Review

As introduced in Chapter 1, this research is aimed at investigating the sensing capabilities of various phosphor materials for use within an optical sensor to detect the skin temperature of a patient (27-37 °C[6, 7]) within a MRI scanner. A critical review of current literature in the fields of optical sensors as well as the luminescent characteristics of thermographic phosphors is undertaken to gain insight into up-to-date fluorescence thermometry techniques, and to identify the most appropriate phosphor for use in the fabrication of the sensor. A comparative study of phosphors has been performed for verifying the suitable candidates which are sensitive to temperature variations over the range of 5- 60 °C.

2.1 Temperature range of human skin

The normal surface skin temperature of a person is from 32-34 °C[19-21] compared to the normal core temperature of 37 °C[22]. However, 'normal' varies from person to person depending on gender, fitness, age and diet. For example, women tend to have a lower skin temperature by 1-2 °C compared to that of men due to women having a higher ratio of skin surface (heat dissipation) to volume (heat generation) than men and thus shed heat faster[23]. In addition, it is evident that different parts of the body have different skin temperatures and relatively large temperature gradients may develop both in the tissue and in the air close to the surface[6, 19, 24]. Skin temperature also depends on numerous external factors like (i) ambient air temperature (ii)time spent in that environment (iii)changes of the physiological condition such as skin blood flow and sweating[19, 24].

The sense of hot and cold within the body is determined by the flow of energy to and from the skin[19]. The human skin temperature will not fall below that of surrounding air due to heat dissipating from higher to lower temperature[19]. A person's skin temperature would rise if he was to be in a warm room and his skin temperature was cooler than air. Typically, a MRI scanner is located in an enclosed area at ambient temperature, and thus a normal person being scanned is expected to have a typical skin temperature at approximately 34 °C. However, an unhealthy patient who contracted hyperthermia or hypothermia would have a few degrees higher or lower than of the normal skin temperature. As a result, the skin temperature range that of interest for investigation is 27-37 °C[6, 7].

2.2 Review of temperature sensing methods for human skin temperature

The first temperature measurement instrument was the thermoscope, invented in 1594 by Galileo and Fludd[25] which used the air trapping within a bulb to show that air expands or contracts in response to an increase or decrease in temperature. A couple of centuries later, the modern scientific thermometer with temperature scale was proposed by Daniel Gabriel Fahrenheit in 1724[26]. The Fahrenheit (F) scale, named in his honour, is still in use today alongside the Celcius scale (°C) and the Kelvin scale (K). This has led to the development and commercialisation of both invasive and non-invasive instrumentation systems for various applications[1, 2, 27] within the fields of science, engineering, security and medicine.

Numerous methods have been exploited for measuring temperature including thermal paints, radiation pyrometer, thermocouples, liquid crystal tape and phosphor thermography[3, 24, 28]. Specifically, the remote temperature sensing technology of phosphor thermography is of particular interest within the body of this work due to the electromagnetically hostile environment within a MRI. A MRI scanner uses a strong magnetic field and radio waves to generate images of the inside of the body[29]. As a consequence, metallic temperature sensing tools such as thermocouples may distort the image quality if it is placed near the body part being scanned. In addition, the MRI's external magnetic field may also induce a dangerous eddy current in a piece of closed-loop metal and subsequently induce some degree of heat. The quality of the image improves with increasing magnetic resonance, however, the drawback of applying a greater magnetic strength is the inducement of heat into the body tissue. In addition, the MRI machine produces a tremendous amount of noise during a scan making the verbal communication between the patient and the radiologist difficult. Therefore, monitoring the patient's temperature inside MRI is vital, particularly in the case of an infant or a critical-care patient where verbal communications are hindered. The solution is an optical-based sensor which is independent of an external triggering source and electromagnetic interference.

Such a solution is Phosphor Thermography (PT) - a sensing method for measuring the temperature of a material employing thermographic phosphors[1, 27]. The concept of a phosphor-based optical sensor is to excite the phosphor on the end of the probe via a

UV light source and the resulting fluorescence is monitored. The temperature is subsequently determined by measuring the decrease of fluorescence intensity with respect to time after the UV excitation has ceased. The first phosphor based thermometry was preformed by Urbach [30, 31] in 1951, who measured the temperature distribution on a flat wedge using several phosphors such as $ZnMoO_4$, $Na_2W_2O_7$ and $CdWO_4$. . Later in 1970s, Wickersheim and co-workers[5, 32, 33] explored the possible use of rare-earth activated phosphors in numerous applications, including lasers, neutron detectors and x-ray detectors. Their research at determining the temperature sensitivity was significantly valuable and eventually led to the commercialisation of thermometry based on fluorescence. Additionally, fibre optic temperature sensors are already widely used in biomedical application. For instance, sensors exhibiting variable reflection with temperature using liquid crystals and black body type sensors for use at high temperatures[2, 24].

In recent years, applied researchers have become increasingly interested in fibre optic thermometry for use in electromagnetically harsh environments, for instance in the challenging MRI environment. In 1980s, Wickershiem et al.[5] from Luxtron Corporation have developed two generations of fibre optic temperature sensing which have found acceptance for a variety of scientific and medical applications. The first generation Luxtron system, represented by Model 2000 using the ratio of two emission intensities of a rare-earth phosphor as a function of temperature, whereas the second generation technology (Model 750) utilises the change in the fluorescent decay time of a phosphor with temperature[5]. The phosphor they used for the decay time approach is magnesium fluorogermanate doped with tetravalent manganese over the temperature range from -60 to 400 °C[5].

2.3 Phosphor

A phosphor is defined as a solid material which converts absorbed energy into electromagnetic radiation over and above thermal radiation, usually in the visible range, or sometimes in the infrared (IR) or ultraviolet (UV) region[27, 34]. In terms of their composition, phosphors may be divided into two classes: organic and inorganic. This study has focused on inorganic phosphors which consist of two components as shown in Figure 2-1: a host lattice and an activator from which the light is emitted [1], for example, La_2O_2S: Eu, where the europium is the activator and lanthanum oxysulphide is the host lattice. Many different phosphors are extensively used in the lighting, display and sensing industries. The applications of phosphors can be classified according to the excitation source. Such examples are the cathode ray tube (CRT) which is excited by a beam of electrons; fluorescent lighting excited by UV rays; scintillators and x-ray conversion screens excited by x-ray [1]. Other excitation sources include neutrons, gamma rays, and visible light.

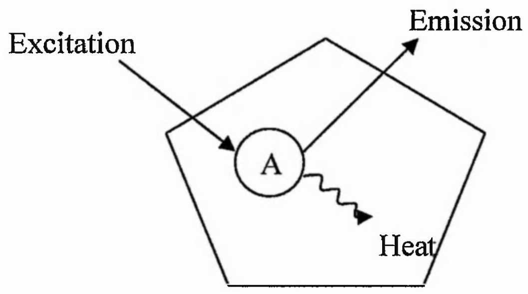

Figure 2-1: A luminescent ion A in its host lattice. Emission (radiative return to the ground state); Heat (non-radiative return to the ground state) [34].

2.3.1 Historical background of phosphors

The word 'phosphor' was invented by an Italian alchemist, Vincentinus Casciarolo of Bologno in the 17th century[27] to indicate the discovery of a stone known as 'Bolognian stone' which emitted red light in the dark after exposure to sunlight. 'Phosphors' also means 'light bearer' in Greek [27]. In fact, the first use of phosphors was discovered in an interesting cow's painting that was presented to the second emperor of the Song dynasty (976 – 998) [27]. At the time the officials could not explain the reason why the cow appeared during the day as eating grass outside the pen, but resting in it at night. Later, a monk explained that the ink (colour) that was shown only in the night was mixed with pearl shells collected from a seashore while the ink that was shown only during the day was made from the rock fell from a volcano[27] which are now known to contain phosphorescent materials.

The beginning of scientific research of phosphors started in 1866[27] when a young French chemist, Theodore Sidot, succeeded in growing zinc sulphide (ZnS) crystals which exhibited phosphorescence in the dark. This important finding has driven the evolution and development of phosphors for use in various applications, especially the display market. During the 19th century, Philip E.A. Lenard and co-workers in Germany[35] investigated the luminescence properties of different phosphors based on alkaline earth chalcogenides (sulfides and selenides) and ZnS: which are now also referred to Lenard phosphors. They established the principle of firing the metallic impurities, also known as luminescence activators into the phosphor compound to form luminescence centers within the host. In the late 1920s, P.W. Pohl and co- workers in Germany pioneered the configurational coordinate model of luminescence centers by investigating Ti^+-activated alkali halide phosphors and were able to grow single crystal phosphors. Humbolt Leverenz and co-workers at Radio Corporation of America (US) performed extensive studies on ZnS type phosphors. They exploited the characteristics and capability of many practical phosphors to be used in CRTs and their achievements are published in 'An introduction to luminescence of solids'[36] which still remains a valuable source of information today.

Scientific research on phosphors was largely the domain of academia until the introduction of the fluorescent lamp in 1938 by GEC, UK[1, 37] and resulted in numerous industrial laboratories to delve into the development of phosphors for commercial lighting applications. At that time, the degradation of the luminescent output with temperature was problematic in lamp applications and this led to the need to study the thermal characterisation of phosphors. As early as 1937, Neubert [38] suggested the use of phosphor use within a device for indicating the temperature distribution of hot bodies. Later on, Urbach [31, 39] carried out early phosphor thermometry approaches on measuring the temperature distribution on a flat wedge in a supersonic flow sonic field. Research on phosphors and solid-state luminescence has evolved radically since the end of World War II, especially gaining a deeper understanding of the optical spectroscopy of solids and the concept of the configurational coordinate model of luminescence centers.

With the television industry growing explosively in 1950s, research on phosphors was extensively carried out where suitable phosphors were put to practical use in cathode ray tubes (CRT) to create a full colour fluorescent screen. The screen consisted of the blue-emitting ZnS: Ag (peaking at 450 nm), the green emitting Zn_2SiO_4: Mn^{2+} (525 nm), and the red-emitting $Zn_3(PO_4)_2$: Mn^{2+} (638 nm) phosphors[27]. However, these tubes suffered from a number of problems such as insufficient brightness, long persistence in the image, an imbalance in the beam currents, and instability of the red-emitting phosphor. In addition, the broad luminescence band of $Zn_3(PO_4)_2$: Mn^{2+} and (Zn, Cd)S: Ag spread into the deep-red region where human's eye is least sensitive. As a consequence, the concept of an ideal red-emitting phosphor for colour televisions - 'sharp peak in the area of 610 nm' was proposed in 1955 and extensive research to explore this phosphor was soon followed. In 1962, an ideal candidate was discovered, europium doped yttrium vanadate oxide, YVO_4: Eu (618 nm)[40]. This phosphor was however only used for a relatively short period, it was replaced in 1967 with europium doped yttrium oxysulphide [27], Y_2O_2S: Eu (626nm), developed by the Radio Corporation of America (RAC). Y_2O_2S: Eu has an 80% higher luminous efficiency and a good balance in the beam currents of all the electron guns for producing a white screen. The successful achievement with the rare-earth red has led the researchers to delve into the development of various phosphor hosts activated with rare-earth ions due to their high luminescence efficiency, narrow spectral band outputs and sensitivity to temperature variations.

2.3.2 Luminescence

Luminescence refers to the absorption of energy by a material, with a subsequent emission of light. The emission of light of the inorganic materials is often split into two categories which are related to the lifetime of the activator: fluorescence refers to the same process as luminescence but having the emission lifetimes of typically $10^{-9} - 10^{-3}$s; and phosphorescence (also known as afterglow) which has greater luminescence duration of approximately $10^{-3} - 10^{3}$s [1, 41]. The luminescence properties of rare-earth doped ceramic oxide and oxysulphide phosphors have characteristic temperature dependencies that make these materials useful in a variety of thermometry applications.

2.3.2.1 Photoluminescence

There are several forms of luminescence which are excited by different external means for various applications, such as electroluminescence (EL) excited by electric field for the thin film electroluminescent (TFEL) devices, cathodoluminescence (CL) excited by electron beams for the CRT and also radioluminescence (RL) excited by high energy radiation for the radiographic imaging plate[41]. The method that is of interest in this project is photoluminescence (PL), the emission of light from a material excited by photons, typically from the UV region of the optical spectrum.

A visual representation of the photoluminescence system is shown in Figure 2-2, it shows the difference of a phosphor powder sample, La_2O_2S: Eu prior to and under excitation. Like many other phosphors, La_2O_2S: Eu is a white powdered phosphor (it is important to note that La_2O_2S: Eu turns slightly pink after being compacted due to mechanical stressing within the pellet die, this will be discussed in Chapter 3). When the phosphor pellet is excited by an UV source, it produces red luminescence as shown in the picture. The mechanisms of photoluminescence are explained below.

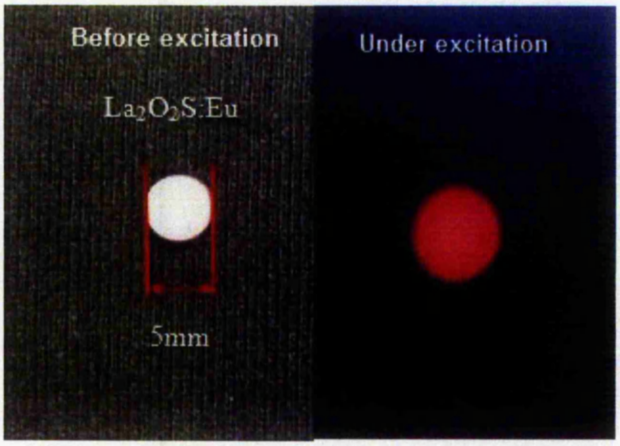

Figure 2-2: Picture illustrates the phosphor pellet before excitation and the emission of luminescence under UV excitation.

Typically, an activator is added to a crystal lattice of a phosphor leading to the splitting of energy levels within the crystal field in order to create luminescence, provided a sufficient amount of energy is absorbed. Absorption of radiation does not necessarily take place in the host lattice, but may also occur within the activator and this will be discussed later in this sub-section. For photoluminescence, the optical absorption of a phosphor mainly occurs in the ultraviolet or visible region with energies greater than the width of the forbidden gap, usually several electron volts (eV). To illustrate the photoluminescence processes, an energy level diagram indicating the valence and the conduction bands of a host lattice, as well as an activator sited within the crystal lattice is depicted schematically in Figure 2-3. The valence bands are the energy states with lower energies which are occupied by electrons, whilst the energy bands having higher energies are not occupied by electrons are called conduction bands[42].

As presented, the luminescence processes involve the absorption of light allowing the electrons at the ground state to be promoted to a higher energy level, followed by the emission of either radiation (photon) or non-radiation (phonon) via a relaxation transition back to a lower stable energy state. The radiative emission process produces luminescence whilst the energy of the excited state in the non-radiative process is used to excite the vibrations of the host lattice, i.e. to heat the host lattice[43]. The manifested characteristics to be measured of such energy transitions are represented in Figure 2-4, the excitation and emission spectra of one of the investigated phosphors, La_2O_2S: Eu. The excitation spectrum is determined by monitoring the intensity of an emission peak while the excitation wavelength is varied[1]. In this case, the optimum excitation wavelength at 355 nm is associated with the most intense emission line peaking at 625 nm in the red region of the visible spectrum. The emission lines of rare-earth phosphors usually have a narrow spectral linewidth, this is due to the allowed transitions between the discrete energy levels leading to emission of photons with a certain energy.

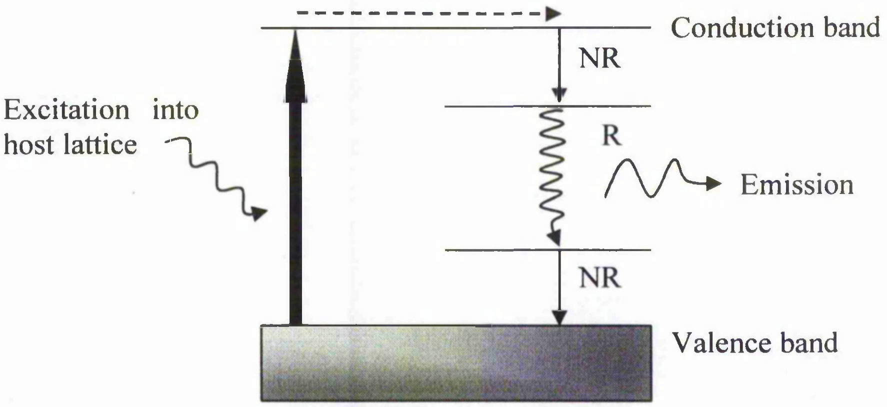

Figure 2-3: Energy level diagram illustrating electron transitions from a valence band state to a conduction band state resulting in the emission of radiation (photon) and non-radiation (phonon).

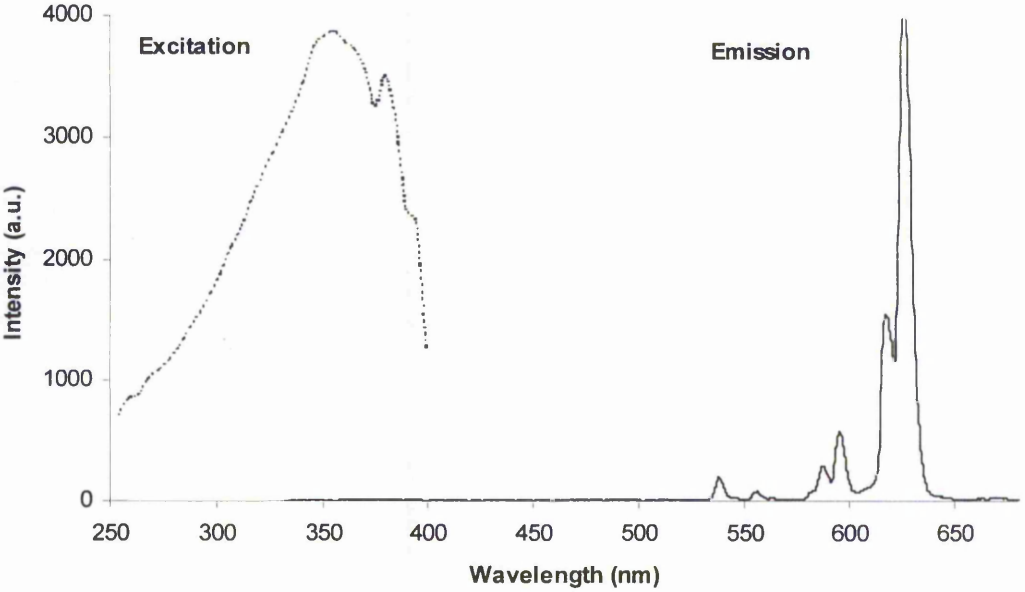

Figure 2-4: Emission spectra of La_2O_2S: Eu excited by a nitrogen laser (337 nm) at room temperature. Excitation spectra for La_2O_2S: Eu provided by Phosphor Technology Ltd.

As discussed earlier, absorption of excitation energy can also occur directly within the activator itself. According to Blasse et al[44], direct excitation of the activator is only possible with ultraviolet and/or visible radiation. On the other hand, examples of the high energy excitation that always excites the host lattice are fast electrons, γ (gamma) rays and X-rays. The well-known phosphor Y_2O_3: Eu $^{3+}$ used for colour television screens, is excited in the activator itself when applied in a luminescent lamp (254 nm excitation), but is excited in the host lattice when used as a cathode-ray or X-ray phosphor[44]. The sharp red emission is primarily characteristic of the impurity ion Eu $^{3+}$. This research is only dealing with ultraviolet radiation by referring to the excitation spectrum of the phosphor candidates provided by the supplier, PTL.

A basic schematic energy level diagram of an activator is illustrated in Figure 2-5. Prior to excitation, the electronic levels of the material are populated in the ground state (E_0). A means of exciting radiation, photons in this case (often denoted in wavelength or electron volt), is absorbed by the activator and thus promoting the electrons to a higher excited state ($E_{n=1, 2, 3, ...}$). Conservation principles dictate that the amount of energy absorbed must be balanced by an equivalent loss [45, 46]. As a result, the excited state returns to the ground state by emission of a photon (radiation) with the energy equal to the energy difference between the levels, by transfer of energy via quantised vibrational (dissipated non-radiatively as a phonon) exchange in the material, or by other more complex energy exchange mechanisms[1]. Each of the radiative and non-radiation transition has a probability of occurrence[47], and thus produces various intensities for the radiative transitions which correspond to the spectral lines of the emission spectrum of a phosphor.

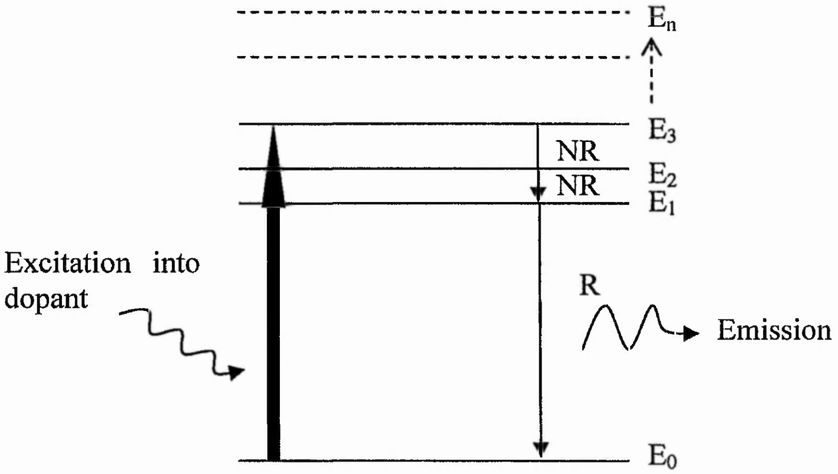

Figure 2-5: Energy level diagram showing energy transitions within an activator.

The wavelength of the emitted light can be determined from this standard equation:

$$E_1 - E_0(eV) = \frac{hc}{\lambda}$$ **Equation 2-1**

Where E$_1$ and E$_0$ are the excited energy value and ground energy value in electron volts (eV) respectively, h = Planck constant, c = speed of light in a vacuum and λ = wavelength of the emitted light. In order to produce photoluminescence, the photons must have enough energy to excite the phosphor material. This occurs only if the excitation energy is higher than the forbidden energy gap of the material ($h\nu > E_g$).

Apart from the direct excitation of the activator with UV and/or visible radiation as mentioned above, it is also important to understand that absorption (excitation) may also take place in another absorbing ion (the sensitizer), or in the host lattice. For instance, a sensitizer can be added to the host lattice in which the ion may absorb the exciting radiation and subsequently transfer its energy to the activator from which an optical transition occurs[43]. Weber[48], a rare-earth laser researcher, notes erbium is a sensitizer for dysprosium, while gadolinium has been found to be a sensitizer for terbium.

2.3.2.2 Dopant concentration

Another important luminescence mechanism is associated with the concentration of the activating impurity. As stated earlier, when an impurity is doped into a crystal host, the optical properties will be altered by the interactions with the crystal and hence produces luminescence. For instance, a host material such as Al_2O_3 is transparent and non-fluorescent until Cr^{3+} is added into it to form ruby[49]. The Cr^{3+} ions directly substitute for the Al^{3+} ions. The impurities will normally be present at a low concentration, say a few percent or less so that the non-radiative de-excitation exchange is minimised between the neighbouring atoms[1]. Allison et al. [3] reported that a phosphor will exhibit brighter luminescence if there are more luminescent centres in a phosphor, up to a point. However, another non-radiative de-excitation pathway becomes important when the concentration levels reach a certain point. As the dopant concentration is increased, the probability that an excited activator will transfer energy non-radiatively to a neighbouring dopant ion increases[1]. The cut-off point in this process is referred to as concentration quenching. In addition, different dopant will have different optimum concentration even when in the same host. For example, the optimum dopant concentration of Y_2O_3: Eu results in the most intense luminescence at 611 nm is 35 atomic %[50], whereas the optimum concentration of samarium (Sm)[1] or dysprosium (Dy)[51] in Y_2O_3 is 0.5 mol %.

Although it is important to identify the optimum dopant concentration of a phosphor to produce the maximum brightness, there are other considerations that need to be taken into account for thermometry applications. For instance, at low Eu concentrations, the emission lines at shorter wavelengths which are temperature dependent tend to be stronger than they are at higher concentrations. This is particularly important for phosphor thermography in determining temperature sensing capabilities of a phosphor.

An example of this phenomenon is shown in Figure 2-6, a comparison of spectral emission distribution for various Eu concentrations in the host of La_2O_2S. Since the luminescence emitted by the host lattice is very weak and therefore the integration time of the spectrometer has been increased to 4 seconds allowing more photons to be captured, compared to only 150 ms for the bright red luminescence emitted from La_2O_2S: Eu at different concentrations. The host lattice has a very broad emission spectrum over the visible region with its characteristic emission lines peaking at 512 nm, 538 nm, 556 nm, 586 nm, 616 nm, 625 nm and 704 nm resulted in an orange luminescence when under UV excitation. These emission lines become far more dominant and have narrower bandwidth (approximately 2.4 nm FWHM) when the dopant, europium is introduced to the host lattice. The red emitting dopant ion, Eu has greatly enhanced the brightness of the undoped La_2O_2S and hence produces a much better signal-to-noise ratio for signal analysis. It needs noting that some emission lines of the host lattice match those of Eu doped La_2O_2S phosphors and thus it is believed that the host lattice may be contaminated by a small amount of Eu impurities. The relationship between the emission intensity with varying dopant concentrations plays an important role in the photoluminescence system. In addition, decay times are also affected by dopant concentrations. This will be further discussed in Chapter 4 and 5.

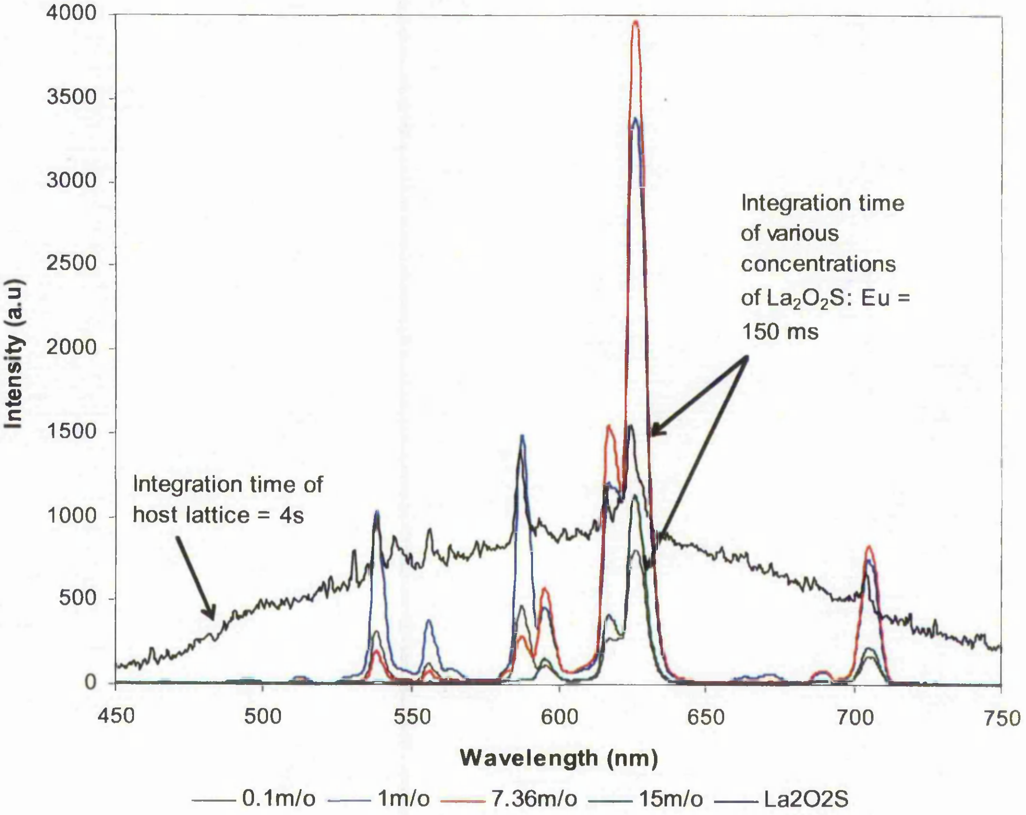

Figure 2-6: Emission spectra of the host lattice and different dopant concentrations of La_2O_2S: Eu.

2.3.3 Phosphor temperature measurement techniques

There are several commonly used measurement techniques to determine the temperature dependency characteristics of phosphorescent materials. Decay time (a.k.a. lifetime) measurement is a preferred technique to determine the temperature dependency of thermographic phosphors mainly due to its independence to fluctuations in the external triggering source.

2.3.3.1 Two peak intensity method (The ratio technique)

The width and the position of the emission peaks can be related to temperature analysis of some phosphorescent materials. Some phosphors emit a single broad peak such as ZnS: Mn (manganese doped with zinc sulphide) and some phosphors exhibit multiple narrow peaks namely La_2O_2S: Eu. The latter is found to be more suitable for temperature measurement using the two peak intensity technique, also referred as the ratio technique as described by Goss et al[52].

The two peak intensity technique involves using the ratio of two emission peak intensities excited by a single excitation wavelength [52]. This technique will ideally use one emission wavelength from the spectrum whose intensity increases or decreases with temperature, along with another one which is independent to temperature and thus acts as a reference[53]. By monitoring the ratio of the two peaks, the temperature of the phosphor can be determined, as demonstrated in Figure 2-7. Since both of the emission peaks are dependent upon the same environmental changes and variations in the excitation source, a self-reference measuring system is provided.

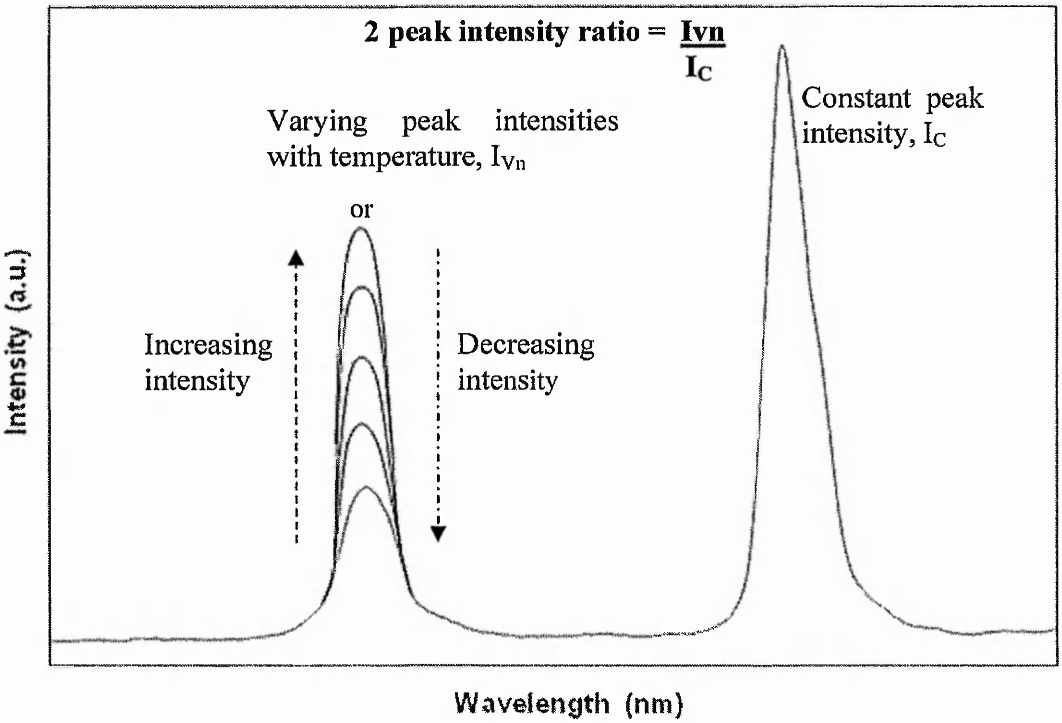

Figure 2-7: Two peak intensity method.

Goss et al. [52] demonstrated the intensity ratio technique using dysprosium doped yttrium aluminium oxide, YAG: Dy, whose spectral line intensity increases with temperature. Ervin et al[54] carried out a phosphor thermographic experiment with a heated cylinder in cross-flow and temperature distribution on the curved surface was recorded over 24 – 55 °C using this ratio technique.

2.3.3.2 Shift in wavelength

The wavelength of an emission peak of a phosphor which varies slightly with temperature is referred to as wavelength shift. Allison et al.[1] reported this phenomenon as a line shift. The emission peak will shift to longer wavelengths with an increase in temperature[55]. According to Allison et al.[1], a variation in the line-width (the spectral width at half the maximum of the line intensity, FWHM) and line shift as a function of temperature is generally insignificant and hence this approach is rarely employed in fluorescence thermometry. As an example, Kusama et el.[56] used this method for cathode ray tube (CRT) thermometry using Y_2O_2S: Eu and they observed a shift of approximately 0.2 nm in the blue region from 582.8 nm to 583.0 nm over -15 to 72 °C, as shown in Figure 2-8.

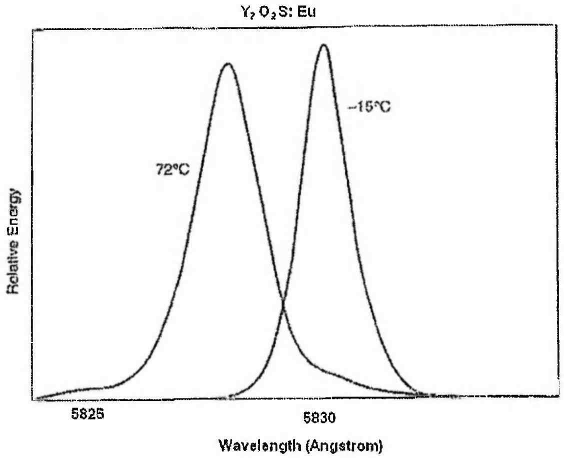

Figure 2-8: Line width and line position at – 15 and 72 °C for Y_2O_2S: Eu [56].

2.3.3.3 Decay time measurement

The variation of the decay time, or lifetime of phosphorescence [57] is another aspect of thermographic phosphor fluorescence that has been successfully exploited for the measurement of temperature. For example, Lutz et al. [58] and Noel et al. [59] have employed the decay time sensitivity of rare-earth phosphor fluorescence for surface temperature measurement on a heated turbine disk and turbine engine respectively. Furthermore, Wickersheim et al.[5] have utilised this approach for fibre optic thermometry. More interestingly, Ranson et al.[9] at NTU have reported a novel methodology using the rise time of phosphorescence to determine the temperature dependent characteristics of the phosphors. This rise time characterisation was previously referred as 'dead-time' and thus it was ignored in the temperature analysis.

When a phosphor is excited by a UV pulsed source, a decrease of fluorescence intensity with time can be observed after the exciting radiation has ceased. The intensity of emission is related to the number of excited states that have resulted from the excitation process. In turn, these excited states are unstable and will naturally fall back to a lower stable state. The rate at which they return to the lower stable state is dependent on internal energy transfer and can be quantified by probability. This can be mathematically explained as follows:-

The value of N_e gives the number of luminescent ions in the excited state after an excitation pulse, t the time, and P_{eg} the probability for spontaneous emission (expressed as the transition probability per unit time, s^{-1}) from the excited state to the ground state[60, 61].

$$\frac{dN_e}{dt} = -N_e\ P_{eg}$$ **Equation 2-2**

We can relate the number of electrons in the excited states to time by integrating equation 2-2. $N_e(0)$ is defined as the value of excited luminescent centres at t= 0, which make a transition to the ground state by emitting luminescent radiation, and the population N_e in the excited state at any time, t, is given by:-

$$N_e(t) = N_e(0)\exp(-P_{eg}t)$$ **Equation 2-3**

After the population of the excited state has decreased to 1/e, the probability of de-excitation can be defined as a reciprocal of the radiative decay time:-

$$\tau_d = P_{eg}^{-1} \qquad \textbf{Equation 2-4}$$

Since the emission intensity, I(t), is proportional to the number of photons, N_e (t). The lifetime of the excited state can therefore be deduced in terms of fluorescent intensity level according to equation 2-3:

$$I(t) = I_O \exp(-\frac{t}{\tau_d}) \qquad \textbf{Equation 2-5}$$

where I(t) = intensity at time t, I_0 = initial intensity at time 0 and τ_d = decay time or excited state mean lifetime is the time at which the intensity has decayed to 1/e (approximately 37%) of the original value. Figure 2-9 illustrates the fluorescence intensity of La_2O_2S: Eu (at 512nm) decaying exponentially with time and the rate of decay is temperature dependent. The decay time of the phosphor is observed to decrease with increasing temperature. Hence, an empirical correlation of decay time with temperature can provide the basis for a temperature measurement.

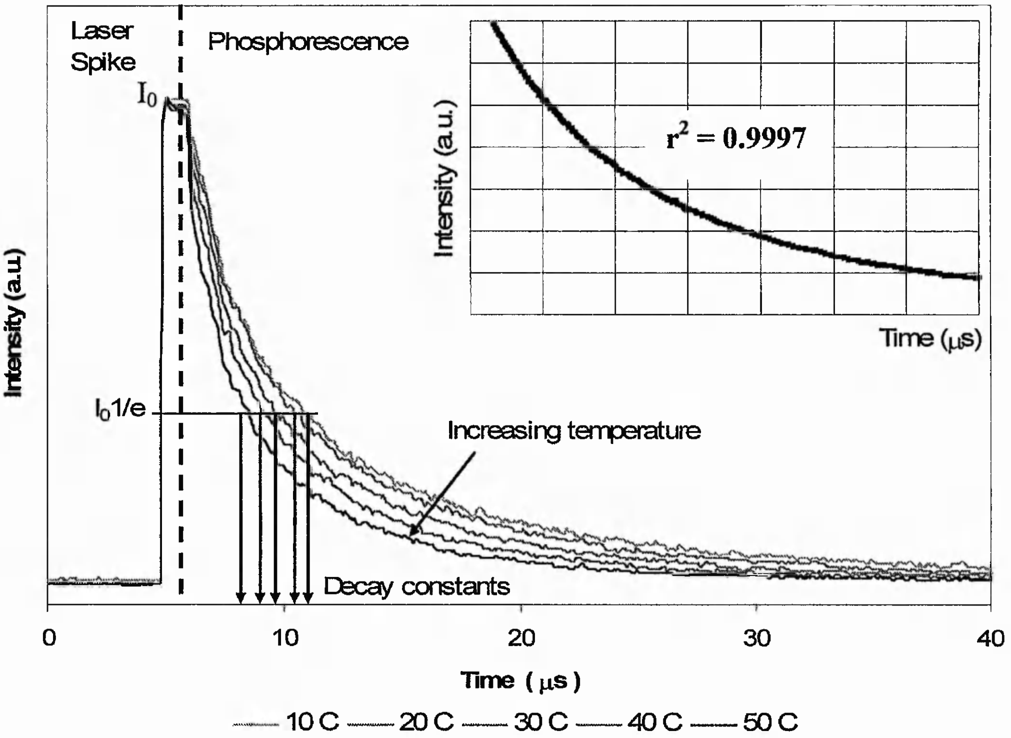

Figure 2-9: Example of single exponential decay profiles of La_2O_2S: Eu at various temperatures under 337nm excitation. The inset graph indicates a single exponential decay fitting with an accuracy of >99.9%.

As illustrated in Figure 2-10 , the decay time of a phosphor can also be determined by a linear least squares fit of intensity (ln) against time relating to Equation 2-5:

$$\ln I(t) = \ln I_0 - \frac{t}{\tau_d} \qquad \textbf{Equation 2-6}$$

This shows a linear relation solid line is well fitted with an accuracy of >99.5% which indicates that La_2O_2S: Eu has a single-exponential decay characteristic. The decay time of the phosphor calculated from the gradient is 5.2 μs which is in agreement with the decay time calculated using Table Curve automated software, 5 μs. This linear least squares fit approach is useful to validate and compare the decay time characteristic of a phosphor that is determined using the commercially available curve fitting software.

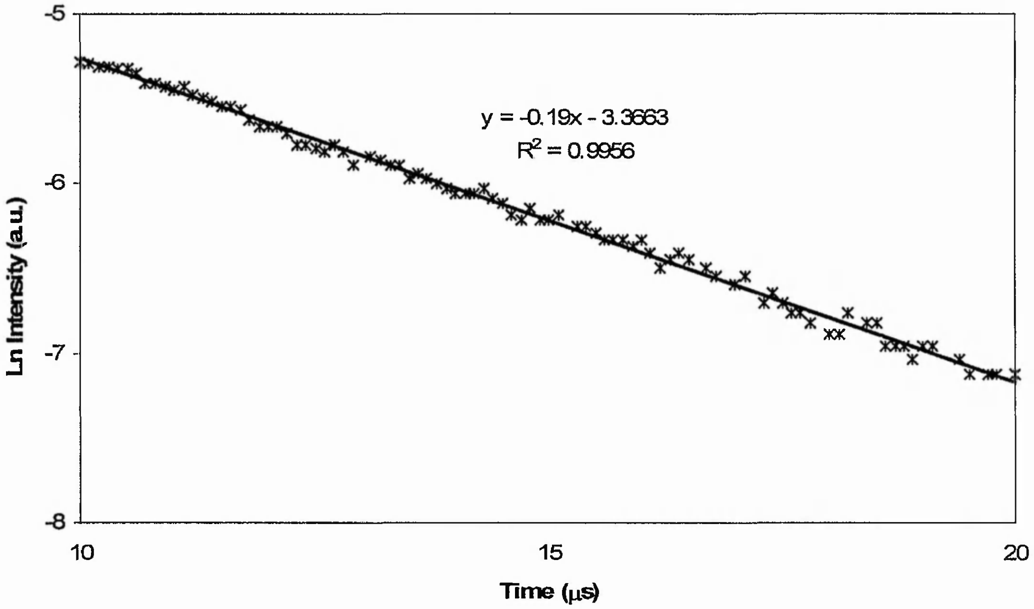

Figure 2-10: Plot of luminescence intensity (ln) against time for La_2O_2S: Eu at 10 °C. The inset graph shows a linear relationship between intensity and time which yields a single exponential profile with an accuracy of >99.5%.

Simons et al. [62] proposed a simple model aimed at describing how strongly the fluorescence lifetime of a material depends on its temperature. The relevant expression is:

$$\tau_d = \tau_q \exp\left[-Q\left(T - T_Q\right)\right] \qquad \textbf{Equation 2-7}$$

By definition, the decay constant (τ_d) is related to the component temperature (T) above the quenching point (T_Q), where τ_q is the decay time at the quenching point. The quenching rate Q is simply the temperature change needed for the decay time to decrease by 1/e and is therefore a measure of the temperature sensitivity of the phosphor. An example of this decay constant variation can be seen in Figure 2-11. It is worth to note that this empirical equation is an approximation to Equations 2-8 to 2-10 which relate to the probability of occurrence of the radiative and non-radiative transitions which will be discussed below.

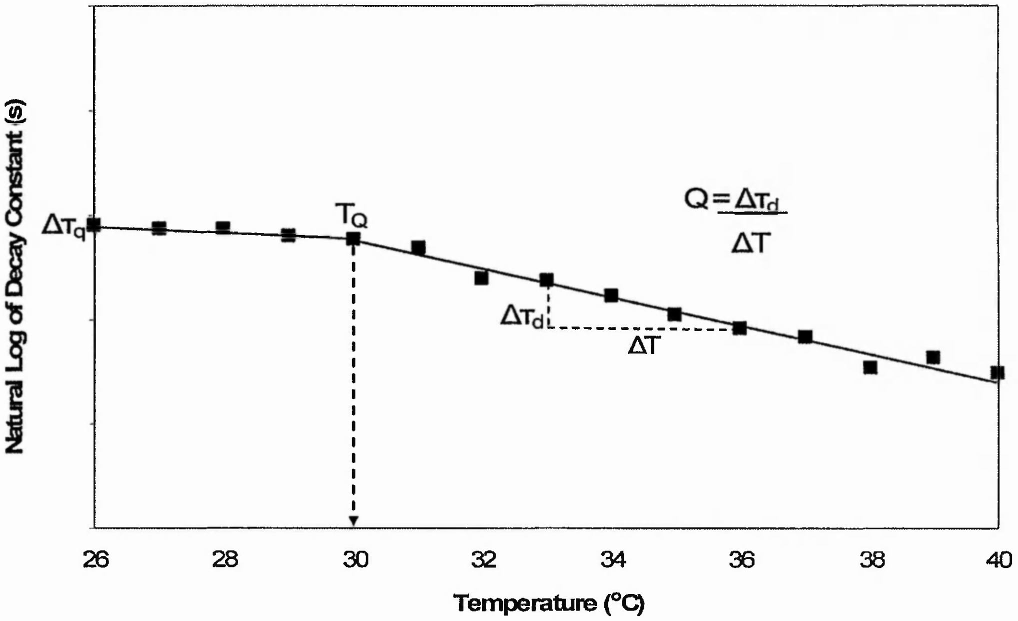

Figure 2-11: Temperature dependent characteristic of La_2O_2S: Eu.

The temperature sensing capabilities of a phosphor, relating to Simons' model, can be explained with reference to the configuration coordinate model depicted in Figure 2-12. The configurational axis represents the mean distance between the luminescent centre and the surrounding ions; the vertical axis refers to the energy of the electrons of the luminescent centre[28, 63].

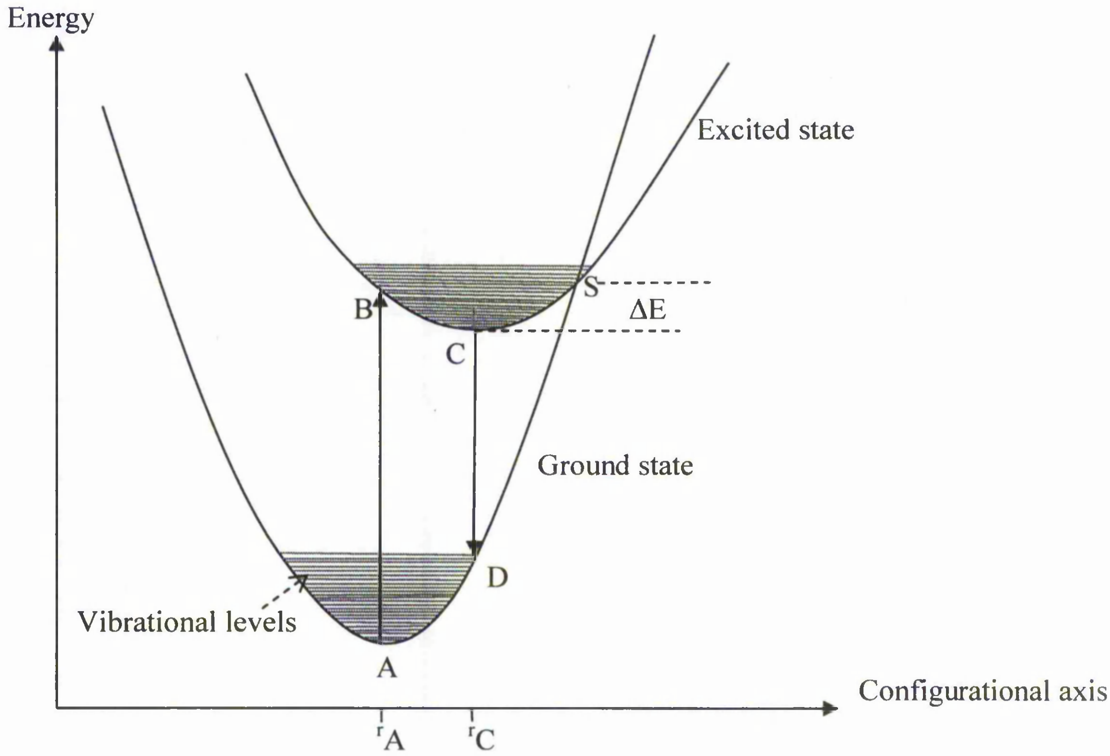

Figure 2-12: A schematic representation of configurational coordinate model showing energy of valence electrons of the luminescent centre against configuration coordinate. Path A-B represents absorption of the excited energy followed by the emission process through path C-D[60, 61].

At room temperature, the thermal energy is not adequate to significantly populate any of the excited energy states. The most likely state for an electron is the ground state at point A, which contains a number of distinct vibrational energy states, each with differing energy levels. For the excited energy to be absorbed, it must have sufficient energy to excite the electrons from the ground state to the excited state at point B. The luminescent centre moves from point B to the lowest point C (equilibrium coordinate) of the excited state by vibrational transitions, whereby the energy that is lost is released as a phonon (thermal energy)[28, 61]. From this state the excited electron may return to the ground state at point D via two routes. The first route results in the emission of a photon and is called fluorescence. The second route is where the centre is thermally activated from point C to the crossing point S (the intermixed of the excited state and the ground state), and subsequently thermally released as a phonon from S to D on the ground state. The energy ΔE required to excite the centre from C to S is referred to the thermal activation energy[61].

Relating the number of excited luminescence centres in a unit volume to the probability of de-excitation P_{eg} from Equation 2-3 , the equation can be rewritten by denoting the sum of the radiative, W_R and non-radiative, W_{NR} transition probabilities[61]:

$$P_{eg} = W_R + W_{NR} \qquad \textbf{Equation 2-8}$$

Hence, the decay time from Equation 2-4 can be rewritten as:

$$\tau_d = (W_R + W_{NR})^{-1} \qquad \textbf{Equation 2-9}$$

The probability of the non-radiative transition, W_{NR} that makes the transition from point C to S by thermal activation is given by:

$$W_{NR} = s\exp\left(-\frac{\Delta E}{kT}\right) \qquad \textbf{Equation 2-10}$$

where k is the Boltzmann constant, s is the frequency factor and T is the temperature. This non-radiative mechanism is strongly temperature dependent. At higher temperatures, the non-radiative transition becomes more likely due to the thermal activation energy ΔE can be more easily provided[28, 61], resulting in thermal quenching which causes a reduction in emission efficiency and shortening the decay time of the luminescent centre.

In summary, the decay time system is a preferred and more reliable method to determine the temperature of the phosphor because of its insensitivity to ambient light and fluctuations in the excitation source. In addition, decay time measurement has a wide temperature sensing range based on the selection of suitable phosphor which can be carried out typically to ± 0.2 °C or better accuracy over most of the working range of temperatures[2], compared to an accuracy of 9–50 °C obtained by the two-peak intensity method[52]. Due to the limitations of intensity based approaches in terms of performance, this research therefore concentrated on the decay time measurement as the main temperature dependent characterisation for the chosen phosphors.

2.4 X-ray diffraction (XRD)

X-ray diffraction is a useful tool for determining the crystalline structure and orientation of a single crystal or polycrystalline material. In 1913, Sir W.H. Bragg and his son Sir W.L. Bragg developed a mathematical relationship, Bragg's Law[64, 65] to explain the interference pattern of X-rays scattered by crystals. When an X-ray is incident upon a sample, the radiation will be scattered by the electrons of the atoms in the material. The scattering process results in a variety of constructive and destructive interference patterns. Where the combining waves are out of phase and there is no resultant energy leaving the solid sample, this is referred to as destructive interference. Peaks form when constructive interference occurs whereby Bragg's Law is satisfied. The waves are in phase and there will be well-defined X-ray beams leaving the sample at various directions, as shown in Figure 2-13.

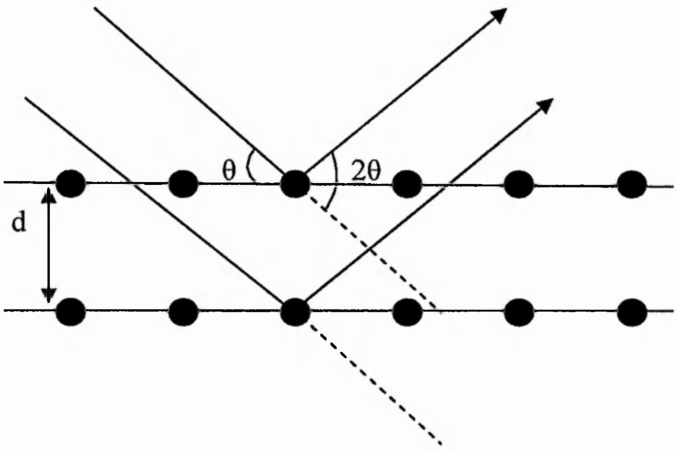

Figure 2-13: X-ray reflections in a crystalline material. (2θ is the measured angle)

A simple geometry illustrated in Figure 2-14 indicates the conditions of constructive interference derived from the Bragg's Law[64]. An X-ray beam is incident on a pair of parallel planes P1 and P2. These planes are separated by an interplanar spacing, d. The two parallel incident rays 1 and 2 create an angle (theta, θ) with planes P1 and P2. If the waves represented by 1' and 2' are in phase, a diffracted beam of maximum intensity will generate. The difference in path length between 1 to 1' and 2 to 2' must be an integral number of wavelengths, λ. Diffractions occur from planes set at angle θ with respect to the incident beam and subsequently generates a diffracted beam at a 2θ angle from the incident beam[66]. This relationship can then be expressed mathematically in Bragg's law[66, 67]:

Path difference = nλ = AB + BC,

$$AB = BC$$

$$n\lambda = 2AB$$

$$\sin\theta = \frac{AB}{d}$$

$$AB = d\sin\theta$$

$$n\lambda = 2d\sin\theta \qquad \textbf{Equation 2-11}$$

where variable d is the spacing between atomic layers in a crystal, θ is the incident angle, n is any integer, and λ is the wavelength of the incident X-ray beam.

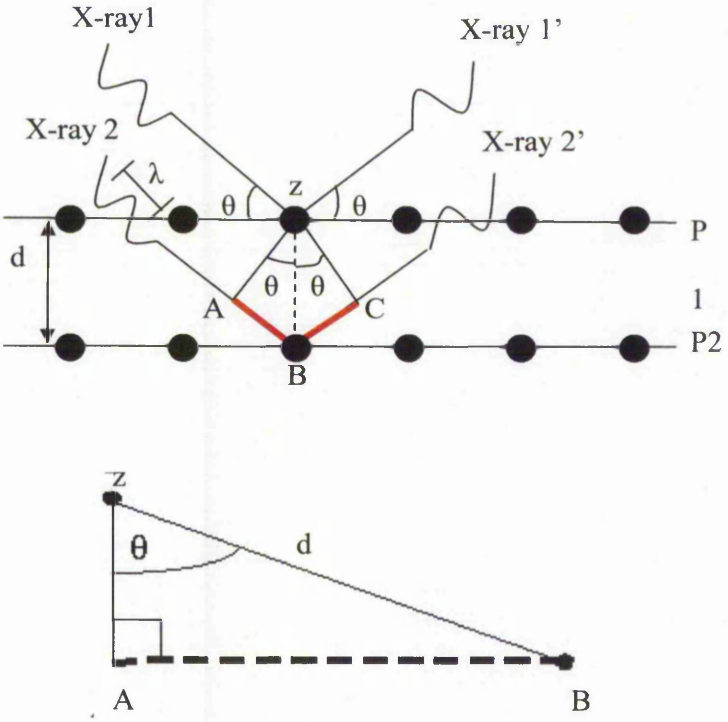

Figure 2-14: Geometry of the Bragg's condition[65, 68].

The crystal field of any given phosphor alters with different levels of dopancy due to the interactions between the dopant ion and the lattice. It is therefore important to carry out an investigation on XRD as a function of dopant concentrations. The optical properties of a phosphor could then be fine-tuned in terms of dopancy to determine an optimum temperature sensing phosphor for thermographic applications.

Considering the luminescence and temperature dependent characteristics of a phosphor are dependent on its crystal structure, XRD measurements have been carried out to aid the investigation of the temperature sensing capabilities of various dopant concentrations of La_2O_2S: Eu and La_2O_2S: Tb by determining the changes in their crystallinity and crystallite size. The XRD results and discussions of both phosphors are included in Chapter 4 and 5 respectively.

2.5 Review of previously analysed phosphors

This detailed review of the current literature in the fields of optical sensors has been carried out to identify potentially the most appropriate phosphor for use in the fabrication of the sensor. This provides the relevant data to gain insight into up to date sensing capabilities and fabrication process as well as the photoluminescent and decay time characterisation systems. A look-up table of a wide range of analysed phosphors from past papers has been produced to show their emitted wavelengths, excitation source used and also their temperature sensing capabilities.

Table 2-1: Data of analysed phosphors and fluorescent materials from literature survey.

Phosphor	Technique	Temperature Range (°C)	Decay Time (µS)	Excitation Wavelength (nm)	Emitted Wavelength (nm)	Ref
Acridine Yellow	Intensity	-50 - 50	-	Xenon,75nm band center 410 nm	500, 580	[69]
Alexandrite	Decay time	20 - 150	-	Green LED	-	[70]
BaClF:Sm^{2+}	Decay time	25- 200	-	417	687.7	[71]
$BaMgAl_{10}O_{17}$:Eu	Wavelength	20- 280	-	UV	Blue, 447	[28]
Chlorpromazine Sulphoxide	Intensity	5- 45	-	335	380	[72]
CuOEP		-180- 20	-	480- 515		[73]
Emetine Hydrochloride	Intensity	5- 45	-	282	318	[72]
EuTTA	-	-20- 80 20- 50 19- 50	500	350	612	[74]
Fluorescein Sodium	Intensity	5- 45	-	487	512	[72]
Guaiphenesium	Intensity	5- 45	-	274	310	[72]
La_0F_3:Dy^{+3}	Decay time Intensity	-70- 60	-	-	-	[75]
La_2O_2S:Eu	Decay time	20- 90	-	337 (N_2)	514	[59]
	Decay time	20-200	-	337 (N_2)	537	[58]
	Decay time	100- 260	0.02-0.12	337 (N_2)	537	[76]
La_2O_2S:Eu^{+3}	Intensity	19- 60	-	355(Nd: YAG)	512	[76]
	Intensity	24- 55	-	-		[54]
	Decay time	0-100	0.8-25	337 (N_2)	512	[59]
	Decay time	95-250	0.8-250	337 (N_2)	538	[59]
La_2O_2S:Tb^{+3}	Intensity	-173-327	-	270	489-545	[77]
Mg_4FGeO_6:Mn	Decay time	70-700	1.2-4000	355(Nd: YAG)	664-637	[78]
Perylene		0- 100	5ns	330- 450	430- 580	[73]
Phenol	Intensity	5- 45	-	270	299	[72]
Quinine Sulphate	Intensity	5- 45	-	350	450	[72]
Rhodamine B	-	0- 80	4ns	460- 590	550- 590	[74]
Ru(bpy)	-	0- 90	5	320, 452	588	[74]
Ru(bpy)/Zeolite	-	-20- 80	-	320, 452	588	[74]
$Sr_4Al_{14}O_{25}$:Eu	Intensity	20- 280	-	UV	Green, 488	[28]
YAG:Ce	Decay Time	7-77	18-27ns	337 (N_2)	550-620	[79]
Y_2O_2S:Eu	-	30- 300	-	337 (N_2)	Red	[78]
Y_2O_3S:Eu	Decay Time	60-150	45-1.5	337 (N_2)	514	[80]
Y_2O_3S:Gd	Decay Time	48-465	-	337 (N_2)	Blue	[78]

As mentioned in 2.3.2.1, apart from the main dopant, the host lattice of a phosphor also plays a very important role in absorption of radiation. The optical properties of a luminescent centre are usually different if a given ion is incorporated into different host lattices as a result of several possible factors:

a) The first factor for the influence of the host lattice on the properties of a given ion is covalency [81-84]. The interaction between the electrons is reduced for increasing covalency because they spread out over wider orbitals. As a consequence, electronic transitions between energy levels with an energy difference shift to lower energy for increasing covalency[85]. For example, the charger-transfer absorption band of Eu^{3+} in the fluoride YF_3 was found to be at higher energy than in the more covalent oxide Y_2O_3[85].

b) Another influential factor is the crystal field [1, 85] which is the electric field at the site of the ion surroundings. The strength of the crystal field determines the spectral position of certain optical transitions. For instance, Cr_2O_3 and Al_2O_3: Cr^{3+} (ruby) exhibit green and red respectively although both of them have the same crystal structure. The reason being the Cr^{3+} ions (colour emitters) in ruby occupy the smaller Al^{3+} sites, so that they undergo a stronger crystal field than in Cr_2O_3[85]. As a result, the optical transitions in ruby are higher than in Cr_2O_3 resulting in a different colour for the two compositions. In addition, the splitting of certain optical transitions are also dependent upon the crystal field[85]. Therefore, a relationship between the host lattice and crystal field can be established: different host lattices have different crystal fields which will result in different splittings of the optical transitions, and thus produces different emission spectrum.

From the literature survey, two phosphors are identified as primary candidates; namely europium doped lanthanum oxysulphide (La_2O_2S: Eu) and terbium doped lanthanum oxysulphide (La_2O_2S: Tb) due to their temperature sensing capabilities over the temperature range of interest. In addition, during a conference at Nottingham Trent University, a phosphor specialist Professor Jack Silver from Brunel University suggested that La_2O_2S: Tb could be an ideal phosphor to fulfill the objectives of this research[86]. The personal conversation with Professor Silver has again validated the viability of these two potential phosphors La_2O_2S: Eu and La_2O_2S: Tb that possess the identical host lattice to be used for comparison purposes over the temperature range of 5- 60 °C to investigate their temperature dependent characteristics. In addition, Sobon et al[87] have suggested that La_2O_2S is an excellent optical host, exhibiting high transparency from 350 nm in the ultraviolet region to beyond 8 μm in the infrared region. Results of both phosphors are discussed in Chapter 4 and 5.

Chapter 3 Experimental Techniques

As discussed in previous chapters, an investigation into the temperature dependent characteristics of the chosen thermographic phosphors has been carried out at low temperatures up to 60 °C. This chapter details the experimental procedures of PL, decay time and X-ray diffraction (XRD). Determining the spectral emission of a phosphor is required to determine the wavelength and intensity of the peaks which can be used for decay time characterisation. An important aspect of this research is the varying of dopant concentration within the host lattice. Varying dopant concentration will also vary the crystallinity of a phosphor. Therefore a study of their x-ray patterns and crystallite size has been determined by XRD. In addition, intensity variations and wavelength shifts may occur at different dopant concentrations due to the changes in crystal field of a phosphor. The sensing capability of a phosphor is determined by the decay time characterisation and hence the optimised dopant concentration within the phosphor will be used for the sensor design which will be discussed in Chapter 6.

3.1 Creation of the phosphor pellet for characterisation

Thermographic phosphors investigated in this research were supplied by Phosphor Technology Ltd (PTL). At the preliminary stage, a series of photoluminescent (PL) and decay time experiments were performed using 7.36 m/o La_2O_2S: Eu (SKL63/ F-R1) and 0.91 m/o La_2O_2S: Tb (SKL65/ N-C1) followed by a further investigation using a range of different dopant concentrations. All phosphors which have been characterised, existed in the form of a powder.

Prior to analysis, the phosphor powders were pressed to form a pellet which could then be held on a test coupon within an incubator. Figure 3-1 depicts the cross sectional diagram of a powder press and a complete set of Specac evacuable pellet die. Firstly, all the apparatus such as spatula, stainless steel pellets, plunger and the die have to be cleaned after each use with Acetone and disposable wiping papers to ensure that the components are free of impurities to reduce the risks of contamination to the sample. The whole operation of inserting the stainless steel pellets and filling the phosphor powder between the pellets is done with the die inverted. The die is held steadily in one hand while adding components from the other to allow access to the bore of the cylinder. The die base is then placed on the die assembly for pressing as shown in Figure 3-1 (a). An oil hydraulic pump is used to press the pellet to a pressure of 3000 lb/inch^2 and the pressure is maintained for five minutes. Further pumping is required if the pressure falls below 3000 lb/inch^2 over this period. After this period of time, the pressure is released and the inverted assembly is placed on top of an extractor ring, as illustrated in Figure 3-1 (b). Light pressure is applied to the die until the phosphor pellet has cleared the bore of the cylinder body. The compacted phosphor pellets are 5 mm in diameter and 2 ± 1 mm in thickness.

During the phosphor pellet preparation, unusual colouration of the phosphors is often observed. When a phosphor powder, for instance La_2O_2S: Eu/ Tb was pressed in the stainless steel pellet die, the colour of the phosphor changed from white to its characteristic hue. For La_2O_2S, a pink violet colour appeared due to the absorption bands peaking at 520 nm in the emission spectra. A sulphur odour was noted every time the samples were pressed. T.Nishimura et al. [88] has reported the colouration of the phosphors caused by mechanical stress may be due to optical absorption bands in the visible region. It can be assumed that the characteristic colour of an oxysulphide originates from the trapping of electrons at some atomically dispersed defects induced by the stress on the crystal lattice. Their results also showed the c-axis of the unit cell shrinks in the coloured samples. However, colouration did not depend on presence and quantity of rare earth impurities. At our laboratory, the undoped material La_2O_2S showed the same colour as those of oxysulphides which were doped with up to 15 m/o Europium or 50 m/o Terbium after being pressed. As a result, PL measurement was carried out on several phosphors to compare their luminescence efficiency prior to pressing, as supplied powder, and after formation of the pellet. Importantly, the results showed that the colouration caused by mechanical stress did not reduce the brightness of the phosphors, nor alter their luminescent properties.

In summary, the colouration of the phosphor pellets due to mechanical stressing has no impact on the light output of the phosphors. Forming a phosphor pellet is therefore a simple and desired preparation method due to several reasons such as allowing high emission efficiency of a phosphor, no calibration required as well as time and cost efficient.

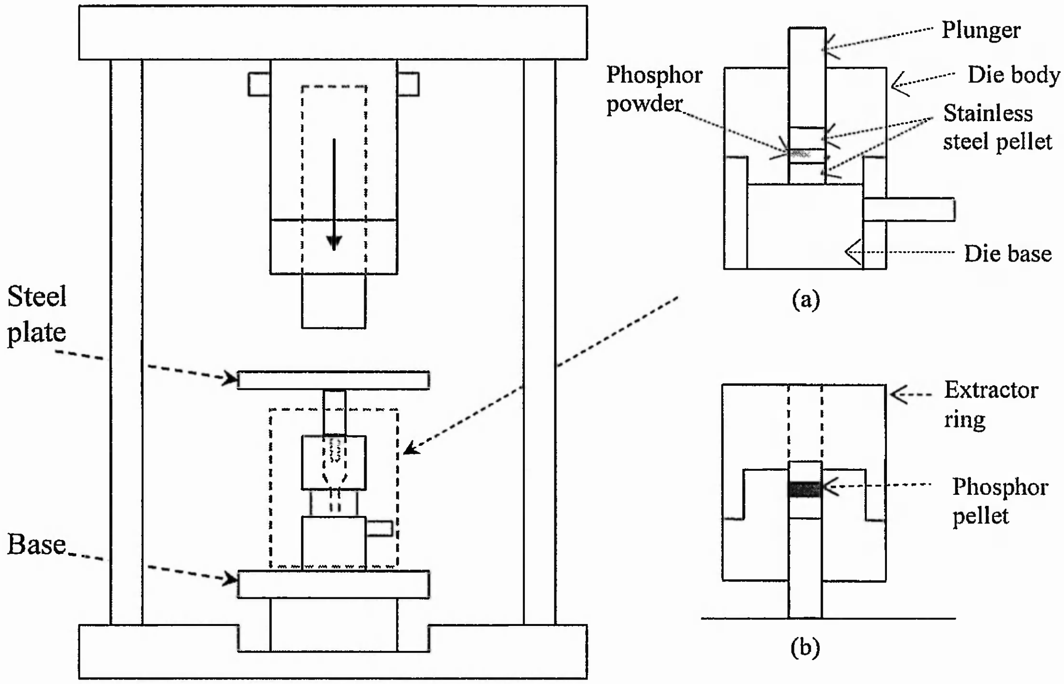

Figure 3-1: Cross-section diagram of the powder press and the pellet die: (a) assembly view of the components and phosphor powder within a die; (b) evacuation of phosphor pellet.

3.2 Controlled temperature environment for phosphor characterisation

3.2.1 Incubator

Temperature dependent measurements were conducted with the sample situated within a high precision cooled incubator (model IPP 200, Memmert). The programmable incubator has an operating temperature range of 5- 60 °C and a setting accuracy of 0.1 °C. The Peltier heating and cooling system is integrated in the rear of the incubator. Measurements of decay time were taken over 5- 60 °C, with the temperature being given sufficient time (approximately ten minutes) to stabilise between measurements.

In order to perform temperature measurements, several requirements were taken into consideration for designing the window of the incubator, such as the window must act as an efficient heat insulator, as well as being able to allow the UV excitation beam to reach the sample and also to allow the luminescence from the sample to be collected. As a result, the original double layered glass door of the incubator was removed as the glass material would absorb the UV radiation. Modification of the glass door to fulfill the requirements can only be custom made by the manufacturer at an expensive cost. The glass door was consequently replaced by a piece of polystyrene. Polystyrene is a cost effective thermoplastic as well as an efficient insulator at low temperatures. The melting point of polystyrene is 240 °C [89] suggesting that it is a suitable replacement for being modified as a window to maintain the temperature within the incubator up to 60 °C.

Three apertures (about 15 mm in diameter) were pierced in the middle of the polystyrene as shown in . The first aperture, named the 'excitation port', allowed the excitation beam to access the incubator and fire onto the sample. The second aperture, the 'collection port', was located in front of the sample holder and this aperture allowed the insertion of a quartz rod (12 mm in diameter and 290 mm in length) into the incubator for collecting and transmitting the emitted luminescence to the photomultiplier tube (PMT). To maximise the signal strength going through to the photomultiplier tube, the collection quartz rod is positioned perpendicular to the emitting surface (4 mm in diameter) and as close as possible – approximately 5 mm away. The use of a quartz rod has overcome the main problem of collecting inadequate luminance of a phosphor from within the furnace using optical lenses. The luminescent signal entering the quartz rod will have angles larger than the total internal reflection angle of quartz and thus prevent losses of light through the walls of the quartz rod[90]. The third hole is a 'spare port' for permitting an alternative excitation path using a light emitting diode (LED). This will be discussed further in Chapter 6.

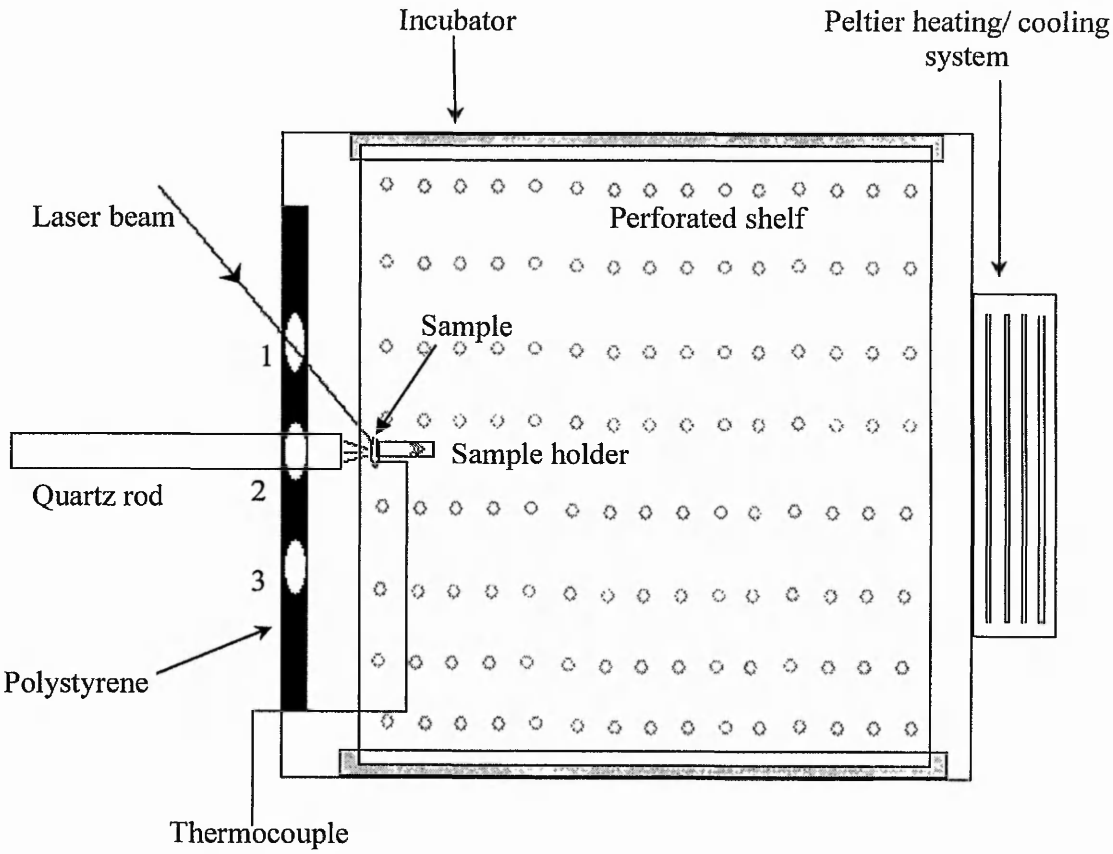

Figure 3-2: Top cross-sectional view of the incubator. Polystyrene is used to insulate the internal heat of the incubator. Aperture 1 in polystyrene is the 'excitation port', aperture 2 is the 'collection port' and aperture 3 is the 'spare port'. With a quartz rod in place, the setup is aligned for decay time measurement. The quartz rod will be replaced by an optical fibre for PL spectra measurement.

3.2.2 Temperature calibration of the controlled temperature environment

When the modified polystyrene was mounted to the incubator, a temperature difference of set value and actual value was expected to be greater than 0.1 ˚C due to probable heat loss or uneven heat distribution in the incubator. To ensure an accurate temperature measurement of the phosphor, its actual temperature was monitored from within the incubator utilising a Type T thermocouple (copper- constantan, suitable for −200 to 350 °C and an accuracy of 0.01 ˚C) and hence the set temperature can be adjusted manually to match the temperature that is of interest. A thermocouple data logger (TC-08, Pico Technology Limited) was plugged into a RS232 connection port on a computer and was used to acquire and record the actual temperature of the phosphor during experimentation.

As part of the calibration process, the actual temperature was monitored over a period of three hours with varying set temperatures and the temperature profiles were subsequently displayed on Picolog Recorder, the data acquisition software. The aim of this exercise was to investigate the repeatability of the temperature control for subsequent analysis. An average of three temperature readings was taken at an interval of five minutes for each set temperature and the temperature difference was calculated as tabulated in Table 3-1. The results showed that the error of measured temperatures was less than 0.5 % over 15 minutes and the average temperature difference was approximately 0.5 ˚C throughout the working temperature range. This has proven that polystyrene is capable of maintaining a fixed temperature within the incubator efficiently and thus providing a reliable and consistent temperature controlled environment for characterisation of phosphors.

Table 3-1: Temperature difference between set temperature and measured temperature.

Set temperature (± 0.1°C)	Measured temperature (± 0.01°C)				Temperature Difference (± 0.01°C)
	Reading 1	Reading 2	Reading 3	Mean	
4.8	5.36	5.27	5.31	5.31	0.51
8.0	8.58	8.44	8.63	8.55	0.55
9.5	9.88	9.90	9.88	9.89	0.39
9.7	9.97	10.00	9.97	9.98	0.28
14.7	14.98	14.80	14.80	14.86	0.16
14.9	14.89	14.94	14.92	14.92	0.02
15.0	15.03	15.05	15.03	15.04	0.04
19.9	20.42	20.31	20.42	20.38	0.48
24.8	25.40	25.35	25.37	25.37	0.57
29.8	30.45	30.43	30.45	30.44	0.64
34.8	35.40	35.42	35.40	35.41	0.61
39.8	40.44	40.47	40.46	40.46	0.66
44.8	45.36	45.40	45.53	45.43	0.63
49.8	50.44	50.46	50.48	50.46	0.66
54.8	55.03	55.01	55.03	55.02	0.22
59.8	59.98	60.00	59.96	59.98	0.18

3.3 Photoluminescent measurement

When excited by an UV pulsed laser, a phosphor will exhibit luminescence at various wavelengths and intensities. The emission wavelengths and their intensity of a given phosphor are dependent on the concentration of the activator. Varying the dopant concentration may induce wavelength shifts and could also result in a reduction or increase in the peak intensity. As a result, it is a standard procedure to characterise the brightness, followed by decay time characterisation of a phosphor as a function of dopant levels.

For PL measurement, a nitrogen pulsed laser (VSL-337ND, $\lambda_{\text{excitation}}$ =337 nm, <4 ns pulse width and a repetition rate of 20 Hz at an average excitation power of 6 mW) was utilised to excite the phosphor within the incubator. The experimental set-up was aligned on an optical bench as illustrated in Figure 3-3.

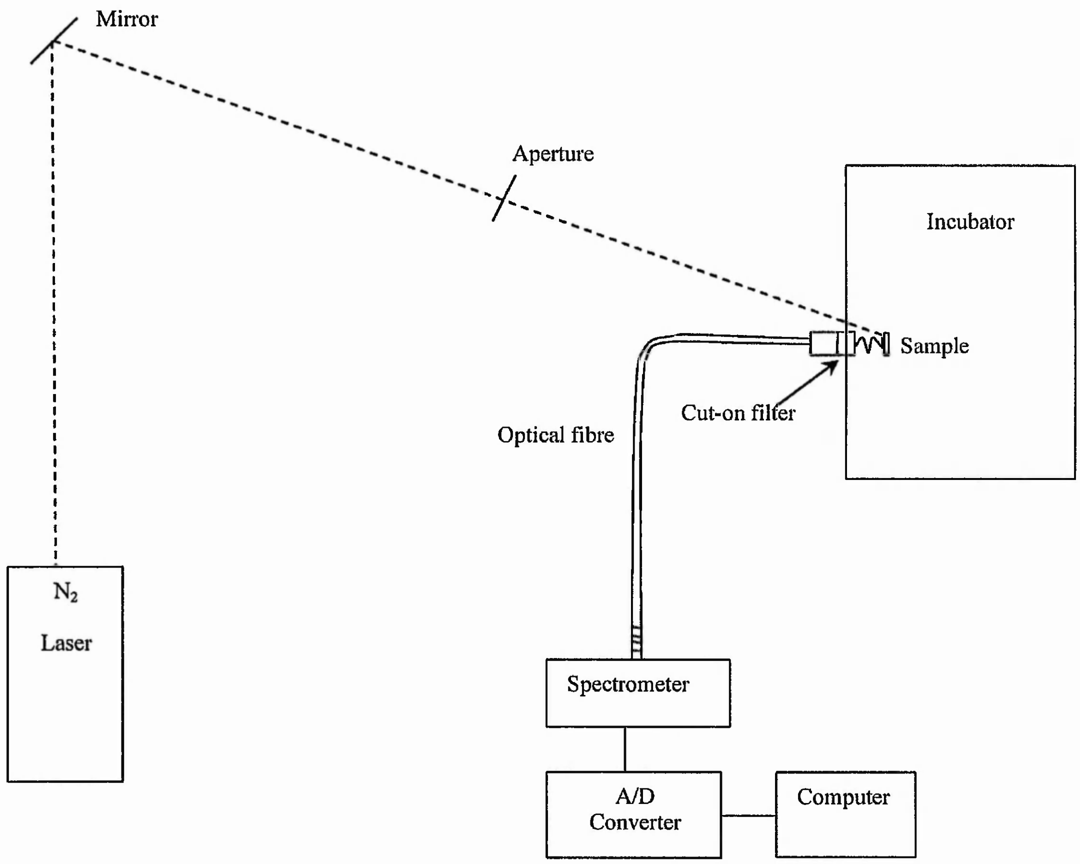

Figure 3-3: Experimental set-up for PL spectral measurement.

The process of the laser beam delivery to the phosphor sample and collection of sample luminescence is as follows. Firstly, the excitation laser beam is fired onto a tilted mirror at 45° which subsequently guides the laser beam through an adjustable aperture. This aperture was set to approximately 4 mm in diameter allowing the reduced beam to match the diameter of the phosphor situated within the incubator. As a result, the laser beam was able to be focused onto the middle of the phosphor pellet, and thus reduce the effect of stray laser beam within the incubator. In addition and for safety precautions, two beam blocks were placed around the sample to prevent the diffused laser light scattering within the incubator.

The quartz optical fibre (600 μm in core diameter, FC-UV600-2) with an UV cut-on filter (wavelength > 380 nm) attached at the collection end was positioned closely to the sample to collect the emitted luminescence. The output end of the optical fibre was coupled into a preconfigured spectrometer (S2000, Ocean Optics Inc. (OOI)) which is responsive from 332. 3 – 1009.57 nm with 1 nm full width at half maximum (FWHM) optical resolution. The spectrometer accepts and disperses the transmitted light energy via a fixed diffraction grating across a high-sensitivity 2048-element linear charged-couple device (CCD) array detector[91]. The spectrometer was connected to an external analogue-to-digital converter (ADC 1000, OOI) which has 1 MHz sampling frequency for data acquisition within 3 ms.

Lastly, the full emission spectrum was acquired using the OOIBase32 spectrometer operating software and displayed on a computer as represented in Figure 3-4. The parameters of the spectrum acquisition can be altered in the software; for instance the integration time, which is the amount of time the detector captures the incoming photons. The longer the integration time the more intense the peak intensities become due to more photons being captured. On the other hand, the length of the integration time needs reducing for a brighter phosphor to avoid detector saturation.

For comparison purposes, the integration time was constant throughout a full series of emission intensity measurements using different dopant concentrations. An integration time of 300 ms was selected, which enabled both the brightest luminescent signal, without saturating the detector, and the weakest luminescent signal, providing sufficient reading for characterisation, to be captured.

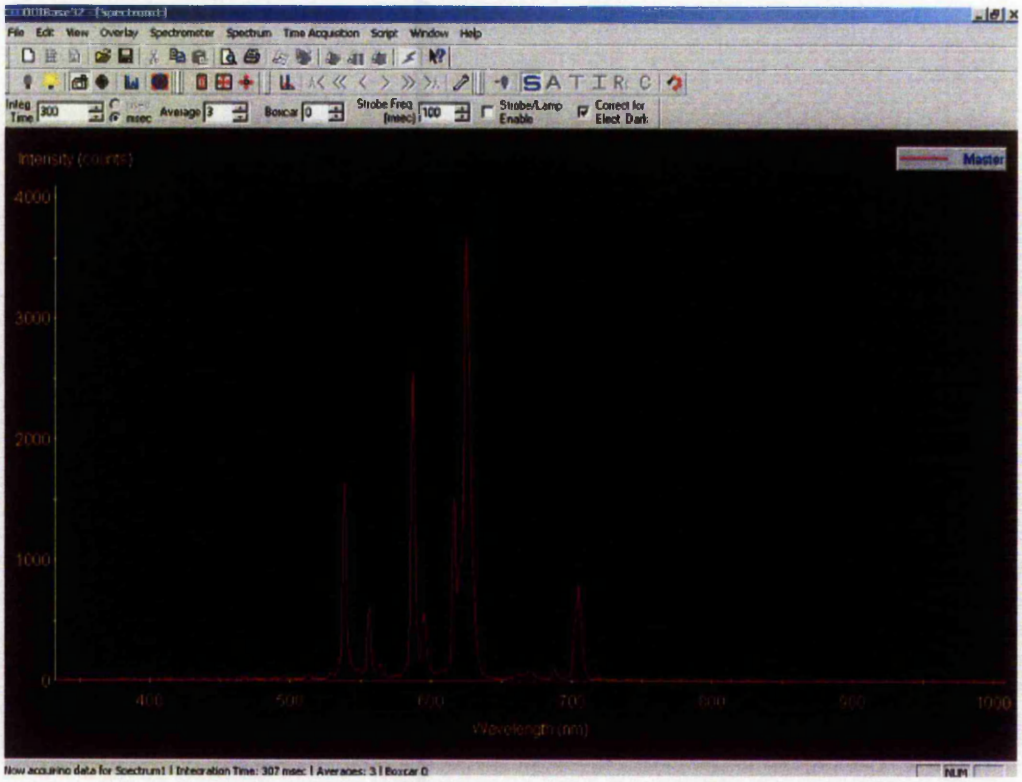

Integ Time 300 ● msec

Average 3

Boxcar 0

Strobe Freq (msec) 100

☐ Strobe/Lamp Enable

☑ Correct for Elect Dark

Now acquiring data for Spectrum1 | Integration Time: 307 msec | Averages: 3 | Boxcar 0

Figure 3-4: Acquisition of emission spectrum of La_2O_2S: Eu.

In order to ensure repeatability of the experiments, a calibrated tungsten halogen light source (LS-1-CAL, OOI) was used to calibrate the absolute spectral response of the complete PL system consisting of the spectrometer and the optical fibre. The calibrated data is represented in Figure 3-5. It is important to note that an excellent match between the calculated data (dashed lines) and the known light source spectral response (crosses) was achieved over the wavelength range of 300 -1000 nm.

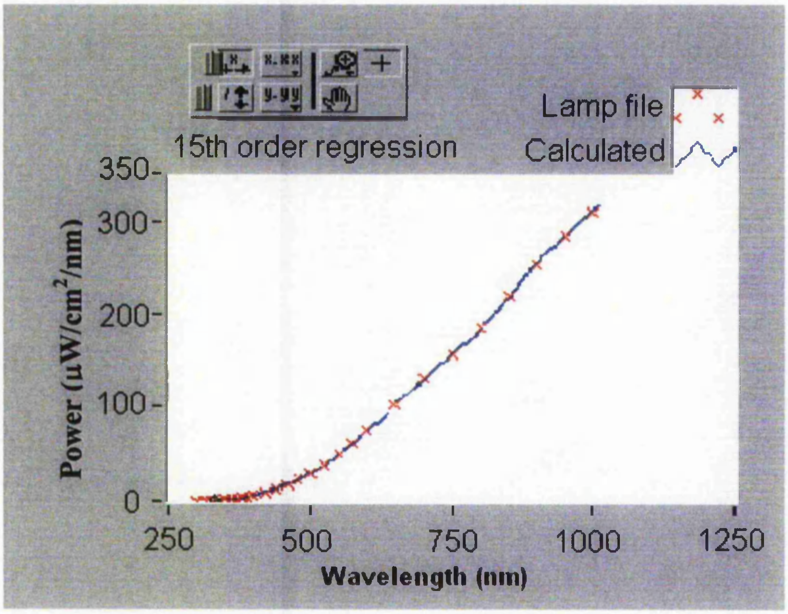

Figure 3-5: Calibration output for the spectrometer S2000 using an optical fibre (FC-UV600-2) and a calibrated light source. Red cross indicates the light source profile whilst the blue line represents the calculated data.

3.4 Decay time characterisation

In general, a phosphor-based optical temperature measurement system will require the following components:

a) an excitation source

b) a means to guide the energy beam to the sample

c) thermographic phosphor

d) an optical system to collect and convey the luminescence of phosphor illuminated by the excitation energy

e) a detector to measure the luminescence signal

f) a data acquisition system that analyse and calculate the temperature of sample

The primary components of the decay constant characterisation system were aligned in the marked position on an optical table as illustrated in Figure 3-6.

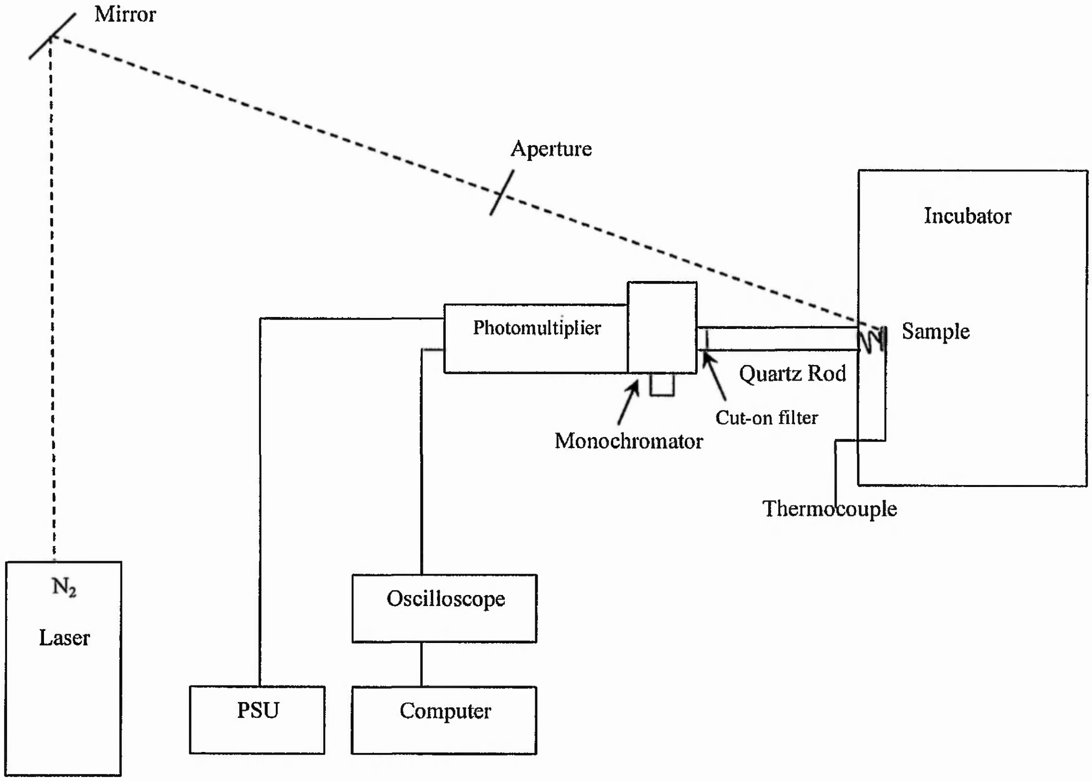

Figure 3-6: Schematic diagram of decay time system.

For decay time measurements, the same nitrogen pulsed laser mentioned earlier was utilised to excite the phosphor within the incubator. A calibrated T-type thermocouple was attached at the back of the sample and the temperatures over time were displayed and recorded using the Picolog software. The emitted luminescence was collected by an optical quartz rod (12 mm in diameter, 290 mm in length). This was positioned perpendicular to the emitting surface in order to maximise the collection of emitted light, which was subsequently passed through a cut-on filter (wavelength > 380 nm) attached to the entrance slit (300 μm) of a monochromator (DMC1-03, Optometrics LLC.). The manually operated monochromator utilises a digital counter for wavelength selection with a readout of 1 nm per division. By rotating the dial via a precise lead screw mechanism, the diffraction grating will rotate, thus positioning the selected wavelength at the exit slit.

The monochromator transmits the selected wavelength of the luminescence to a photomultiplier tube (PMT model 9558 QB, Electrons Tube) that serves as the detector to convert the light into a current output. PMTs are made from a glass vacuum tube which consists of a photocathode, several dynodes and an anode[92]. The photocathode is a negatively charged electrode which is present at the entry window of the PMT. It absorbs the incident photons which have sufficient energy to be ejected as photoelectrons from the surface of the material as a consequence of the photoelectric effect[92, 93]. These photoelectrons are subsequently directed by the focusing electrode towards the positively charged electron multiplier, known as dynodes, where the electrons are multiplied by the process of secondary emission[94]. As the photoelectrons are accelerated by the electric field towards the first dynode, more secondary electrons are emitted and these electrons in turn are accelerated towards the second dynode. This secondary electron emission is repeated at each of the successive dynodes. The electrons emitted from the last dynode are collected by the anode which outputs the electron current to an external circuit. A high voltage power supply is used to operate the PMT and the gain is divided and distributed to each dynode via a voltage-divider circuit. A voltage of 1.1 kilovolts (kV) was supplied to 9558 QB PMT in order to attain the maximum gain and hence sensitivity to low PL emission.

A waveform processing oscilloscope with a 100 MHz bandwidth and a sampling rate of 400 ms^{-1} (DSO 4072, Gould) was used to display, digitise and store the decay data for subsequent analysis. The oscilloscope was set up to average the signals received over a period of approximately 1 minute in order to enhance the signal-to-noise ratio. This equates to an average of 1200 luminescent decay signals. Optimisation of the decay time output signal on the oscilloscope can be made by altering the scale of the vertical trace (volts per division) and/ or the horizontal trace also known as time base control (seconds per division), as well as by adjusting the trigger level to meet a certain threshold condition to display an accurate output signal.

Subsequently, the optimised decay curve was transferred to the computer via Labview software[3], as shown in Figure 3-7. The initial sharp rise in the emission is due to the dominating excitation pulse. For comparison purposes, the decay constant was always calculated from the same time domain (3-5 μs after the 4 ns laser excitation pulse) with the standard form of the single exponential equation as derived in Equation 2-5 using a unique curve-fitting and data modeling software TableCurve 2D v5.01. The goodness of fit of a decay profile was determined by a coefficient of determination (r2) value.

The repeatability of decay constant measurements was carried out using five independent pellets of La_2O_2S: Eu and La_2O_2S: Tb over 10-50 °C. Each pellet was labelled P1– P5 ('P' = pellet) respectively. The pellets were investigated in turn: i.e. the first pellet was replaced by another pellet after a series of decay constant experiments being performed. The repeatability results showed that the accuracy of the decay constants for both phosphors is approximately ± 5% within the temperature range of interest.

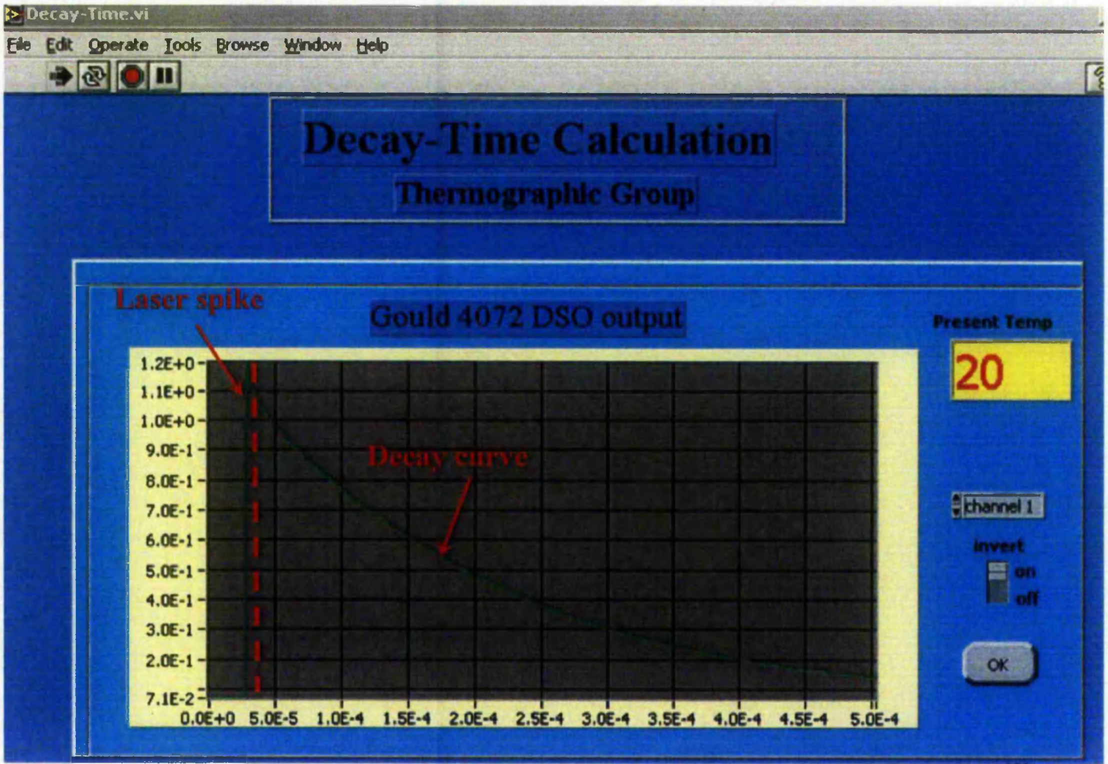

Figure 3-7: Decay constant transferred from oscilloscope using LabView[3] programme.

3.5 X-ray Diffraction

X-ray diffraction is a nondestructive technique to identify crystalline phases and orientation of a single crystal or polycrystalline material. The electromagnetic radiation wavelengths used in XRD are between approximately 0.1 Angstroms (Å) and 100 Å which are similar to the distance between atoms in a crystalline material [64] in order to allow crystal structures to diffract X-rays.

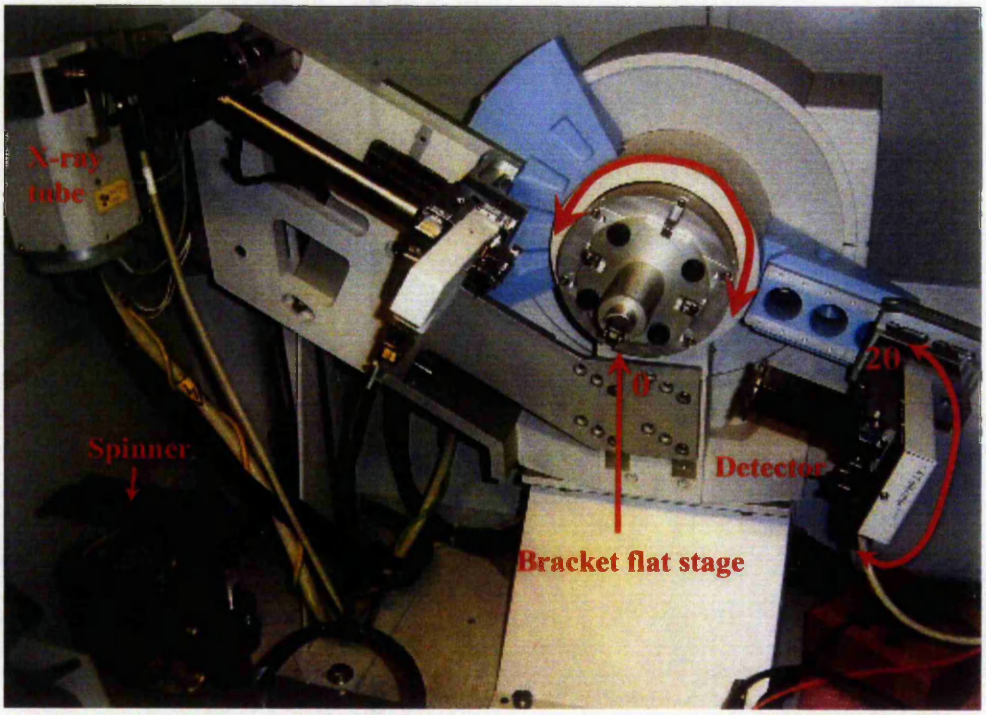

Figure 3-8: PANalytical X'Pert PRO x-ray diffraction system.

Figure 3-8 shows the diffraction system from Phillips, PANalytical X'Pert PRO with a monochromated Cu-$K_{\alpha 1}$ radiation source, $\lambda = 1.54056$ Å. The X-ray beam will pass through a set of divergence slits and reach the sample. The x-ray that is diffracted from the sample will subsequently go through another set of receiving slits, diffracted from the secondary beam monochromator and finally measured by the detector. The sample stage is interchangeable between the automatic multi-sample spinner (up to 15 samples) and the bracket flat stage. The spinner stage with PW 3065 15 position sample changers is used for powder diffractometry while the bracket flat stage is suitable for attaching thin film materials for reflection and transmission applications. All parameters for both stages such as scanning angle and step size are programmable via the software X-Pert Data Collector. Prior to XRD measurements, a number of sample holders (27 mm diameter, 5 mm depth) were used to house different concentrations of powdered phosphors as shown in Figure 3-9 for being held on the spinner for phase identification and quantitative analysis.

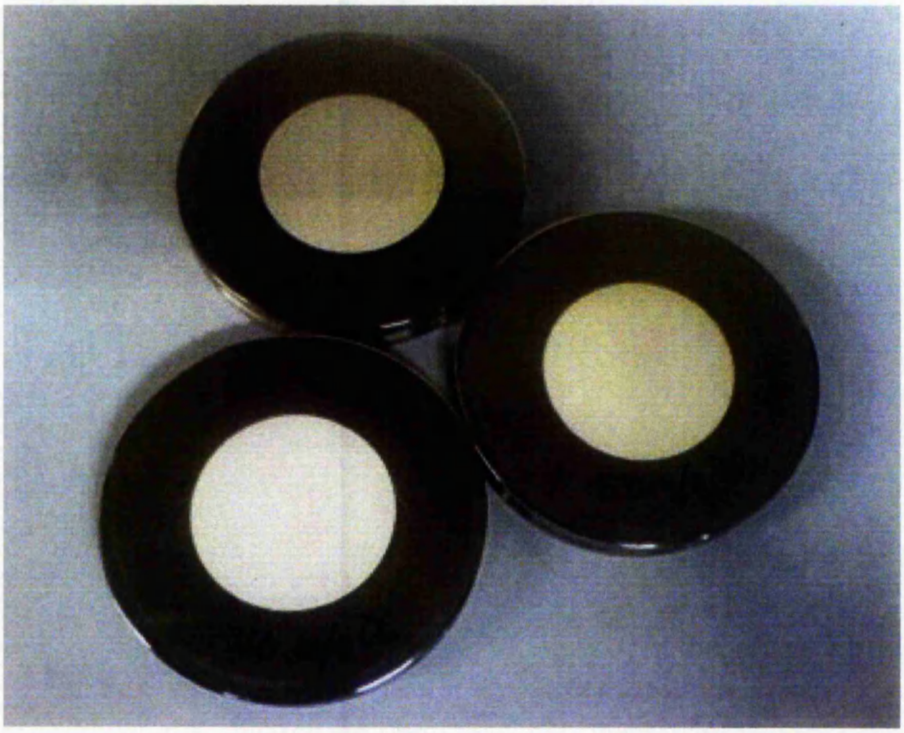

Figure 3-9: Sample holders filled with phosphors to be placed on the spinner for XRD measurements.

These investigated polycrystalline powder phosphors at various dopant concentrations were examined using the XRD system and the operating conditions were, tension = 45 kV and current = 40 mA. To ensure the studied data was self-consistent, XRD measurements for different concentrations of a specific phosphor were carried out on the same day and a Silicon standard was used as a control sample allowing repeatability. Experiments were concentrated on the $25^{o} \leq 2\theta \leq 27^{o}$ Bragg angles consisting of the (100) and (002) reflections which will give the variation in the *c* cell parameter of the unit cell as a function of dopant concentration. The data were collected with 0.008^{o} step size and a count time of 150 seconds per step. During or after each measurement was undertaken, the measured XRD patterns can be displayed individually or combined using the X'Pert

Data Viewer as illustrated in Figure 3-10. This figure illustrates variation of crystallinity due to dopant concentration which will be discussed in detail in Chapter 5. Finally, the XRD formatted files were converted and exported to excel files for further analysis.

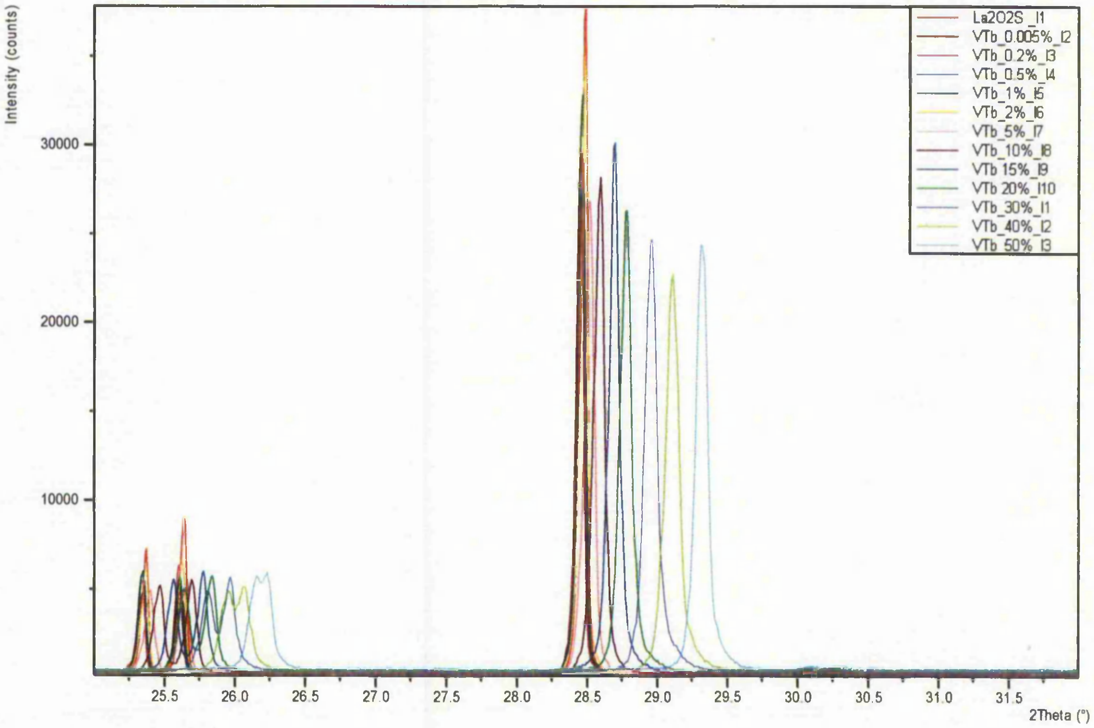

Figure 3-10: XRD patterns of various concentrations of La_2O_2S: Tb acquired by the X-Pert Data Viewer software.

X'Pert HighScore Plus is a comprehensive powder pattern analysis tool for phase identification and crystallographic analysis. For phase identification, each of XRD patterns of La_2O_2S: Tb and La_2O_2S: Eu was profile fitted and smoothed to match the peaks of a reference profile. The auto- residue scoring feature was switched on to allow automatic phase identification and removes similar, multiple phase entries from the candidates list. These match the reference pattern (PDF code: 00-027-0263) of the parent compound La_2O_2S as represented in Figure 3-11. This indicates that the hexagonal crystal structure of La_2O_2S is consistent in the doped materials and its crystal lattice parameters lie within the interval of $3.41 < a < 3.51$Å and $6.79 < c < 6.94$Å (the *a*-axis and *c*-axis of a unit cell[9]).

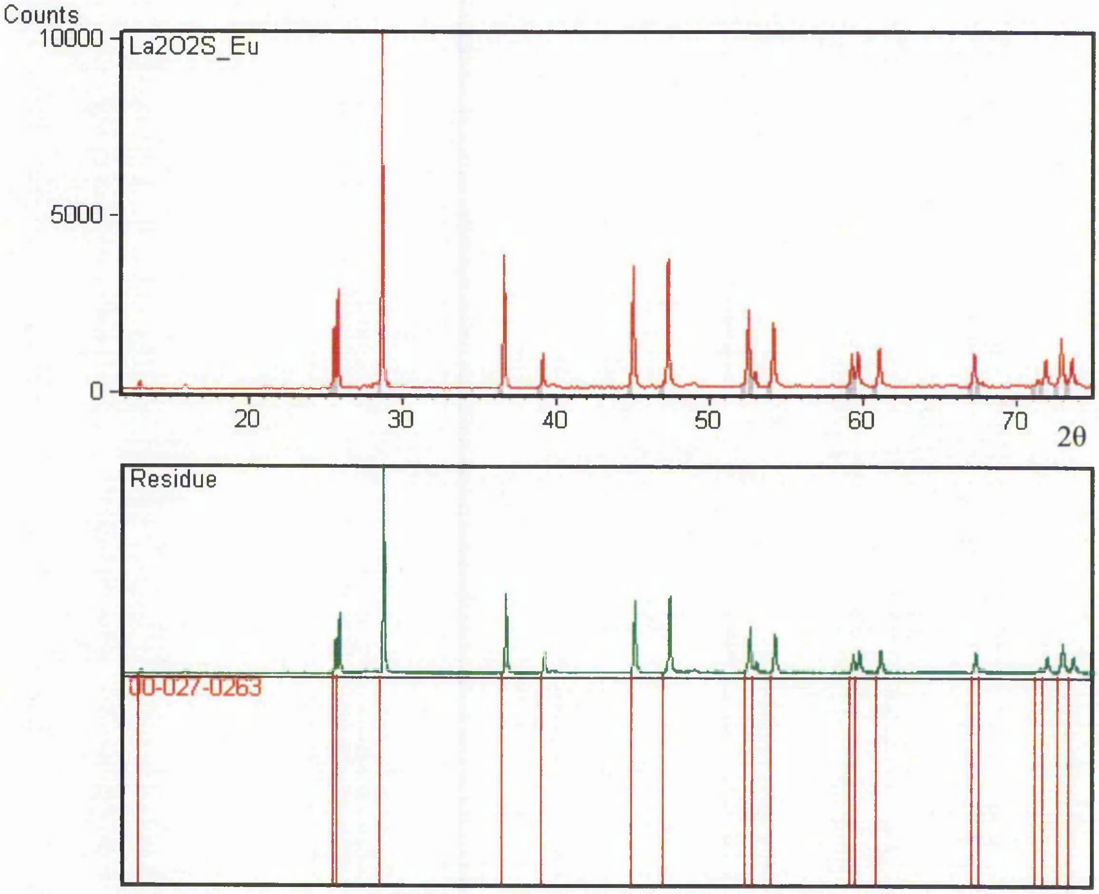

Figure 3-11: Profiles matching for XRD patterns of La_2O_2S: Eu with the reference file (PDF code: 00-027-0263).

The Scherrer calculator in the X'Pert HighScore Plus is used to determine crystallite size or lattice strain by comparing the profile width of a standard profile with a sample profile according to the the Debye- Scherrer equation[27, 95]:

$$D = \frac{K\lambda}{(\beta \cos\theta)}$$ Equation 3-1

Where:

D = crystallite size of a material

K= the constant K is the shape factor which is typically close to unity and ranges from 0.8-1.39

λ = wavelength of the incident radiation

β = full width at half maximum height of peak (FWHM)

θ = the position of the maximum diffraction/ 2

Figure 3-13 demonstrates the Scherrer calculator in HighScore Plus software. B indicates the structural broadening of a peak profile in degrees 2θ. The shape factor K is used to correlate the particle size of sub-micrometre crystallites from the measured width of their diffraction curves. The typical value for this dimensionless shape factor is 0.9 but it varies with the actual shape of the crystallite[96]. As soon as sufficient information is present in a row of the table (by inputting the peak positions and width values (FWHM) obtained by peak searching and profile fitting as shown in Figure 3-12), the other items are automatically calculated using Equation 3-1. When the wavelength is changed, new peak positions and either a new crystallite size or a new lattice strain is calculated for all rows with sufficient input.

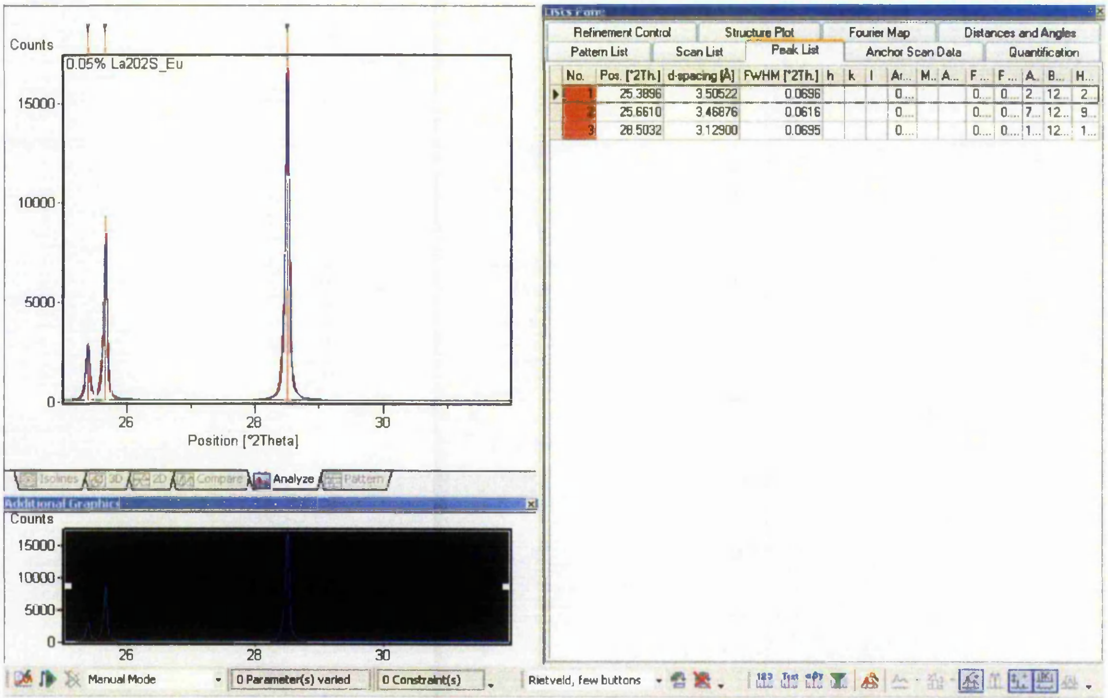

No.	Pos. [°2Th.]	d-spacing [Å]	FWHM [°2Th.]	h	k	l	Ar...	M...	A...	F ...	F ...	A...	B...	H...
1	25.3896	3.50522	0.0696				0...			0...	0...	2...	12...	2...
2	25.6610	3.46876	0.0616				0...			0...	0...	7...	12...	9...
3	28.5032	3.12900	0.0695				0...			0...	0...	1...	12...	1...

Figure 3-12: Peak list of La_2O_2S: Eu generated by the process of peak searching and profile fitting to indicate the position, d-spacing and peak width of the XRD pattern.

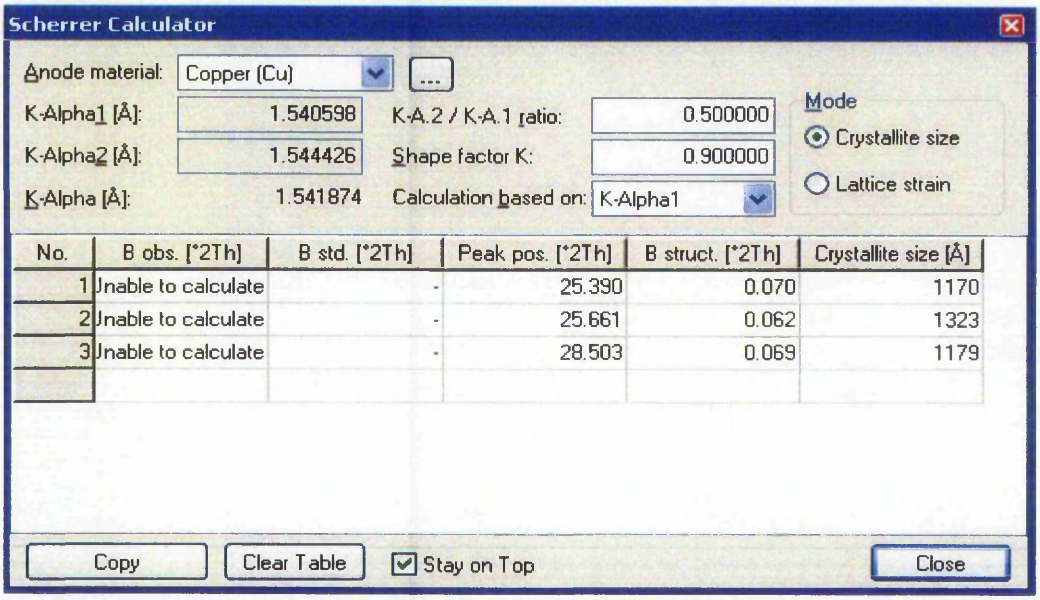

Anode material: Copper (Cu)
K-Alpha1 [Å]: 1.540598
K-Alpha2 [Å]: 1.544426
K-Alpha [Å]: 1.541874
K-A.2 / K-A.1 ratio: 0.500000
Shape factor K: 0.900000
Calculation based on: K-Alpha1
Mode
● Crystallite size
○ Lattice strain

No.	B obs. [°2Th]	B std. [°2Th]	Peak pos. [°2Th]	B struct. [°2Th]	Crystallite size [Å]
1	Jnable to calculate	-	25.390	0.070	1170
2	Jnable to calculate	-	25.661	0.062	1323
3	Jnable to calculate	-	28.503	0.069	1179

☑ Stay on Top

Figure 3-13: Crystallite size of a phosphor can be calculated using the Scherrer calculator with the information provided in the peak list as shown in Figure 3-12.

3.6 Summary

This chapter describes and discusses the experimental procedures that have been designed and developed for characterisations of emission intensity, decay time and crystallinity of a range of powdered phosphors. Both PL and decay time experiments were designed to be carried out within an incubator. Polystyrene was modified in-house to replace the glass door of the incubator for maintaining heat. The temperature calibration data has shown a consistency of 0.5 °C can be achieved and this has proven that polystyrene is an effective insulator particularly for the desired experimental set-up and allowing the decay time measurement to be carried out over the temperature range of 5-60 °C. The phase identification and crystallite size of the phosphors were determined using XRD along with its powerful analysis software packages.

In summary, the experimental set-up has been suitably aligned and calibrated to allow PL and decay time measurements to be carried out. The use of controlled procedures has enabled a repeatability and effective process to be achieved for charaterisations of La_2O_2S: Eu and La_2O_2S: Tb at various dopant concentrations in terms of PL spectra, decay time and XRD.

Chapter 4 Europium doped Lanthanum Oxysulphide

In recent years, rare-earth oxysulphides doped with rare-earth ions have attracted considerable attention, in particular europium doped with lanthanum oxysulphide (La_2-O_2S: Eu), as an effective red emitting material for various applications such as cathode ray tube[97]. La_2O_2S doped with trivalent rare earth ions is also an active phosphorescent material that is suitable for lasers, X-ray imaging and photoluminescent thermographic applications [98, 99]. Furthermore, the increased use of La_2O_2S: Eu for temperature measurement is mainly due to its sensitivity to temperature and the efficient absorption of ultraviolet radiation. This chapter describes the investigation into the feasibility of using La_2O_2S: Eu for temperature measurements over 5-60 °C. The photoluminescent, decay time and X-ray diffraction results of different dopant concentrations of La_2O_2S: Eu are presented.

4.1 Properties of La_2O_2S: Eu

4.1.1 Crystal structure

La_2O_2S has a hexagonal structure (space group P3*m*l) and the structure is very closely related to the A-type rare-earth oxide structure, with the only difference being that one of the three oxygen sites is occupied by a sulphur atom[87, 100, 101]. The primitive unit cell contains one formula unit of La_2O_2S. The lattice parameters for the structure are $a = b = 4.035$ Å, c (length) = 6.914 Å and the band-gap is 4.6 eV[100]. The structure exhibits alternative stacking of $La_2O_2^{2+}$ layer and a layer of anion group (i.e. S^{2-}) due to the occurrence of sulphur and oxygen atoms at different sites[100-102], as illustrated in Figure

4-1. In this structure, the lanthanum ion is located on the three-fold axis with a triangle of three sulphide ions on one side, a triangle of three oxide ions and one axial oxide ion on the other side[101].

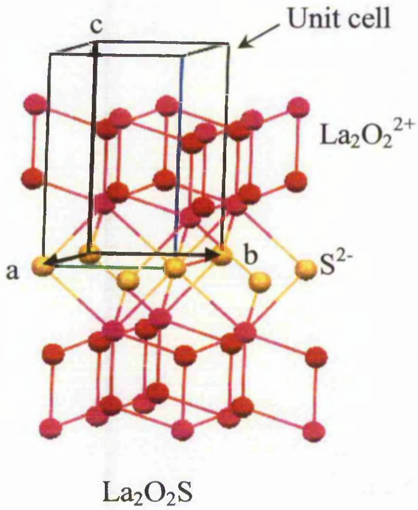

Figure 4-1: Crystal structure of La_2O_2S (O = red, La = magenta, S = yellow). (Courtesy of Dr. Gary B. Hix at NTU)

The valence band, conduction band and energy levels in the La_2O_2S compound are where the electronic transitions at the origin of the absorption properties occur. The conduction band is characterised by the 5d states of La and the splitting of the 5d band is governed by the crystal field[27, 101]. The valence band is characterised by the 3p states of sulphur[101]. However, the nature of electronic transition varies according to the rare-earth.

Figure 4-2 shows the energy levels of the dopant Eu^{3+} ion incorporated into the La_2O_2S lattice. The transitions which occur between the ^5D levels to the ^7F levels of the ground state will exhibit emission lines[103]. The charge transfer state (CTS) of the lattice is labelled La_2O_2S. A complex model for Eu^{3+} ^5D resonance quenching to the charge transfer state in La_2O_2S has been developed successfully by Fonger and Struck[104] to account for the temperature dependence of the emission in the material. For La_2O_2S host, the CTS minima is low enough that excitation in ^5D states can be activated thermally to the CTS. Fonger and Struck showed that the ^5D_J emisions quench sequentially in the order of $^5D_3$, $^5D_2$, $^5D_1$ and $^5D_0$ with increasing temperature. Each ^5D_J level is thermally emptied in its turn to the Franck-Condon CTS via the ^5D_J – CTS crossover, the excitation subsequently occurring in lower ^5D states via lower CTS- ^5D crossovers[33, 104].

In other words, an electron can undergo a ground state transition with no radiative emission when it moves into a charge transfer state. The direct radiative emission line becomes quenched when there are enough transitions undergoing such a path[103, 105]. Therefore as the temperature increases, the excited level such as the $^5D_2$ level increases in energy and eventually 'crosses' the charge transfer line. The temperature dependence of the emission is very prominent near that charge transfer crossing point. In addition, since the lifetime of the radiative transition is directly proportional to the state population, its magnitude drops drastically in the quenching temperature region[106]. The decay time results indicating the temperature dependence of the phosphor emission will be discussed later in this chapter.

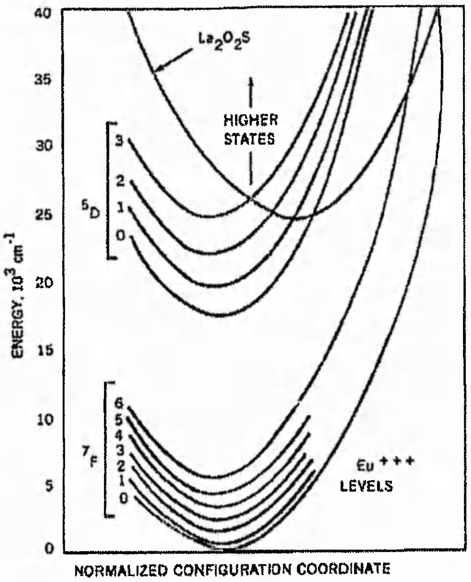

Figure 4-2: Energy levels in Eu^{3+} with the charge transfer state in La_2O_2S[103].

4.1.2 Optical properties of excitation and emission spectra of La_2O_2S

Figure 4-3 illustrates the excitation and emission spectra of La_2O_2S: Eu (SKL63/F-R1) provided by Phosphor Technology Ltd. The excitation spectrum is useful to identify the brightness of respective luminance signals. In addition, the excitation spectrum provides an alternative means of determining the position of absorption features in a phosphor[1]. In practice, the excitation spectrum of a particular phosphor is obtained by monitoring the intensity of an emission peak while the excitation wavelength is varied.

From the given spectrum, it can be seen that the optimum excitation wavelength for the excitation process is 355 nm, and the major emission peak of La_2O_2S: Eu at standard dopant concentration (7.36 m/o) is centred at 625 nm. A pulsed nitrogen (N_2) laser (VSL-337ND) was used as an UV excitation source throughout the research which emits 337 nm with a 4 ns pulse length at a repetition rate of 20 Hz. Although 337 nm is not the most beneficial excitation wavelength for La_2O_2S: Eu but the graph indicates that the excitation wavelength at 337 nm (photon energy = 3.68 eV) is sufficient enough to illuminate the phosphor.

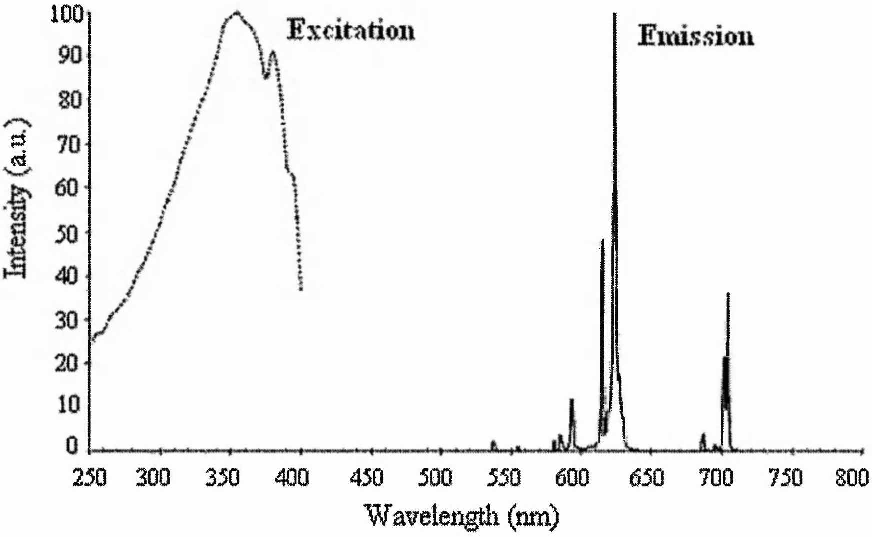

Figure 4-3: Excitation and Emission spectrum of La_2O_2S: Eu provided by Phosphor Technology Ltd (PTL).

4.2 Photoluminescent measurement

La_2O_2S: Eu, when subjected to UV excitation at 337 nm, fluoresces brightly within the visible spectrum in particular the red region. Based on the model developed by Fonger and Struck[104] as previously mentioned, UV excitation into the CTS directly feeds discrete 4f states and gives the visible ^5D_J - ^7F states luminescence characteristic of Eu ion, where J= 0, 1, 2, 3 in the La_2O_2S lattice at room temperature, as shown in Figure 4-4. The resulting luminescence comprises of several sharp emission lines due to the electronic transitions between the discrete levels of the incomplete 4f inner shell of La_2O_2S: Eu. It is worth noting that these peaks are dependent upon both the atomic structure of the rare-earth dopant and the host lattice within which they are sited.

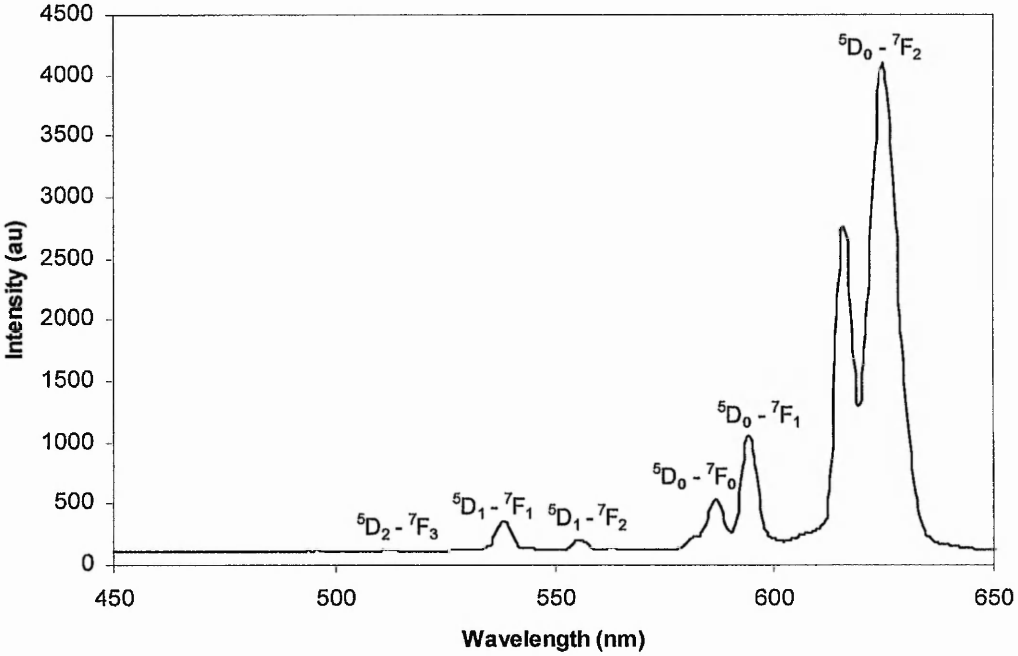

Figure 4-4: Typical emission spectrum for La_2O_2S: Eu excited by a nitrogen laser at room temperature.

During the initial stage of the research, experimental work concentrated primarily on the range near human skin temperature, 26-40 °C[7]. As shown in Figure 4-5, the emission spectra of La_2O_2S: Eu were characterised over the temperature range of interest. Results acquired at NTU indicate that no spectral shift occurs but intensity varies within this narrow temperature range. Repeatability of PL measurement was carried out over a wider range of temperature from 5- 60 °C but no obvious trend is observed for the relationship of emission intensity and temperature. Hence, temperature dependent characterisation of the phosphors has concentrated on the decay time measurement and the appropriate selection of the emission wavelengths is significant for the decay time characterisation. For instance, previous research by Webster et al. [33] has reported that the temperature dependent peaks of La_2O_2S: Eu occur only at 512 nm and 538 nm but other researchers[107] have shown that the temperature dependent characteristics are also found in much lower emission wavelengths such as 467 nm and 495 nm. This will be further discussed in the decay time section in this chapter.

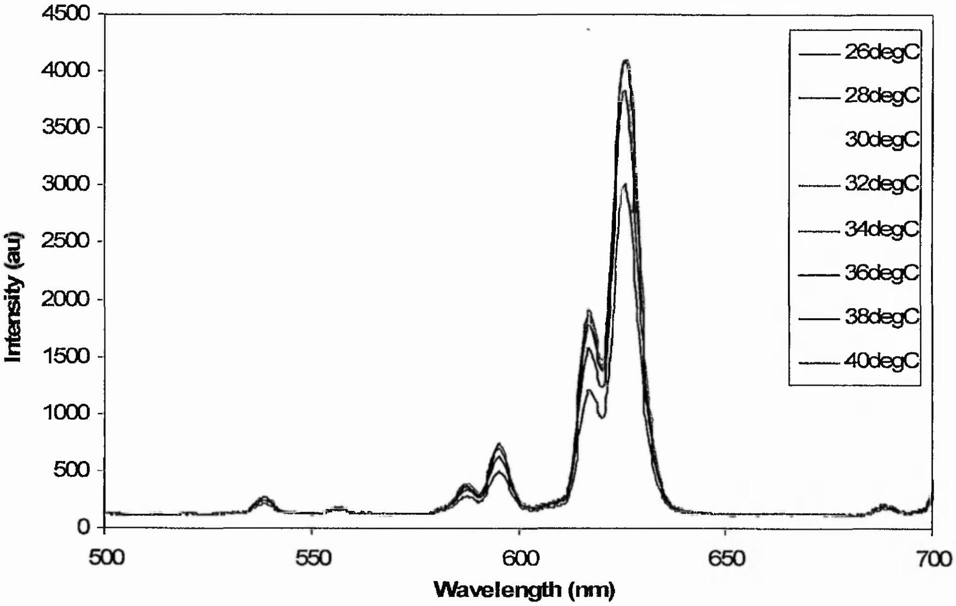

Figure 4-5: Emission spectra of La_2O_2S: Eu excited by a nitrogen laser at various temperatures.

4.2.1 Dopant dependency

The photoluminescence characteristics of a phosphor can be dependent on the concentration of the activating dopant. Generally the intensity, decay time, rise time, relative spectral distribution and response to temperature all are affected to some extent[1].As a result, it is standard practice when characterising the thermal response of a given phosphor to determine its characteristic, primarily brightness, as a function of dopant concentration. The photoluminescent spectra of La_2O_2S: Eu were characterised over a dopant concentration range from 0.1 to 15 m/o, as illustrated in Figure 4-6. It can be seen that the intensities of the phosphors vary with different concentrations, but no wavelength shifts occur.

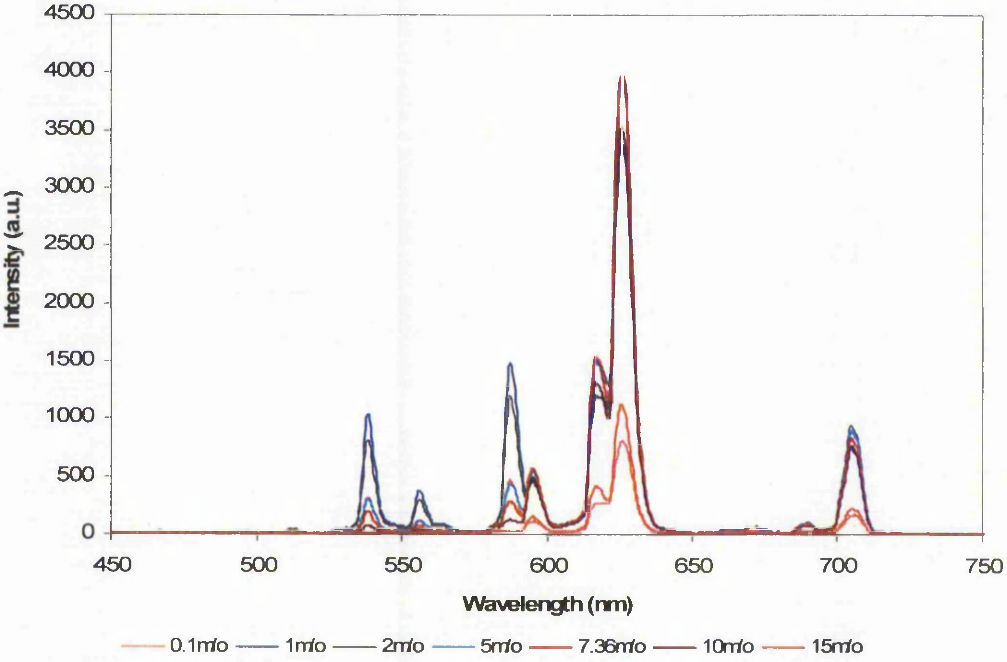

Figure 4-6: Photoluminescent spectra of La_2O_2S: Eu at different dopant concentrations ranging from 0.1 to 15 m/o.

To examine closer the variations of the emission intensities to dopant concentrations, 1 and 7.36 m/o La_2O_2S: Eu were chosen for comparison because 7.36 m/o Eu is the standard dopant concentration provided by PTL, optimised for the brightest luminescence at 625 nm, whilst the lower concentration of 1 m/o Eu has the strongest intensities at shorter wavelengths which are found to be temperature dependent. Their emission spectra are represented in Figure 4-7. Due to the constraint of the spectrometer's resolution and sensitivity, the 467 nm and 495 nm emission wavelengths are only visible in lower concentrations of Eu ($\leq$ 2 m/o) as shown in the inset. These lower emission intensity peaks could be detected at other dopant concentrations via decay time system due to the improved sensitivity of the PMT in comparison with the spectrometer's CCD array.

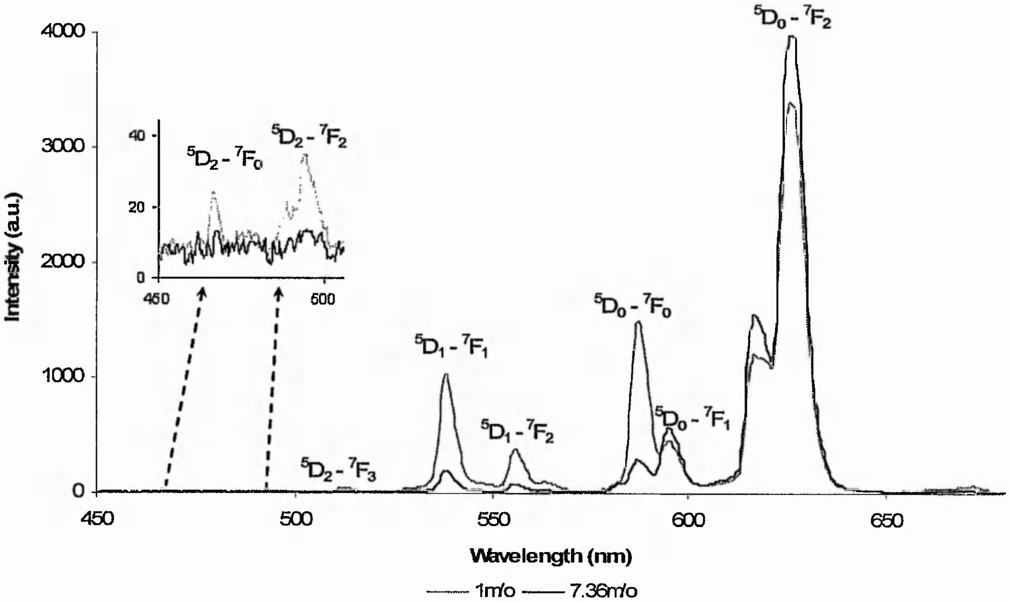

Figure 4-7: Emission spectra of 1 and 7 m/o of La_2O_2S: Eu.

Figure 4-8 illustrates the intensities of the emission peaks vary with various dopant concentrations. Low dopant concentrations of Eu ($\leq$ 2 m/o) appear to have more emission lines especially at the shorter wavelengths, such as 467 nm and 495 nm. In addition, the shorter wavelength lines at low Eu concentrations are far more intense than they are at higher concentrations. The increase in the number of these emission lines in the spectrum is due to the Stark Splitting effect[108] of discrete energy levels between ^5D levels to ^7F levels [103]. It is important to note that these peaks at short wavelengths are temperature dependent and hence they could be used for remote temperature measurements.

Shown in Figure 4-8-Figure 4-9 are the intensity graphs of La_2O_2S: Eu over a number of dopant concentrations. This clearly shows that concentrations of 1-2 m/o of Eu achieving the maximum intensity emission particularly at the temperature dependent peaks and thus they are the optimum concentrations for this phosphor for use within a temperature sensor. A reduction of these emission peaks occurs for 5-15 m/o Eu due to the concentration quenching[109]. The additional Eu ions increase the total concentration of dopant ions so that the optimum brightness is no longer obtained, whereby another non-radiative (heat) de-excitation pathway has become dominant.

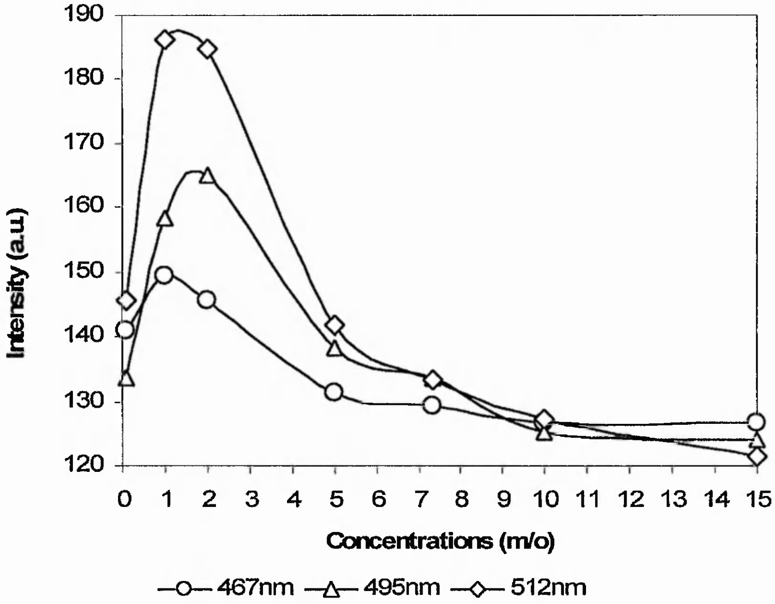

Figure 4-8: Intensity levels of different dopant concentrations of La_2O_2S: Eu at short wavelengths.

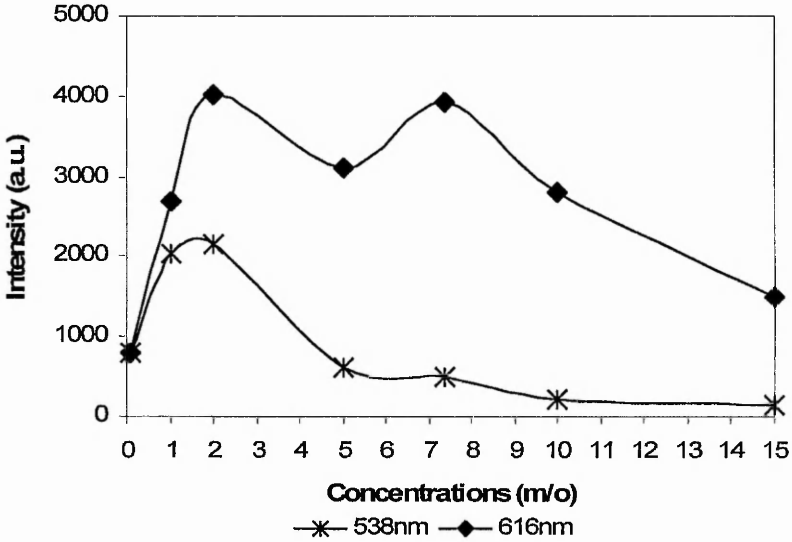

Figure 4-9: Intensity levels of different dopant concentrations of La_2O_2S: Eu at long wavelengths.

These results show the importance of finding the optimum concentration of the interested phosphor to meet the specific needs of the research.

4.3 Decay Time Characterisation

At the preliminary stage of this research, decay constant characterisation was performed over 26-40 °C to investigate the temperature dependent characteristics of the chosen phosphors. As mentioned in Chapter 3, the decay time results presented in this work were deduced according to the single exponential decay relation using Table Curve curve-fitting software and this decay time characteristic has been validated by the linear least squares analysis, as illustrated in Figure 4-10 as an example. It should be noted that a double exponential decay relationship was also fitted but resulted in a less accurate fit (<90% r^2 factor) with both decay constants being within 5% of each other; a clear indication that the single exponential was accurate (r^2> 99.5%).

The results in Figure 4-11 to Figure 4-14 show that low wavelength peaks at 467 nm, 495 nm, 512 nm and 538 nm are temperature dependent whereas the emission peaks at longer wavelengths are insensitive to the temperature range of interest. As a result, further investigation were focused on the temperature dependent peaks over the extended temperature range 5- 60 °C to observe if their decay times would vary strongly enough with temperature over this span to provide a useful means of phosphor thermometry.

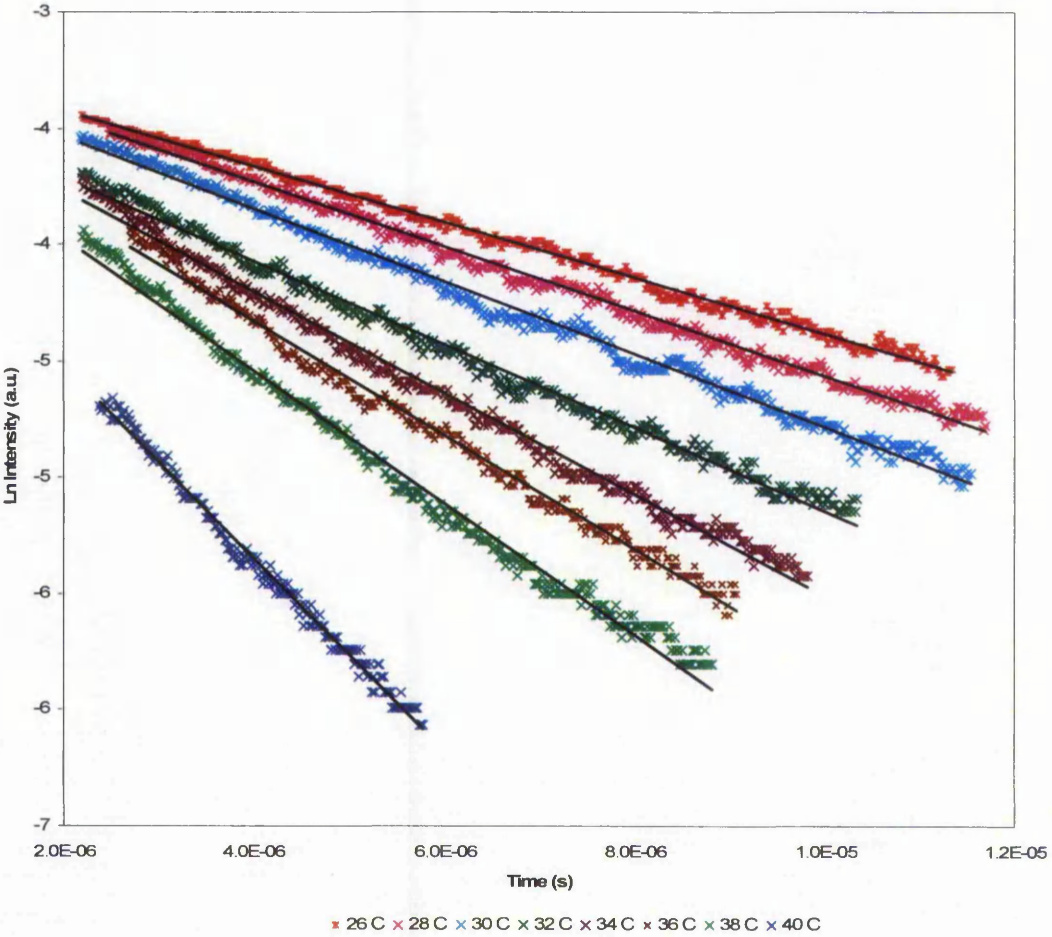

Figure 4-10: Linear least squares analysis of intensity versus time for 7.36 m/o La_2O_2S: Eu at 467 nm.

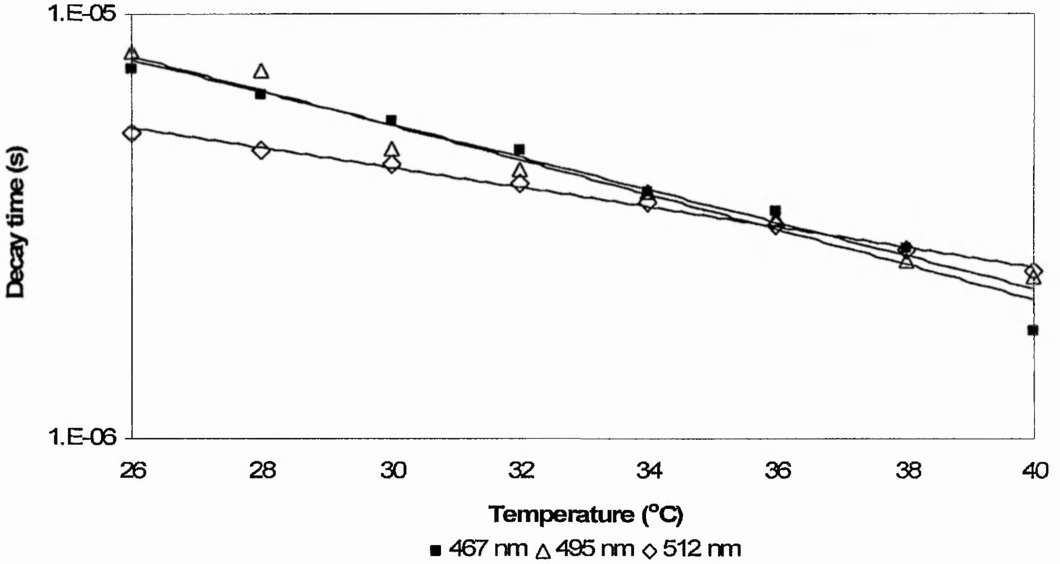

Figure 4-11: Decay constant characteristics of La_2O_2S: Eu at 467 nm, 495 nm and 512 nm.

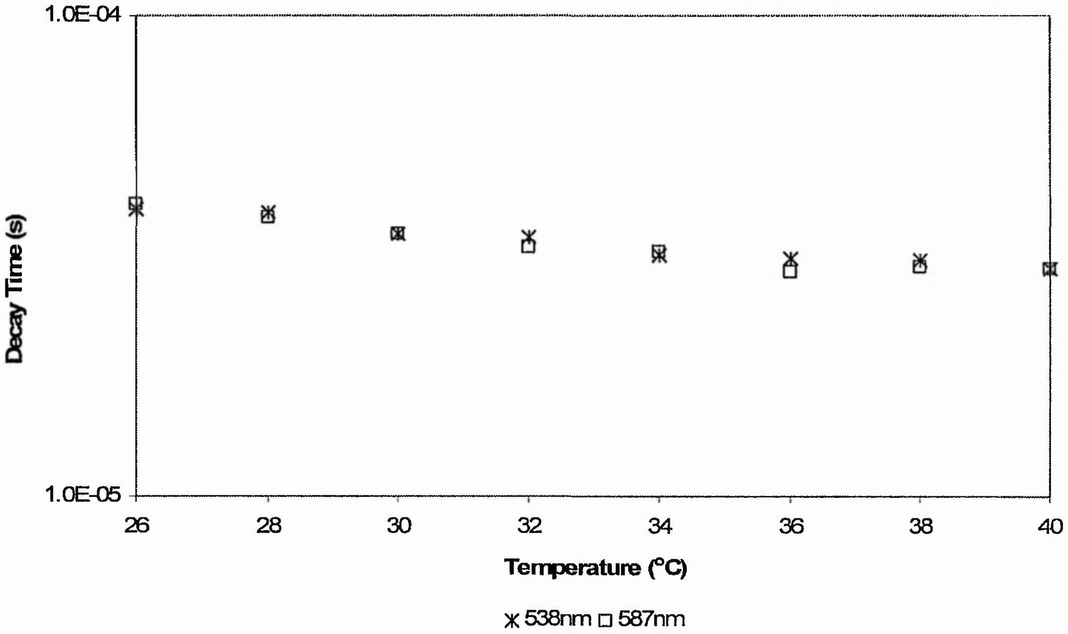

Figure 4-12: Decay constant characteristics of La_2O_2S: Eu at 538nm and 587nm.

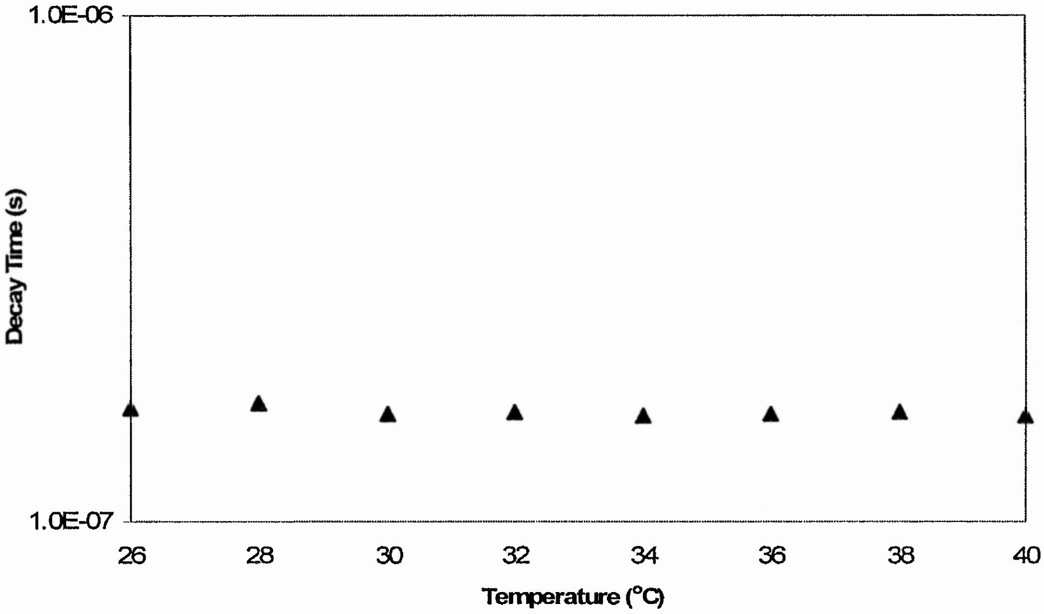

Figure 4-13: Decay constant characteristics of La_2O_2S: Eu at 557nm.

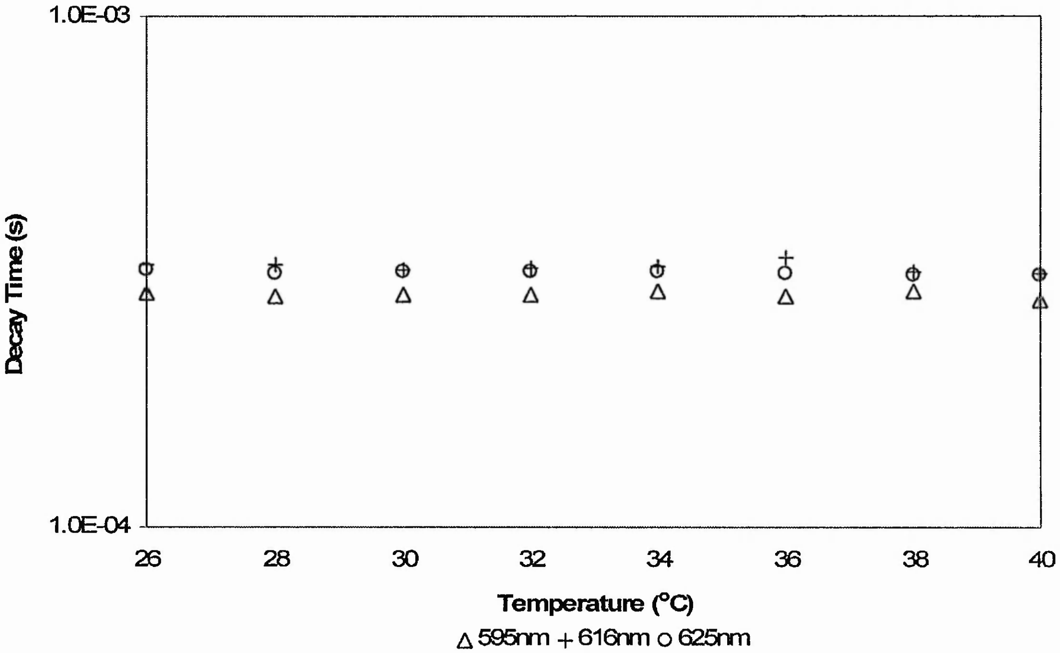

Figure 4-14: Decay constant characteristics of La_2O_2S: Eu at 595nm, 616nm and 625nm.

Following this, the linear least squares analysis of intensity against time for La_2O_2S: Eu at 467 nm has again evident that the decay time characteristic of the phosphor is a single exponential decay as shown in Figure 4-15 and Figure 4-16. A clear indication showing that the phosphor is dependent on the temperature range of interest as well as dopant concentration. Figure 4-17 (a-d) demonstrates the decay time characteristics of La_2O_2S: Eu 0.1-15m/o with a temperature range of 5-60 °C. The decay time characteristics were measured at the temperature dependent wavelengths, i.e. 467 nm, 495 nm, 512 nm and 538 nm. These transitions that occur between the ^5D levels and charge transfer states (CTS) of La_2O_2S: Eu can be described with the model developed by Fonger and Struck [107, 110]. Their analysis suggested the Eu ^5D_J states quench sequentially (J= 3, 2, 1, 0) with increasing temperature. This is because each ^5D state empties thermally via charge transfer. The quenching rates (a measure of the temperature sensitivity of the phosphor – the measurement sensitivity improves with increasing quenching rate) are summarised in Table 4-1.

In addition, another relationship based on the influence of the Eu concentration on the decay time is established. As it can be seen from Figure 4-17, there is a consistent trend indicating the decay time decreases with increasing Eu concentration. The gradient of decay times at lower concentration of 0.1 m/o Eu is greater by an order of magnitude as compared to higher Eu concentration at 15 m/o. This suggests that lower Eu concentrations are more sensitive to temperature variations than that of high Eu concentrations. This again is an indicative of concentration quenching that is associated with the Eu ion interactions leading to non-radiative decay probability increases.

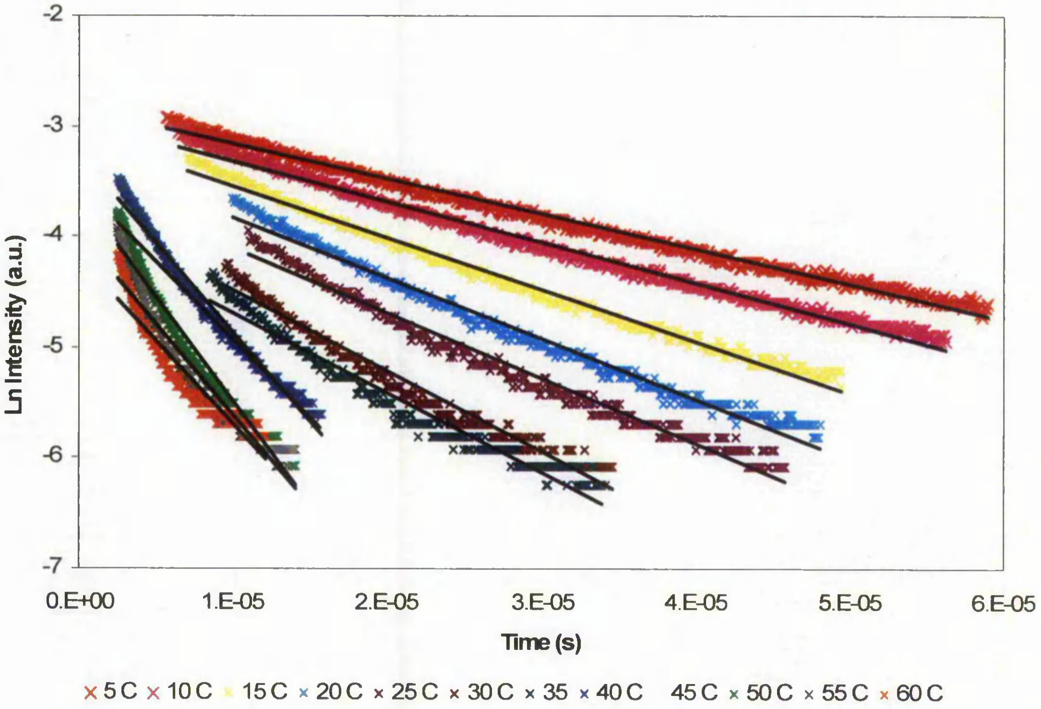

Figure 4-15: Linear least squares analysis of ln intensity versus time for 0.1 m/o La_2O_2S: Eu peaking at 465 nm over 5-60 °C.

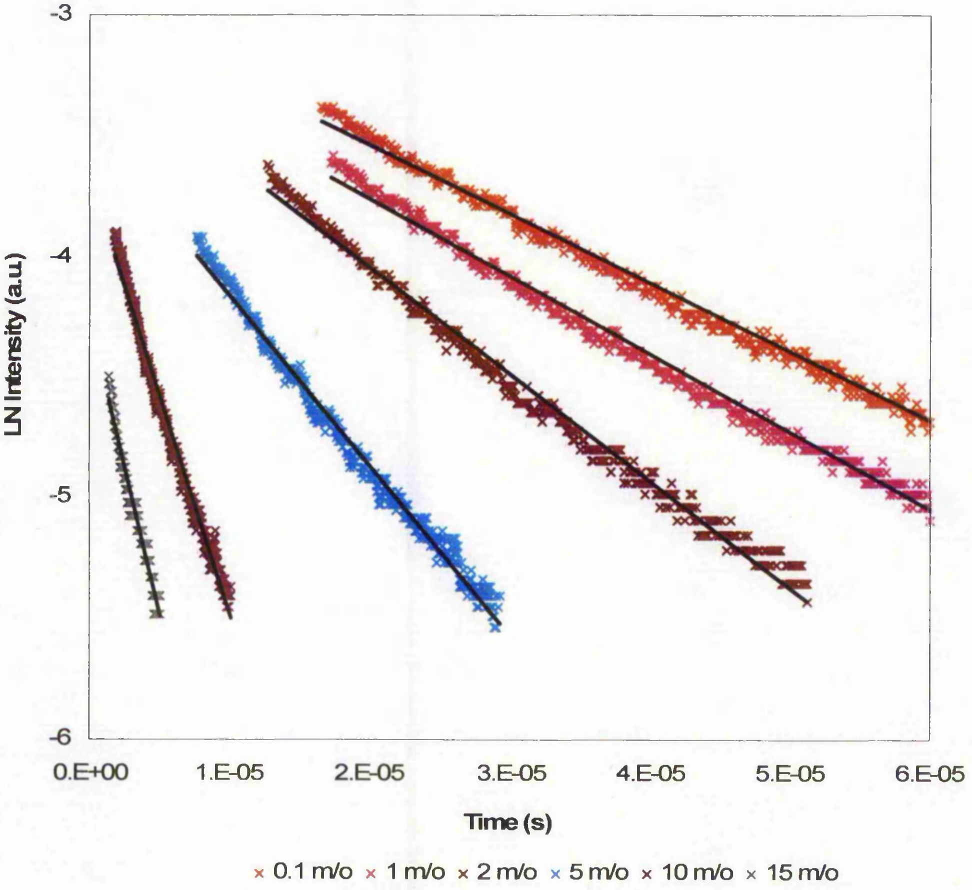

Figure 4-16: Linear least squares analysis of ln intensity versus time for various dopant concentrations of La_2O_2S: Eu peaking at 465 nm at 5 °C.

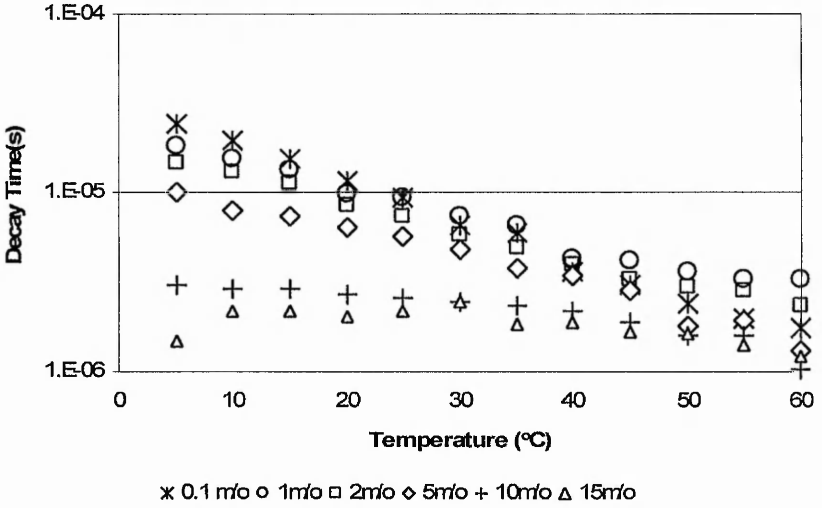

(a) At 465nm, decay time Vs temperature for various dopant concentrations of La_2O_2S: Eu.

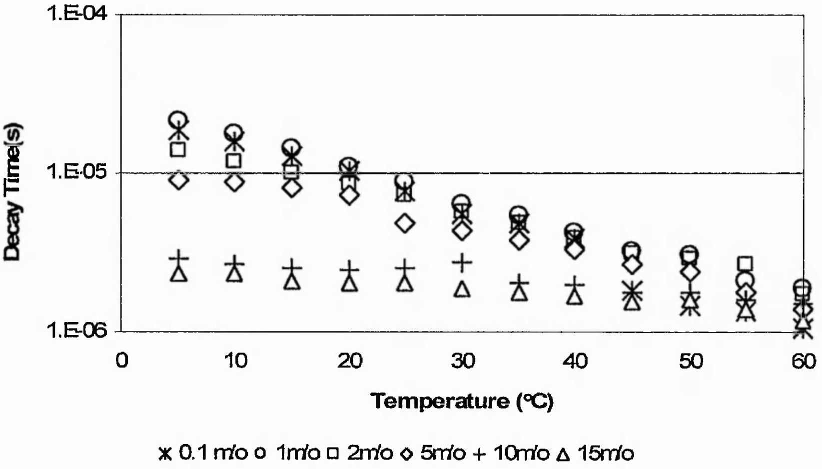

(b) At 495nm, decay time Vs temperature for various dopant concentrations of La_2O_2S: Eu.

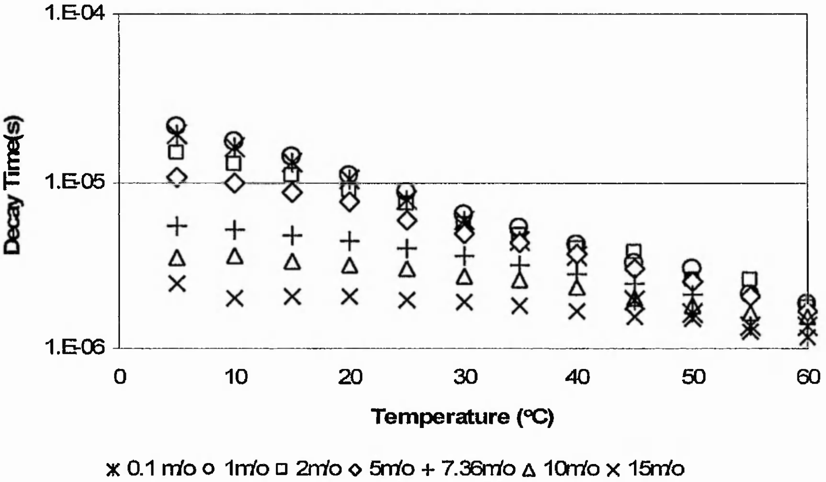

(c) At 512nm, decay time Vs temperature for various dopant concentrations of La_2O_2S: Eu.

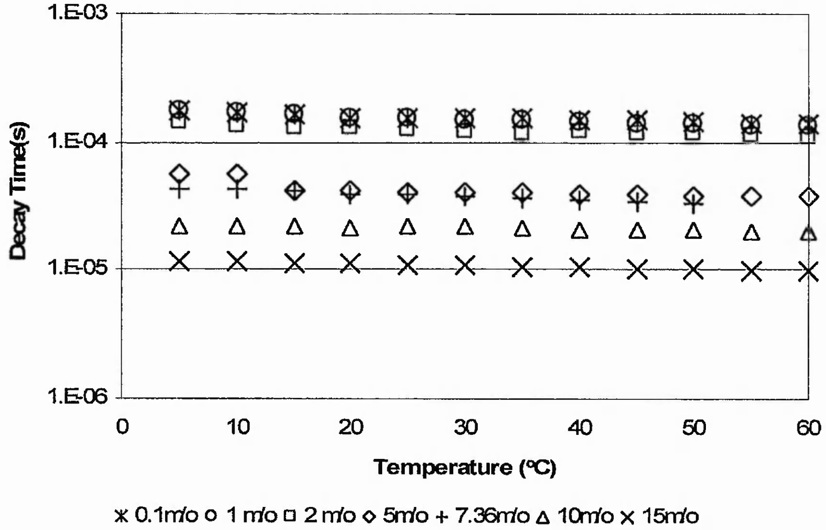

(d) At 538nm, decay time Vs temperature for various dopant concentrations of La_2O_2S: Eu.

Figure 4-17: Decay time of La_2O_2S: Eu as a function of temperature at different emission wavelengths.

Relating back to Equation 2-7, the higher the quenching rate (Q) the better the sensing capability of a phosphor. The data presented in Table 4-1 indicates that 0.1 m/o Eu has the most superior quenching rates of 20.92 $m^{o}C^{-1}$, 24.03 $m^{o}C^{-1}$, 22.23 $m^{o}C^{-1}$ at 467 nm, 495 nm and 512 nm respectedly. There is also a good general trend showing the quenching rates decrease with increasing dopancy levels for these highly temperature sensitive peaks. On the other hand, the 538 nm emission line will be omitted from future analysis due its low quenching rates. Although the emission from 1-2 m/o Eu is more intense but the quenching rates at these two dopancy levels are still weaker than 0.1 m/o. It can be hypothesized that the quenching rates are independent of the brightness of the phosphor. As a result, 0.1 m/o Eu would be the preferred candidate for further investigation.

Table 4-1: Summary of quenching rates for various concentrations of La_2O_2S: Eu.

Emission wavelengths (nm)	Quenching rates ($m^{o}C^{-1}$) of La_2O_2S: Eu								
	0.005 m/o	0.02 m/o	0.05 m/o	0.1 m/o	1 m/o	2 m/o	5 m/o	10 m/o	15 m/o
467	12.50	15.11	19.48	20.92	13.73	14.64	16.16	8.50	4.90
495	14.06	18.73	21.97	24.03	17.10	16.71	14.60	5.28	5.41
512	15.42	18.90	21.51	22.23	19.84	17.08	14.80	6.53	6.02
538	1.76	1.81	4.16	1.77	2.27	2.00	3.12	0.85	1.36

Since the decay time results have indicated that 0.1 m/o La_2O_2S: Eu is the most sensitive phosphor to temperature variance due to its average high quenching rate ~22 mC^{-1} and hence a couple of phosphors at even lower dopant concentrations, i.e. 0.005, 0.02, 0.05 m/o have been characterised to explore whether the decay time trend will continue. Above 0.1 m/o, there is an apparent trend showing that the decay time decreases with increasing dopant concentration whereas the results of concentrations lower than 0.1 m/o do not follow the expected trend. This may be due to the weak emission intensities of 0.005, 0.02, 0.05 m/o Eu at low wavelengths, as shown in Figure 4-18 and Figure 4-19, resulting in a reduction of signal-to- noise ratio and hence problematic for deducing the decay time. However, all these phosphors show temperature dependency but no apparent trend is observed between the decay time and dopant concentration for such a low range of Eu concentration. For comparison purposes, the decay times of the temperature dependent lines of 0.005, 0.02, 0.05 m/o Eu are illustrated in Figure 4-20.

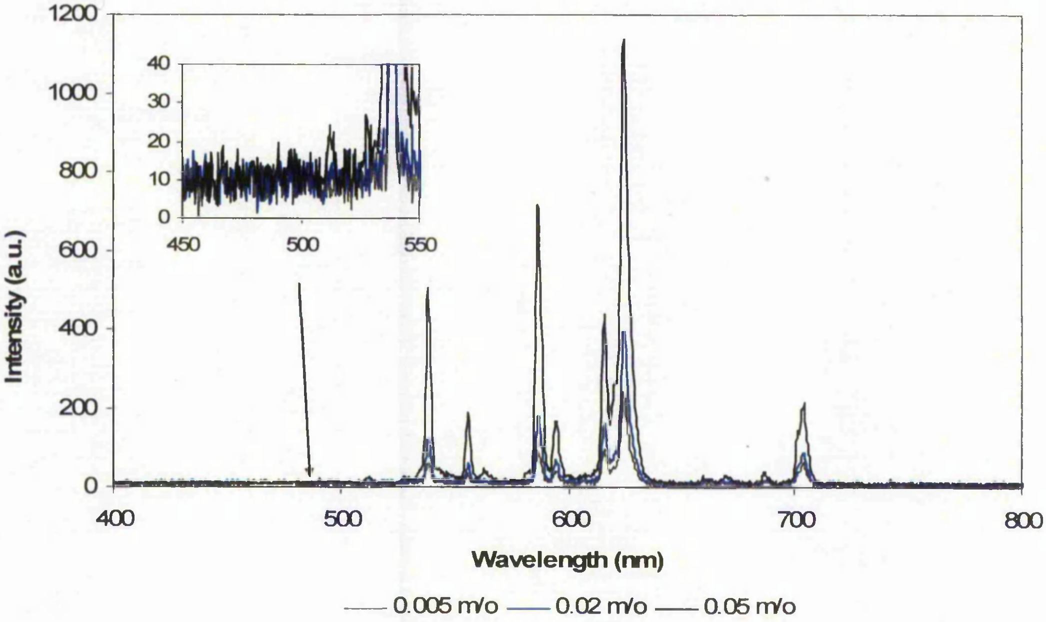

Figure 4-18: Emission spectra of 0.005, 0.02, 0.05 m/o La_2O_2S: Eu under 337nm excitation at room temperature.

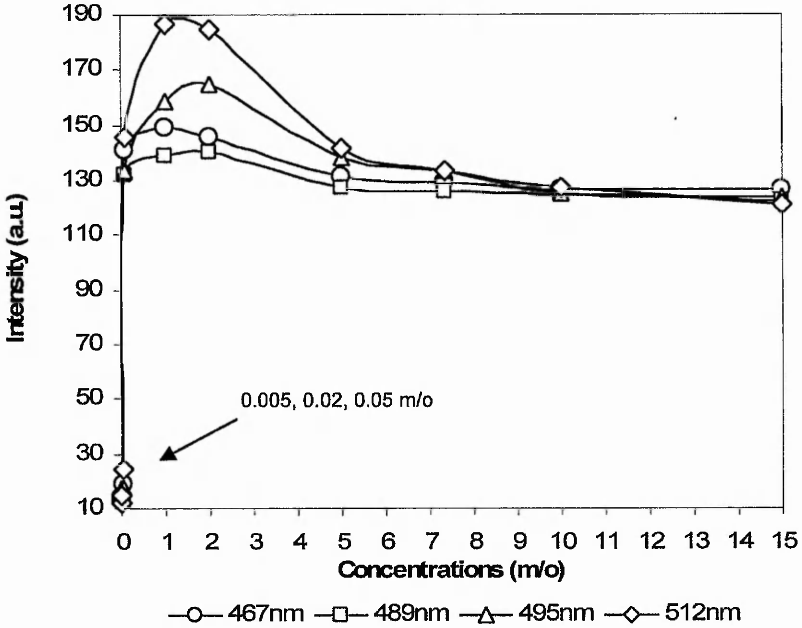

Figure 4-19: Emission intensities against various dopant concentrations of La_2O_2S: Eu.

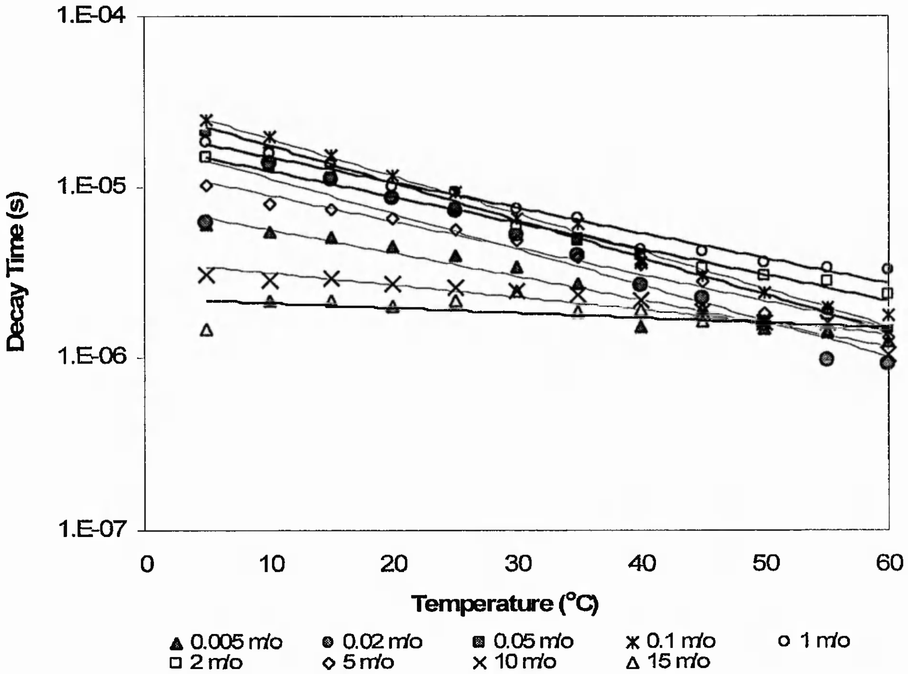

(a) La_2O_2S: Eu at 467 nm.

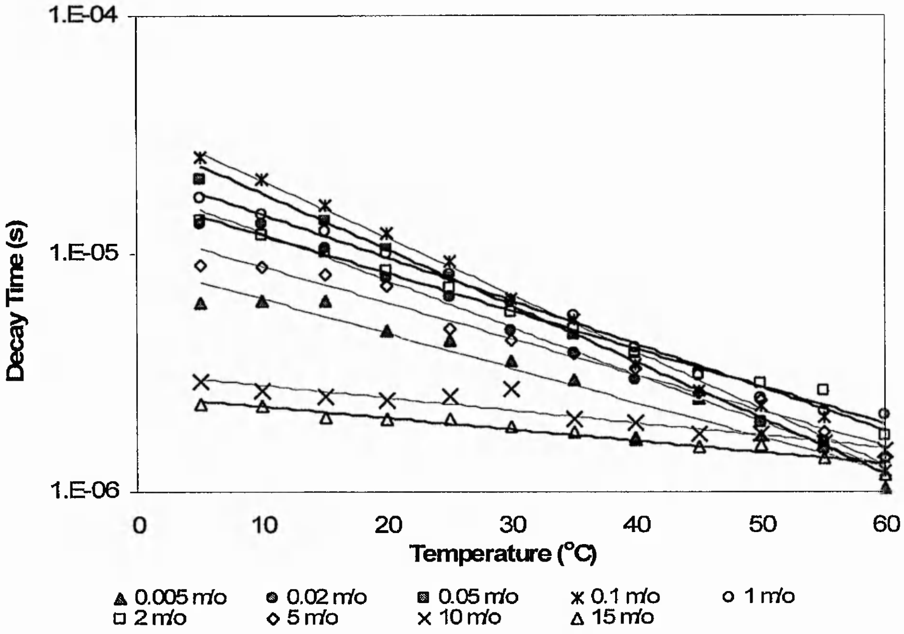

(b) La_2O_2S: Eu at 495 nm.

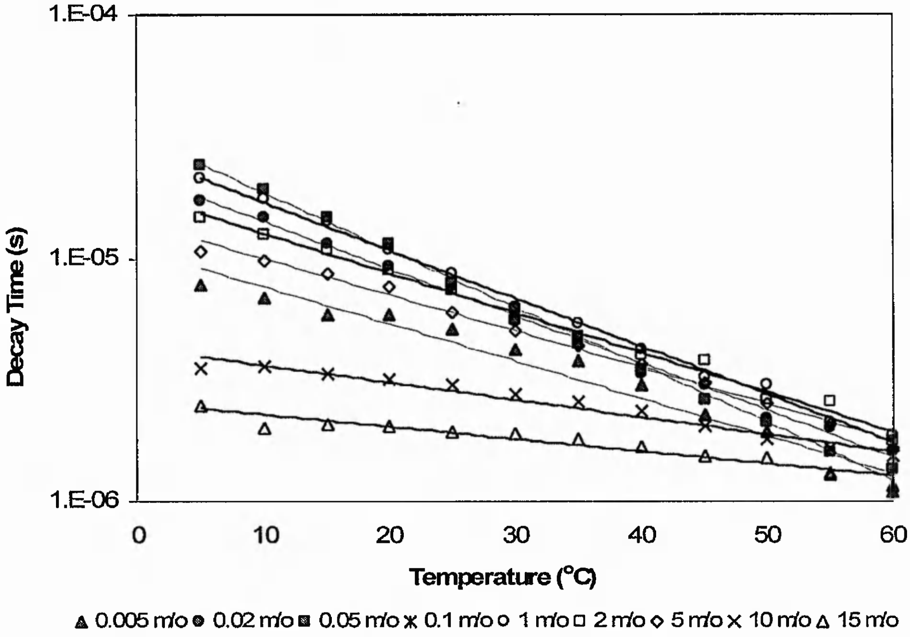

(c) La_2O_2S: Eu at 512 nm.

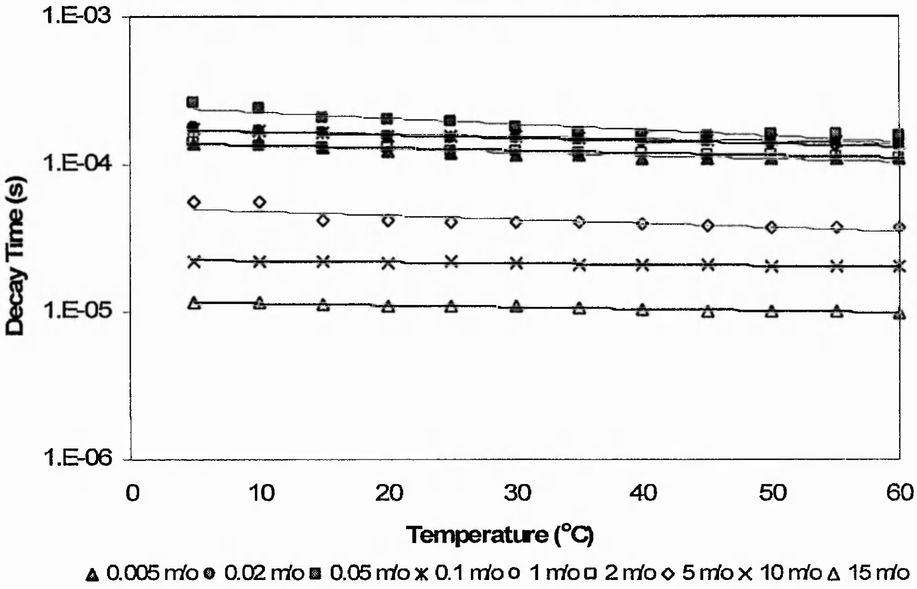

(d) La_2O_2S: Eu at 538 nm.

Figure 4-20: Decay time characteristics of various dopant concentrations of La_2O_2S: Eu as a function of temperature at different wavelengths.

Repeatability of the decay constant measurements is a crucial factor since reproduction of exhibiting similar characteristics is greatly desired. Hence, five different La_2O_2S: Eu pellets were labelled P1, P2, P3, P4 and P5 for comparison purposes. Each pellet sample showed good consistency at every temperature data point with a small standard deviation less than 5 %. The results are summarised in Figure 4-21. In practice, decay constant measurements appear to be a preferred and a more reliable method for temperature characterisation due to its insensitivity to ambient light.

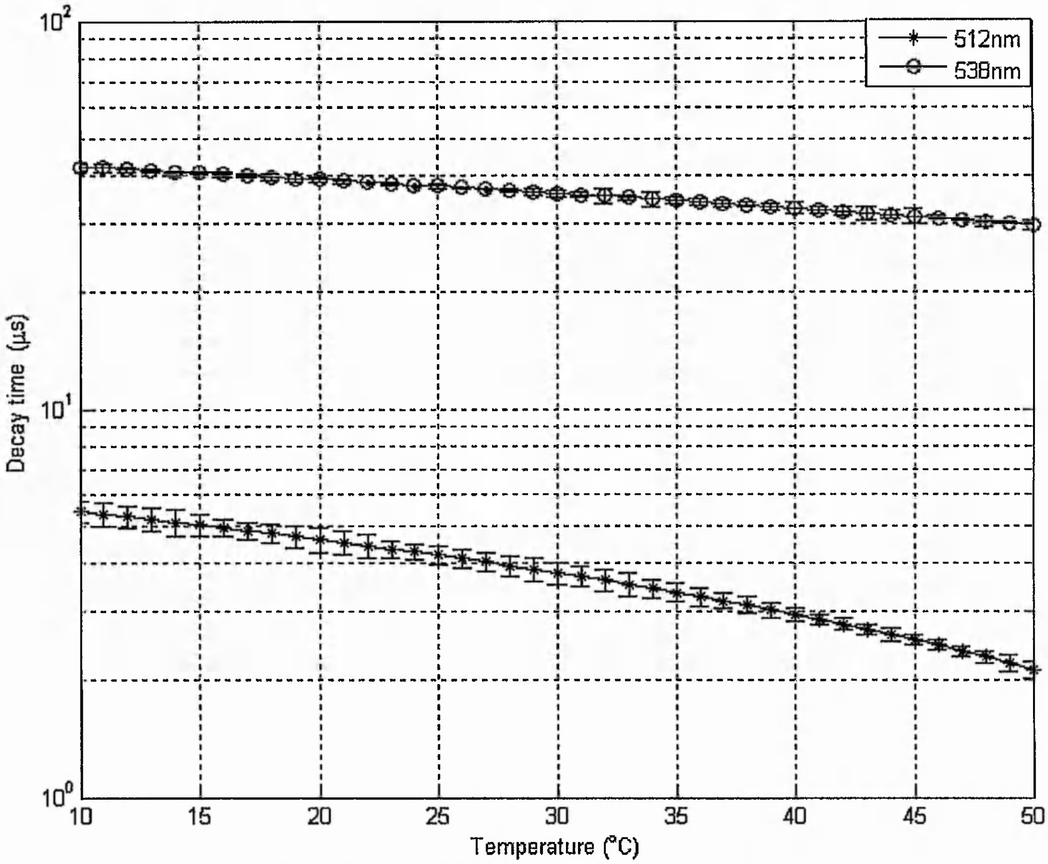

Figure 4-21: A summary of decay time characteristics of La_2O_2S: Eu (repeatability using five different pellets).

4.3.1 X-Ray Diffraction (XRD)

The XRD experiments were performed using Philips X'Pert Pro with monochromated Cu Kα radiation (45kV, 40mA operating mode). Data were collected with 0.008° step size and integration time of 150 s and subsequently stored in computer utilising X-Pert Data Collector.

XRD patterns of La_2O_2S: Eu over the diffraction angles of $5° \leq 2\theta \leq 55°$ are shown in Figure 4-22. These match the reference pattern (PDF code: 00-027-0263) of the parent compound La_2O_2S. This indicates that the hexagonal crystal structure of La_2O_2S is consistent in the doped materials and its crystal lattice parameters lie within the interval of $3.41 < a < 3.51$ Å and $6.79 < c < 6.94$ Å (the *a*-axis and *c*-axis of a unit cell[111]). However, a comprehensive series of experiments required approximately two days to be completed and this had caused spectra variations in the data due to the monochromator changes slightly with temperature. In order to accurately compare the samples, a control sample – Silicon standard needs to be run before and after each batch of samples and then correct the 2 theta position as necessary to compensate for temperature shifts in the analysis. Therefore, the scanning angles were reduced to $25° \leq 2\theta \leq 32°$ and the experiment was performed on the same day to ensure the data to be self consistent.

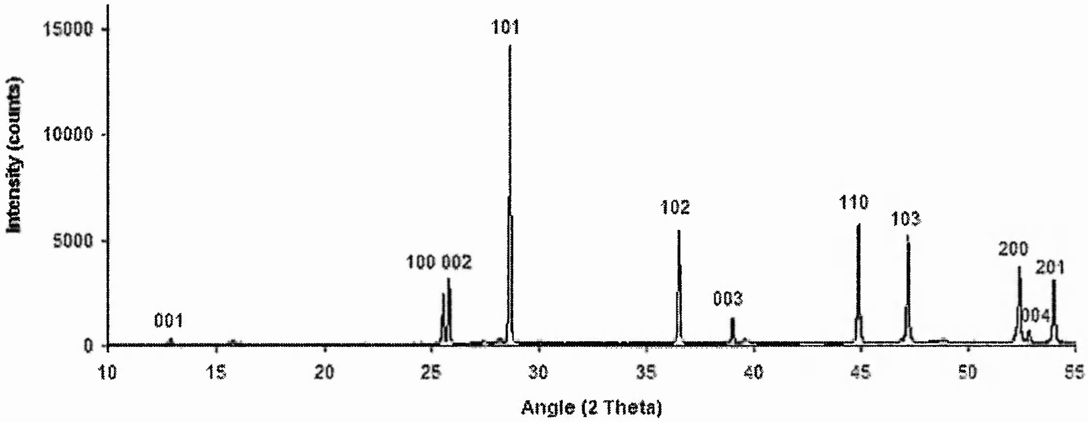

Figure 4-22: Typical XRD pattern of La_2O_2S: Eu.

Figure 4-23 indicates the *c*-axis variations in the position of the (002) reflection peaking at 25.612° as a function of Eu concentration. This has illustrated a pseudo-linear relationship between the Eu concentration and a shift in the position of this peak to smaller values of 2θ as demonstrated in Figure 4-24. These data are consistent since Eu has an ionic radius of 95 pm which is smaller than La (102 pm), and hence an expected decrease in the volume of the unit cell occurs as Eu dopant concentration becomes significant.

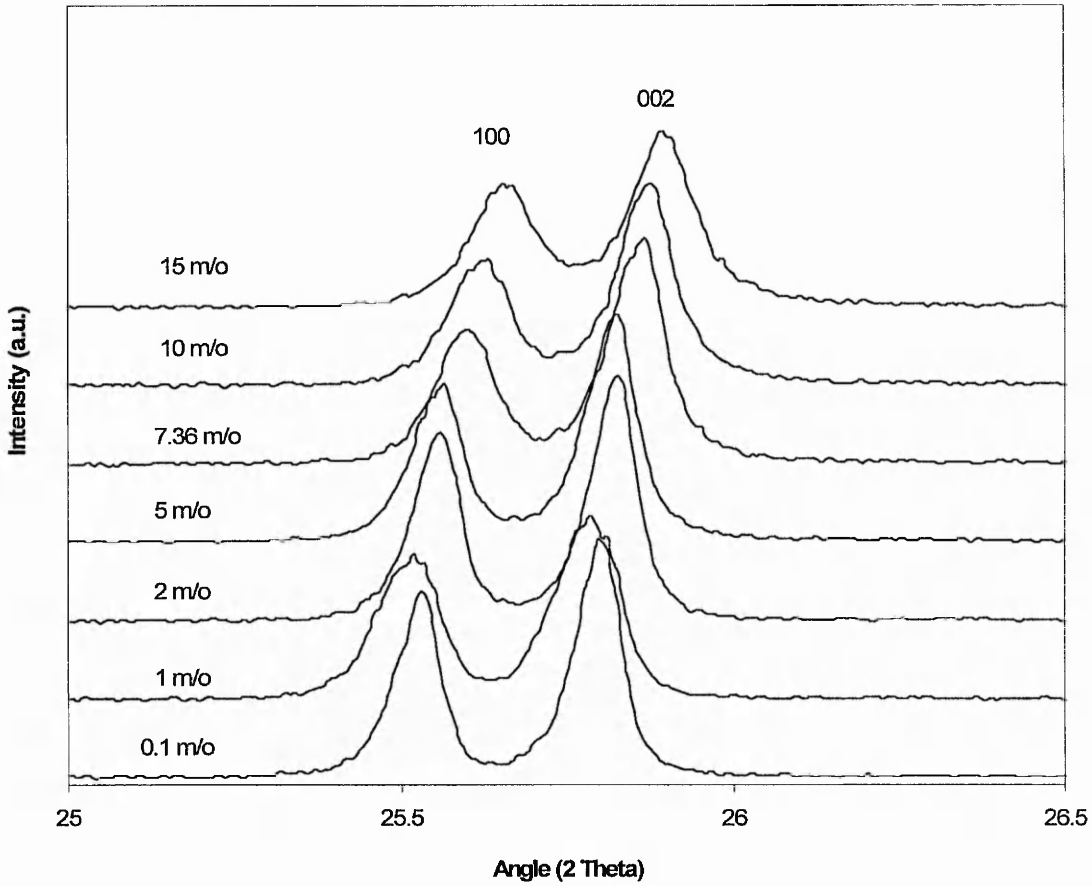

Figure 4-23: XRD patterns of La_2O_2S: Eu at different dopancy levels.

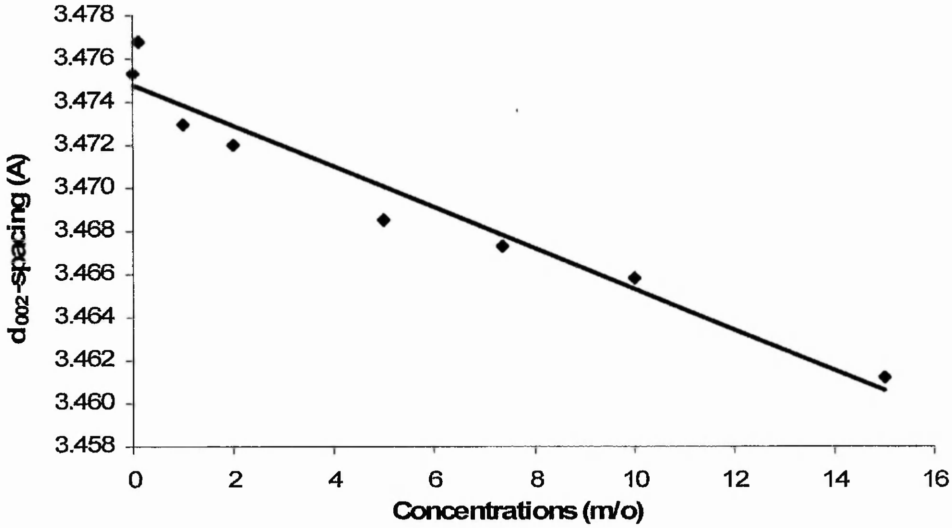

Figure 4-24: ***C*-parameter of the unit cell as a function of Eu content.**

By using the Scherrer calculation from X-Pert High Score Plus, the variation of the crystallite size of La_2O_2S: Eu can be calculated and is shown in Table 4-2. The host lattice La_2O_2S has the biggest crystallite size which is about 0.16 μm than that of the other Eu doped La_2O_2S. The crystallite size of La_2O_2S: Eu has reduced to 2.5 times smaller than the host lattice. A few additional low Eu concentrations 0.005, 0.02 and 0.05 m/o were characterised followed by the assumption made in the decay time section. Results at NTU showed that the commonly investigated La_2O_2S: Eu at higher concentrations with smaller crystallite size has a faster decay rate as demonstrated in Figure 4-17 (a) – (d).

The quenching rates for these phosphors at low dopant concentrations (large crystallite size) are greater than high dopant concentrations (small crystallite size) implying that they are more sensitive to temperature variance and hence a relationship between dopant concentration and decay time is established: a phosphor with lower concentration shows a better temperature dependency.

Table 4-2: Crystallite size for various concentrations of La_2O_2S: Eu.

Dopant Concentrations (m/o)	Crystallite size (Å)
0	1579
0.005	1218
0.02	1148
0.05	1134
0.1	1020
1	1053
2	1015
5	891
7.36	833
10	643
15	656

4.3.2 Summary

The photoluminescent, decay time and XRD analysis of powdered La_2O_2S: Eu showed these phosphors are suitable for the fabrication of the desired optical sensor. Dopant concentration is a key factor that has be taken into account for the measurements described above. The results showed significant changes in emission intensities, decay time and crystallinity with various dopant concentrations over 5-60 °C. For instance 467 nm and 495 nm lines become apparent at low dopant concentrations which are particular useful for phosphor thermographic applications. Consequently, it has been observed that lower Eu concentrations are more sensitive to temperature but this trend does not occur for <0.1 m/o. In addition, the XRD patterns have shown a shift of (100) and (002) planes to a greater 2θ as a function of Eu dopant concentration, this also implies that the c-axis of the unit cell shrinks against dopant concentration.

In this work, 0.1 m/o with a high quenching rate of 24 $m°C^{-1}$ has been identified as the most temperature sensitive dopancy for La_2O_2S: Eu as a sensing phosphor for use within an optical sensor. Previous work carried out by K.A. Wickersheim et al.[112] and L.M. Coyle et al.[113] only focused on the 512 nm temperature dependent line. The decay time results obtained here have shown that 495 nm has a more superior quenching rate of 24.03 m^oC^{-1}, as compared to 13.7 m^oC^{-1} at 512 nm line derived from illustrated data within the publication by L.M. Coyle et al.[113].

Chapter 5 Terbium doped lanthanum oxysulphide

5.1 Introduction

In Chapter 4, the promising results have proved that the red emitting phosphor La_2O_2S: Eu is suitable for potential use as a thermographic phosphor within an optical sensor. This chapter will discuss the results obtained for the second selected phosphor, the green emitting La_2O_2S: Tb, with the aim of determining suitable characteristics that can fulfil the requirements for use within the desired sensor. Many have reported[32, 114, 115] that terbium activated oxysulphides of gadolinium, yttrium and lanthanum have significant potential as input-screen phosphors for x-ray image intensifier use due to their high luminescent efficiencies. Relatively little work, however, has appeared in the thermometry literature concerning the temperature dependency of La_2O_2S: Tb. The following describes the phosphor characterisations of a number of dopant concentrations for La_2O_2S: Tb and the results of photoluminescent emission, decay time and XRD are presented. In addition, an interesting characteristic was discovered in this work whereby the decay time for La_2O_2S: Tb with a dopancy greater than 2 m/o was observed to increase linearly with temperature, which has contradicted the standard decay time characteristic of other phosphors.

5.1.1 Properties of La_2O_2S: Tb

Since both of the selected phosphors possess the same host lattice, lanthanum oxysulphide, and thus the crystal structure of La_2O_2S: Tb^{3+} is identical to the hexagonal atomic structure of La_2O_2S: Eu^{3+} as illustrated in Section 4.1.1. The only difference is that a slight discrepancy in the value of the lattice parameters of the unit cell of Tb_2O_2S: $a = 3.8249$ Å, $c = 6.626$Å, whilst Eu_2O_2S: $a = 3.8716$ Å, $c = 6.6856$ Å[116].

The characteristic properties of the Tb ions are attributable to the presence in the ion of a deep-lying 4f shell which is not completely filled[117]. The electrons of this shell are screened by the outer electron shells leading to a number of discrete energy levels as depicted in Figure 5-1, the energy level diagram of Tb ion sited within the host lattice La_2O_2S. The excited 5d state is strongly influenced by the crystal field which splits the 5d level into several levels which are approximately 15000 to 20000 cm^{-1} apart[117] and the number of these levels is determined by the crystallographic symmetry at the position of the Tb ion. However, the crystal field splittings varies from one lattice to another[117].

Given that the 4f shell may contain 14 electrons, the 4f shell of Tb ($4f^8$, half filled plus one) readily releases an electron and hence the transition $4f^8$-4 $f^7 5d$[117] takes place at relatively low energy. Generally, the emission of terbium corresponds to the electronic transitions $^5D_4 - {}^7F_J$ which are mainly in the green region, but it may also emit blue from the higher level emission $^5D_3 - {}^7F_J$ [118]. In this work, the investigated La_2O_2S: Tb exhibited green luminescence following excitation in the 4f-5d absorption band. The electron is raised to $4f^7 5d$ state as a result of absorbing UV radiation, it subsequently decays sequentially from this state to the $^5D_3$ or the $^5D_4$ state or both, thereby releasing phonons to the lattice[117]. Due to the large distance between the ^5D states and the ^7F levels, the non-radiative process discontinues here and subsequently the electron returns to the ground state by emitting radiation (photon). According to Struck and Fonger, again similar to La_2O_2S: Eu, the thermal quenching of Tb in La_2O_2S is due to the CTS crossover relaxation to Frank-Condon shifted states[107].

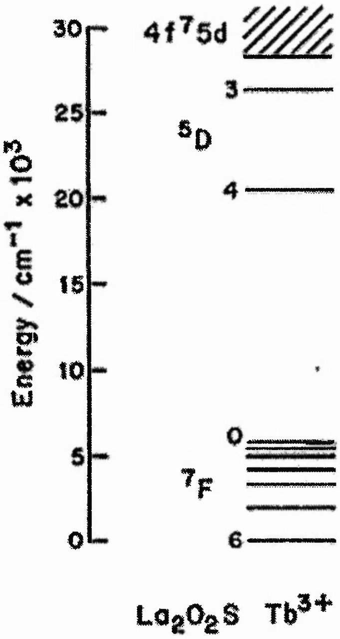

Figure 5-1: Energy diagram of Tb ion in La_2O_2S lattice[119].

As illustrated in Figure 5-2, the emission spectrum of terbium doped lanthanum oxysulphide is determined by the transitions of electrons from an upper ($^5D_3$) and a lower ($^5D_4$) excited state to the ground state of ^7F level. The excitation spectrum for La_2O_2S: Tb provided by PTL indicates that the optimum excitation wavelength is centred at approximately 300 nm but it also shows the 337 nm excitation wavelength by nitrogen laser has enough energy to excite this phosphor. Amiryan et al.[114] reported the cross relaxation between the $^5D_3$ - $^5D_4$ and $^7F_6 - {}^7F_0$ transitions leads to the probability of the former transition increases as the Tb ions become closer. According to this principle, an increase in the Tb concentration will result in an increase in the proportion of the long wavelength lines in the emission spectrum due to the transitions from the $^5D_4$ level[114].

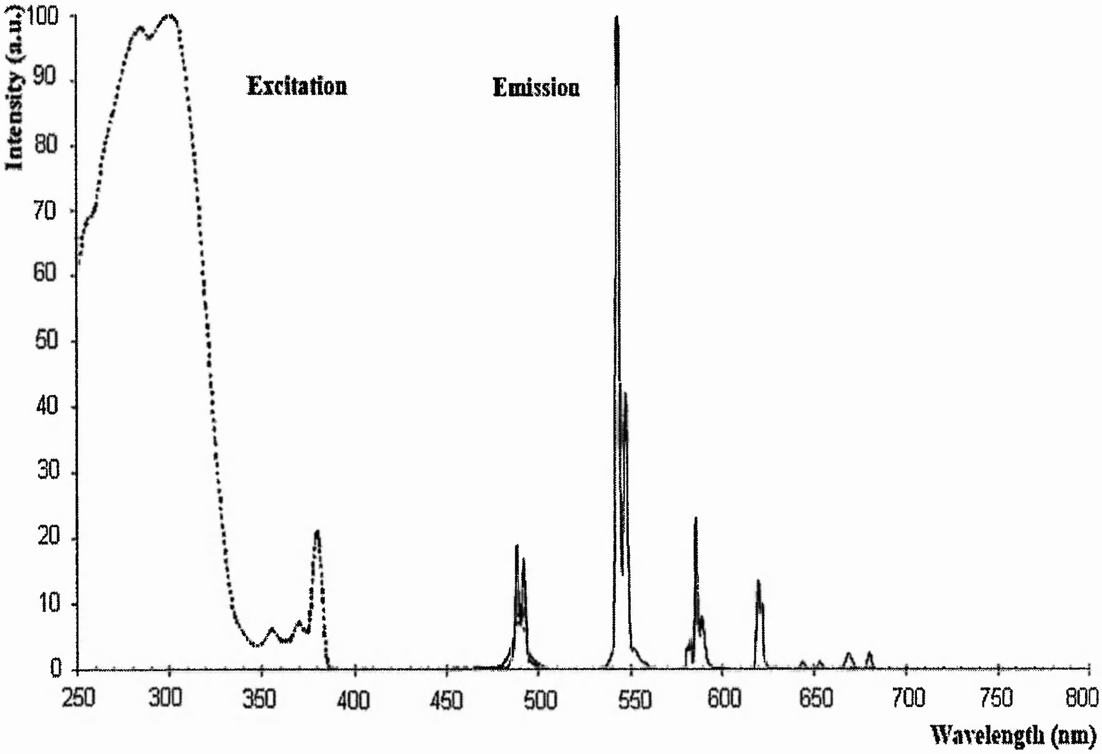

Figure 5-2: Excitation and emission spectra of La_2O_2S: Tb. (Excitation spectra was provided by PTL).

5.2 Photoluminescent measurement

The emission spectrum of La_2O_2S: Tb is determined by the electronic transitions from $^5D_3$ and $^5D_4$ excited level to the level of the multiplet term $^7F_{J\,(J=0,1,2,3,4,5,6)}$ levels of the $4f^8$ configuration[34, 114] as mentioned previously. The PL emission of La_2O_2S: Tb was achieved via the use of a nitrogen laser (337 nm) and the resultant spectrum is shown in

Figure 5-3, comprising of multiple sharp lines at 489 nm, 493 nm, 544 nm, 548 nm, 587 nm and 621 nm. As expected, La_2O_2S: Tb is found to be a green emitting phosphor since the La_2O_2S lattice is activated with terbium ion, thereby resulted in the dominant line peaking at 544nm. Of more importance, the temperature dependent characteristics were found to occur at most of the emission wavelengths of La_2O_2S: Tb, i.e. $^5D_4$ to ^7F_J transitions [77] as compared to only a few emission lines of La_2O_2S: Eu at short wavelengths. The temperature dependency of La_2O_2S: Tb will be discussed later in this chapter.

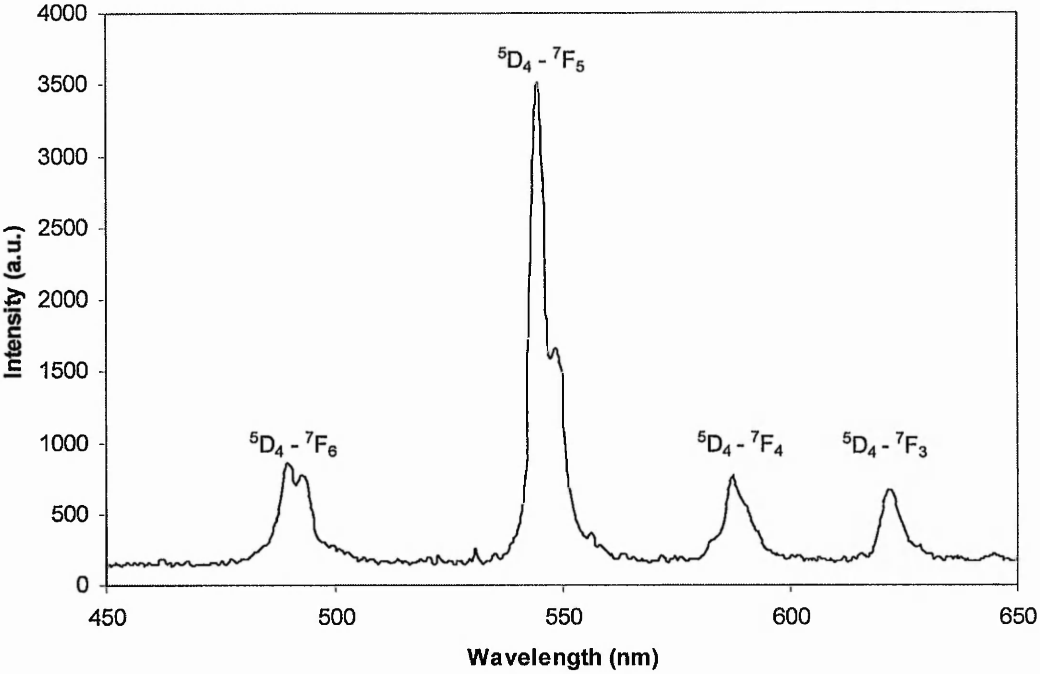

Figure 5-3: Typical emission spectrum for La_2O_2S: Tb excited by a nitrogen laser at room temperature.

5.2.1 Dopant dependency

It has been previously discussed that dopant concentration being a significant influential factor for varying the optical and physical properties of phosphors. Here, this is the first demonstration to correlate a wide range of concentrations 0.005 – 50 m/o Tb with PL emission of La_2O_2S: Tb. The PL measurements were carried out over the full range of dopant concentrations, but as an example, a comparison shown here was made between a lower concentration and a higher concentration (0.2 m/o and 10 m/o Tb respectively). The emission spectra of both phosphors are illustrated in Figure 5-4. At low concentrations ($\leq$0.5 m/o), more lines were exhibited in the emission spectrum due to the Stark splitting effect[108] and the dominant peak has also shifted from the green line 544 nm to the red region peaking at 624 nm. On the other hand, higher Tb concentrations ($\geq$ 0.92 m/o) exhibited six solid emission peaks at 489 nm, 493 nm, 544 nm, 548 nm, 587 nm and 621 nm as a result of a change in the relative intensities of the different transitions. Importantly, these peaks showed temperature dependencies with fast decay time.

From the observations, it has been shown a colour change in the luminescence with dopant concentration. At lower Tb concentrations less than 0.5 m/o, the phosphor emitted orange luminance at 0.5 m/o, then red at 0.2 and 0.005 m/o. This may be due to the domination of the host lattice over the insignificant amount of Tb concentration within the crystal field and hence resulted in the lattice characteristic hue (red). As a result, the emission intensities in the red region ($\geq$ 587 nm) are stronger at lower terbium concentrations as can be seen in Figure 5-5. On the other hand, the maximum brightness occurred at 10 m/o Tb in the green region (489- 548 nm) and the intensities then dropped rapidly with higher concentration. This is mainly due to the effect of concentration quenching.

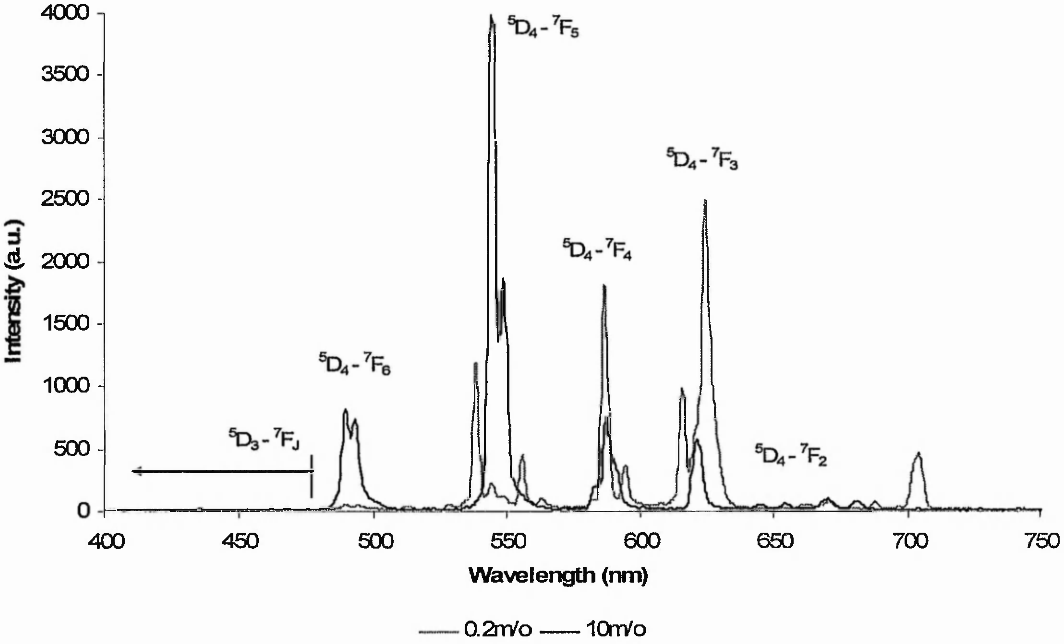

Figure 5-4: Spectra emission distribution for La_2O_2S: Tb at dopant concentrations of 0.2 m/o and 10 m/o at room temperature. (Excitation spectra for La_2O_2S: Tb provided by PTL).

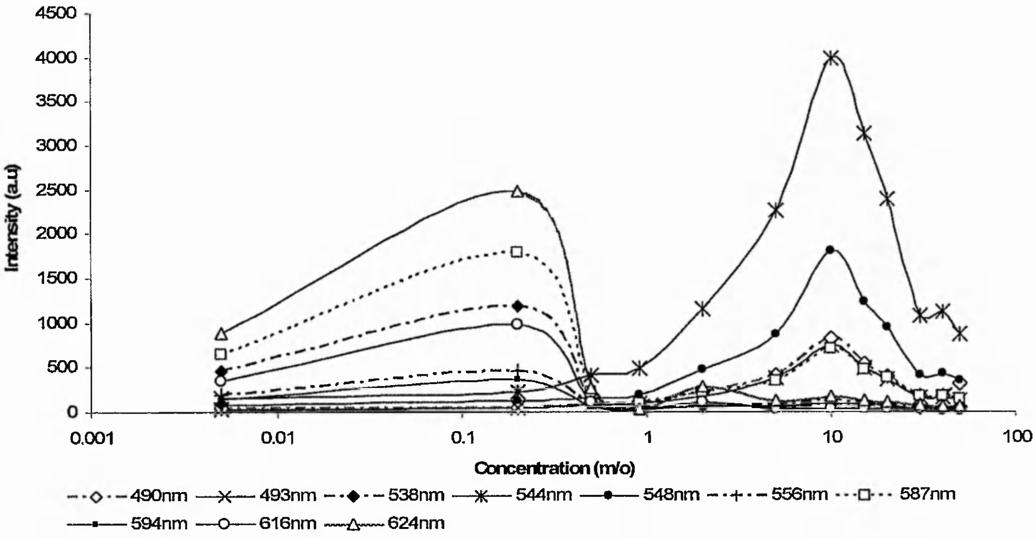

Figure 5-5: Intensity levels of different dopant concentrations of La_2O_2S: Tb at room temperature.

5.3 Decay time characterisation

As stated before, very little work have been reported with regards to the temperature sensing capabilities of La_2O_2S: Tb. Although Struck and Fonger[77] have explained the thermal quenching process of La_2O_2S: Tb but their work only concentrated on 0.5 m/o Tb at the specific wavelength of 545 nm ($^5D_4$ to $^7F_5$). In this research, again, it has first demonstrated the temperature dependent characteristics of La_2O_2S: Tb using a broad range of dopant concentrations from 0.005 – 50 m/o Tb.

For comparison purposes, a selection of decay time profiles at 0.5, 2, 10 and 50 m/o Tb were chosen to represent the numerous set of data, as shown in Figure 5-6. The single exponential decays are normalised and plotted on a semi-log scale. The overall decay time results have shown different concentrations of La_2O_2S: Tb show strong dependency upon temperature at their respective emission wavelengths. The decay time for lower Tb concentrations is about ~10^{-6} to 10^{-7} s while higher Tb concentration are slower by at least an order of magnitude with decay time of ~10^{-3} to 10^{-5} s. Interestingly, an unusual decay time characteristic was observed for 2 m/o Tb and above. The decay times of these high Tb concentrations increase as a function of temperature and this is first reported in the field of phosphor thermography. In order to examine this abnormal phenomenon closely, the decay time measurement concentrated on the dominant wavelength at 544 nm for > 2 m/o Tb.

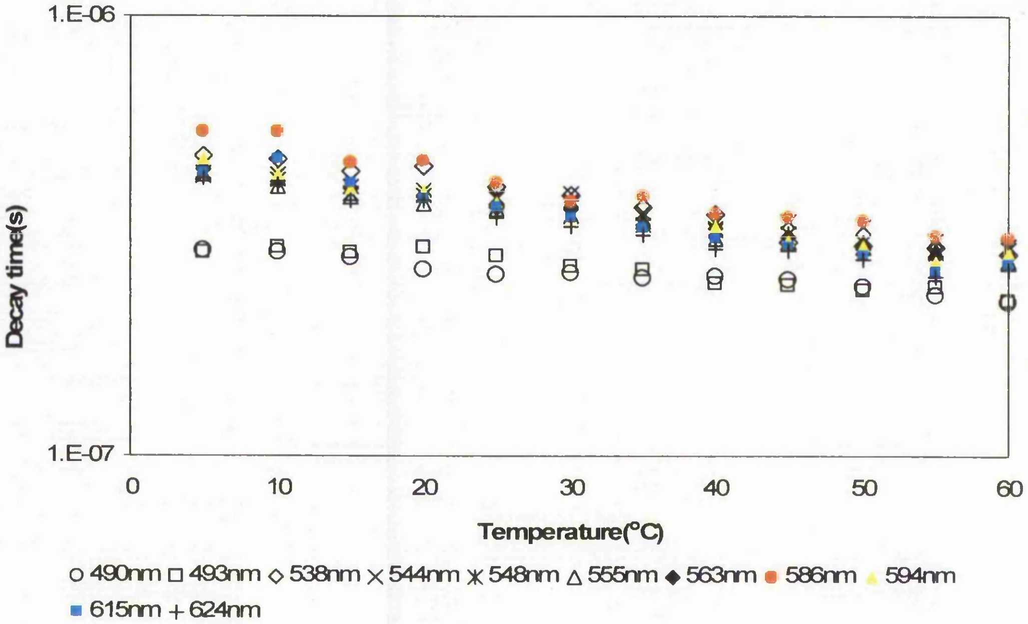

a) La_2O_2S: Tb (0.5 m/o)

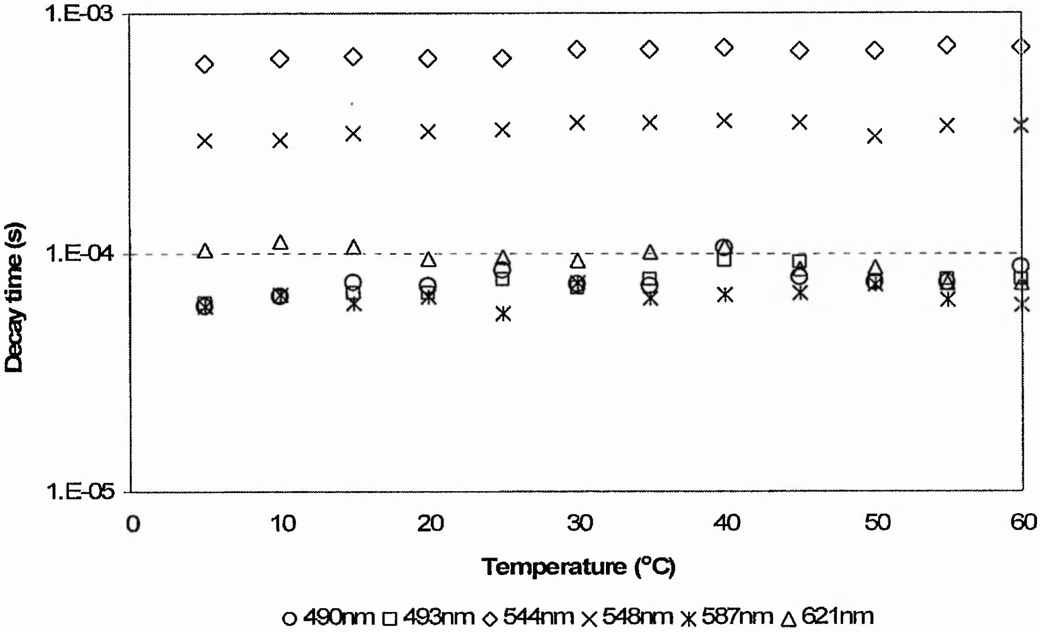

(b) La_2O_2S: Tb (2 m/o)

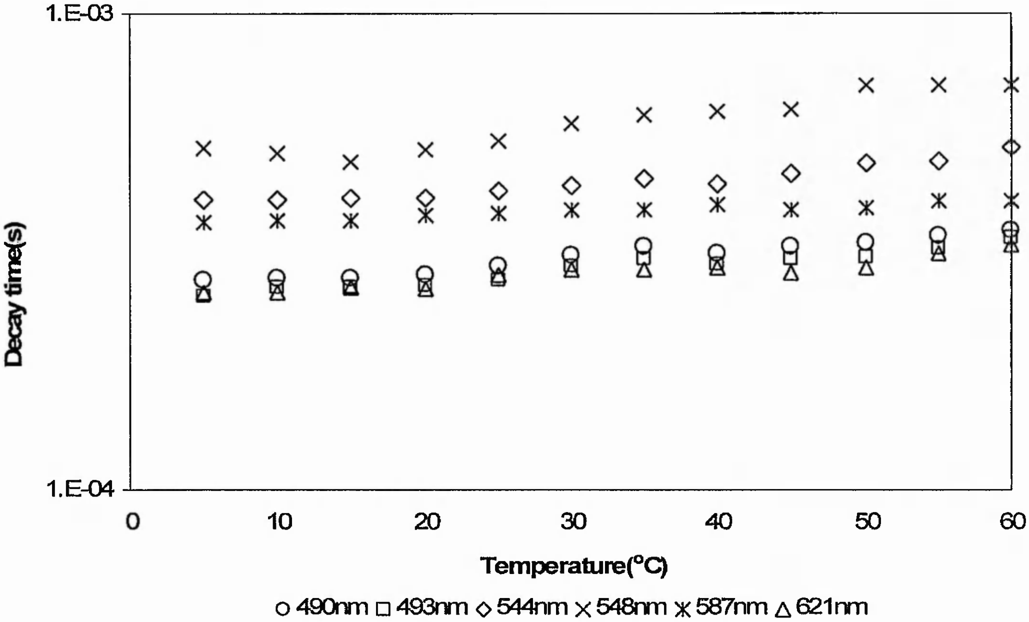

(c) La_2O_2S: Tb (10 m/o)

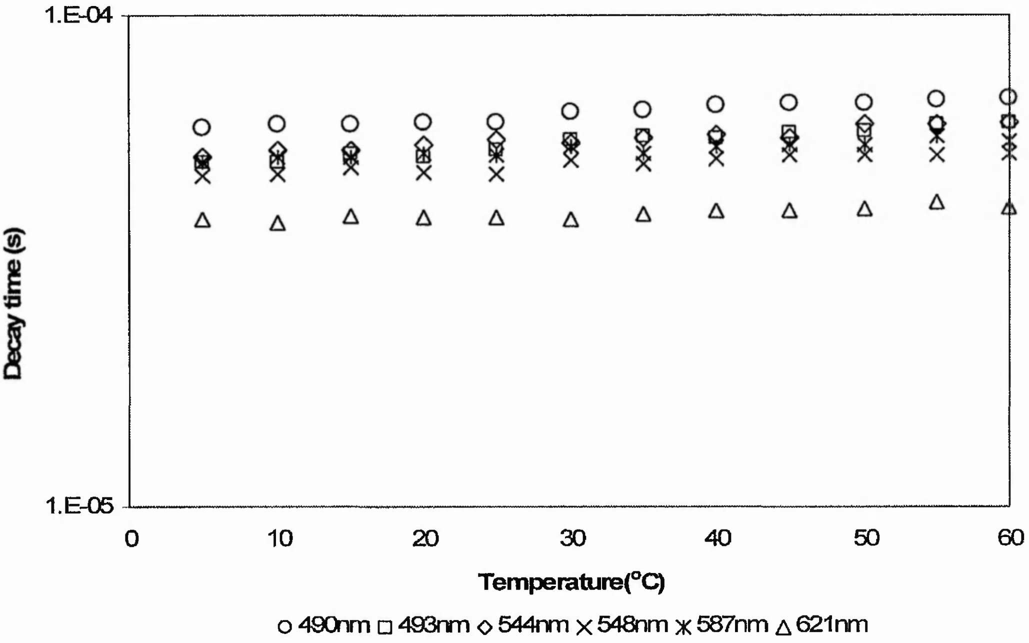

(d) La_2O_2S: Tb (50 m/o)

Figure 5-6: Decay time characteristics of various Tb concentrations at different emission wavelengths.

Like many other cases, the decay time of La_2O_2S: Tb 0.005- 0.91 m/o decreases with temperature. However, it was observed that 2-50 m/o Tb has shown an unprecedented decay time characteristic: its decay time increases with temperature. A good example of this abnormal decay time behaviour is shown in Figure 5-7, the decay time of 544 nm at 5 °C is 269 μs whilst 371 μs at 60 °C and again it has been proven that this unusual trend of decay time has a single exponential decay characteristic as demonstrated in Figure 5-8. In addition, a summary of the decay times at 544 nm of all investigated Tb concentrations is depicted in Figure 5-9. A clear indication of a linear increase in decay time versus temperature for > 2m/o Tb. Although the explanation to this scenario is unclear, it is known that as the dopant concentration is increased, the resulting change in crystal structure will alter the energy levels that exist for excited states (Stark-splitting effect). It would appear that this has induced a trapping state and/or additional energy levels which result in phonon rather than photon emission. This would have two effects - reduction of intensity and an observed slow-down of the luminous decay process, due to the excited states now relaxing to an intermediate state before reaching the photon relaxation energy level.

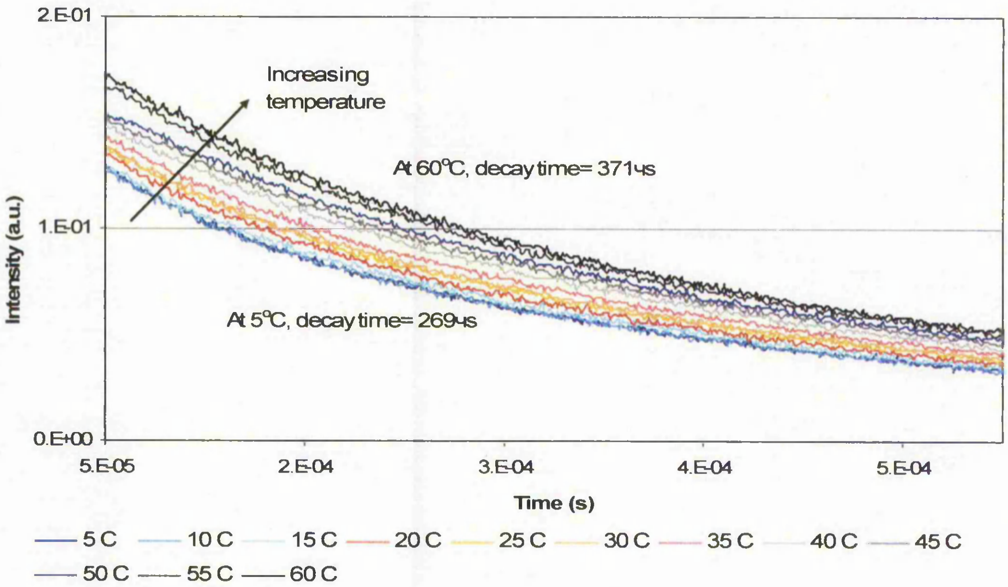

Figure 5-7 Decay curves of La_2O_2S: 15 m/o Tb at 544 nm line from 5- 60°C.

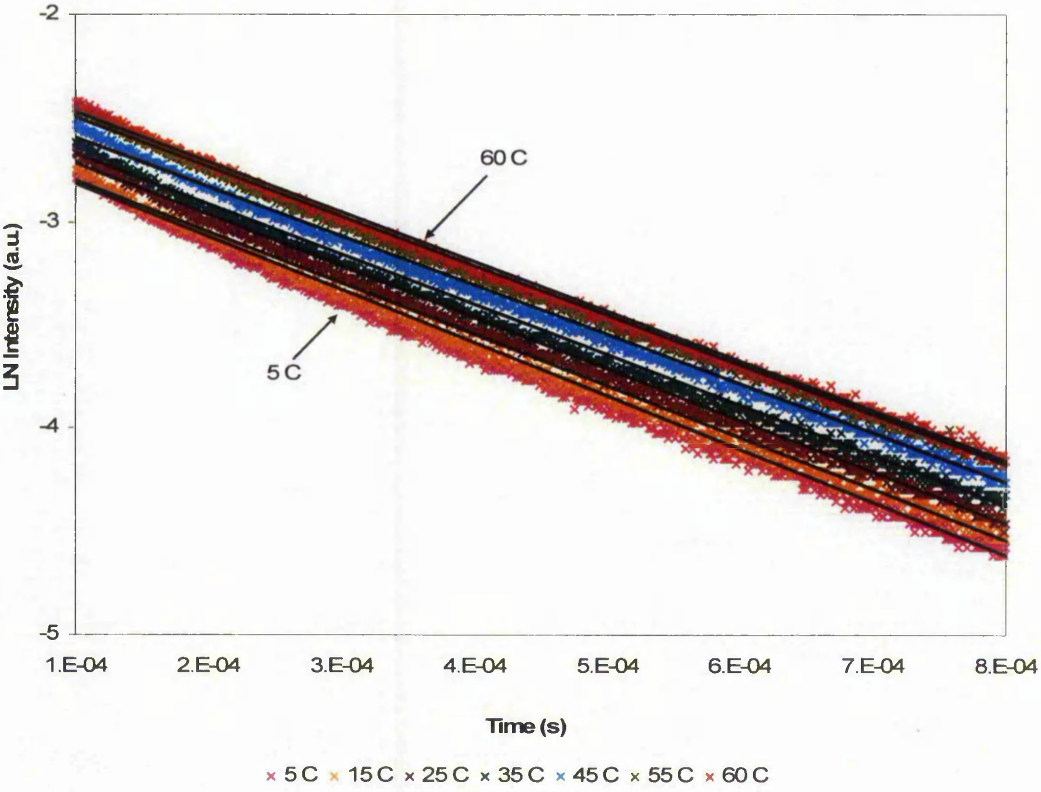

Figure 5-8: Linear least squares fit of ln intensity as a function of time for La_2O_2S: 15 m/o Tb over 5-60 °C.

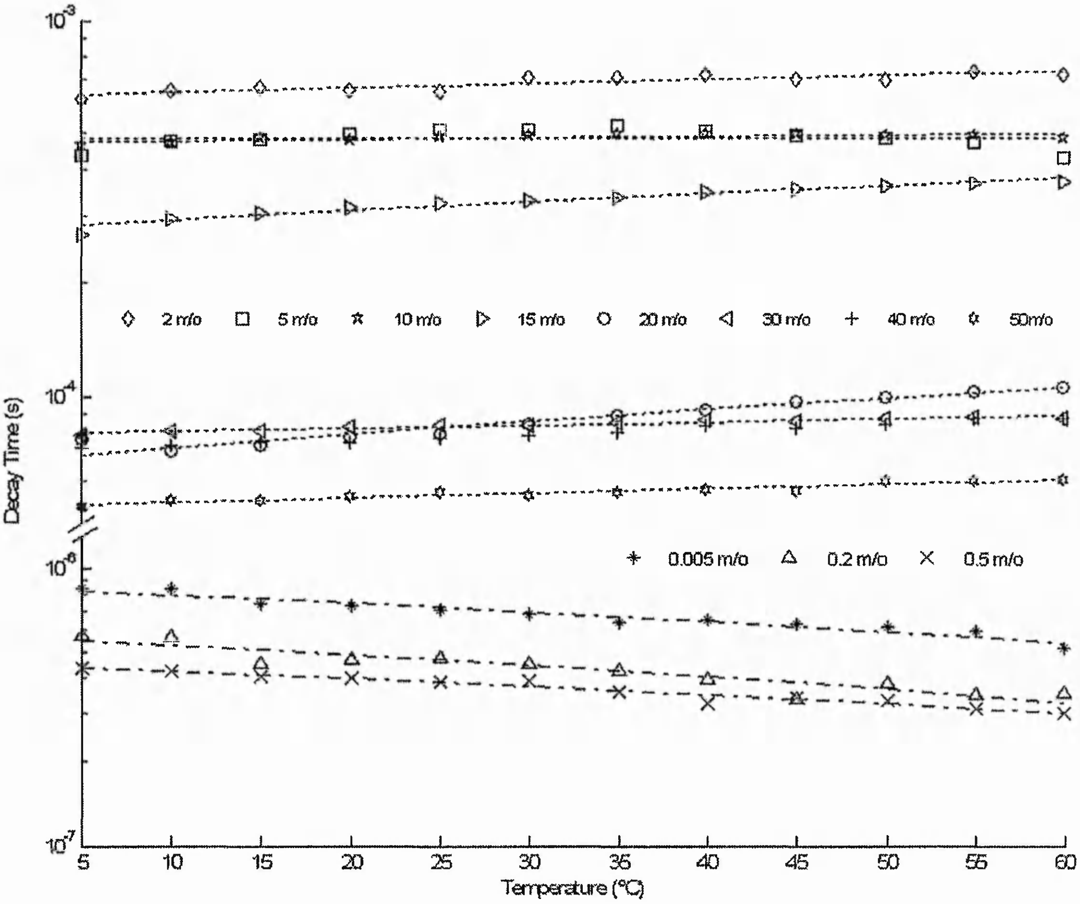

Figure 5-9: Decay time of lower La_2O_2S: Tb concentrations (0.005 – 0.5 m/o) and higher Tb concentrations (2-50 m/o) at 544 nm as a function of temperature.

The quenching rates of various dopant concentrations of La_2O_2S: Tb are tabulated in Table 5-1.Unlike the steep quenching slopes of La_2O_2S: Eu, the average quenching rate of La_2O_2S: Tb is as low as ~ 3 m°C^{-1} with faster decay times depending on the Tb concentrations and also the emission peak. This suggests that La_2O_2S: Tb is a less efficient phosphor when compared to La_2O_2S: Eu. The decay times of the novel decay time behaviour are denoted with (-) sign. At this stage, it is difficult to justify the efficiency of the phosphor based on this inverse manner of decay time characteristic. However, this discovery would certainly draw some attention in the field of optical sensing technologies to attract suitable applications.

To further validate the decay time relationship with dopant concentration as discussed in Chapter 4, higher quenching rate of the temperature dependent peaks was found at lower dopant concentration of the investigated phosphors, i.e. 0.005 m/o La_2O_2S: Tb and 0.1 m/o La_2O_2S: Eu. This again has confirmed that lower doping concentrations are more preferred for use within an optical sensor in terms of sensing capabilities.

Table 5-1 Quenching rates of different Tb concentrations at all emission peaks. (The negative sign (-) is used to denote the increase decay times with increasing temperature.)

Emission wavelengths (nm)	Quenching rates (m°C-1) of La_2O_2S: Tb				
	0.005 m/o	0.91 m/o	2 m/o	10 m/o	50 m/o
467	2.79				
490	2.49	2.10	-2.97	-1.85	-1.12
493	3.29	2.39	-1.81	-2.14	-1.47
512	4.66				
531	3.36				
538	1.39				
544	3.90	3.19	-1.18	-2.01	-1.32
548		3.56	-1.10	-2.42	-0.80
555	4.19				
563	3.63				
587	2.35	4.73	-0.11	-1.58	-1.00
594	4.92				
615	3.28				
621	2.08	4.65	2.53	-1.82	-0.46

5.3.1 X-Ray Diffraction (XRD)

The XRD experiments were carried out using the same parameters as described in Chapter 4. XRD patterns of La_2O_2S: Tb over the diffraction angles of $5° \leq 2\theta \leq 55°$ are shown in Figure 5-10, exhibiting similar characteristics than that of La_2O_2S: Eu.

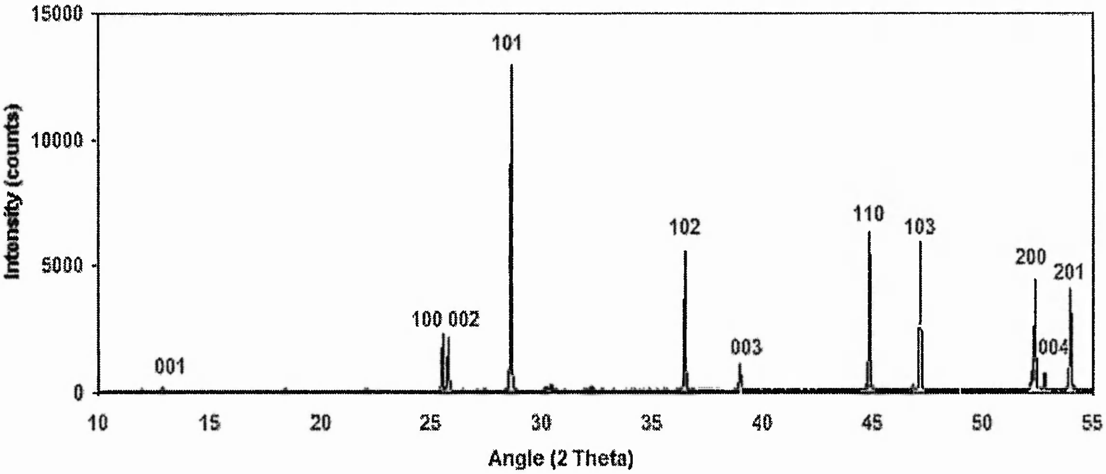

Figure 5-10: Typical XRD pattern of La_2O_2S: Tb.

As shown in Figure 5-11, the shift in 2θ of the (002) reflection with an increase in the Tb dopancy level is mainly due to the variations in the crystal lattice, i.e. *c*-axis shrinks with increasing Tb concentration. This is based on the size of the ionic radius of both La (102 pm) and Tb (92 pm) in the unit cell, which decreases as the Tb concentration becomes dominant. With increasing Tb concentration, the two individual peaks at 25.52° ((100) reflection) and 25.78° ((002) reflection) merge gradually and eventually form a broad peak at 50 m/o Tb. This merging behavior alters the formation of the crystal lattice and hence produces a multitude of probability of occurrence for both radiative and non-radiative transitions. As a result, the changes observed would therefore be an important consideration in determining the temperature sensitivity of a particular phosphor at a favourable dopancy level.

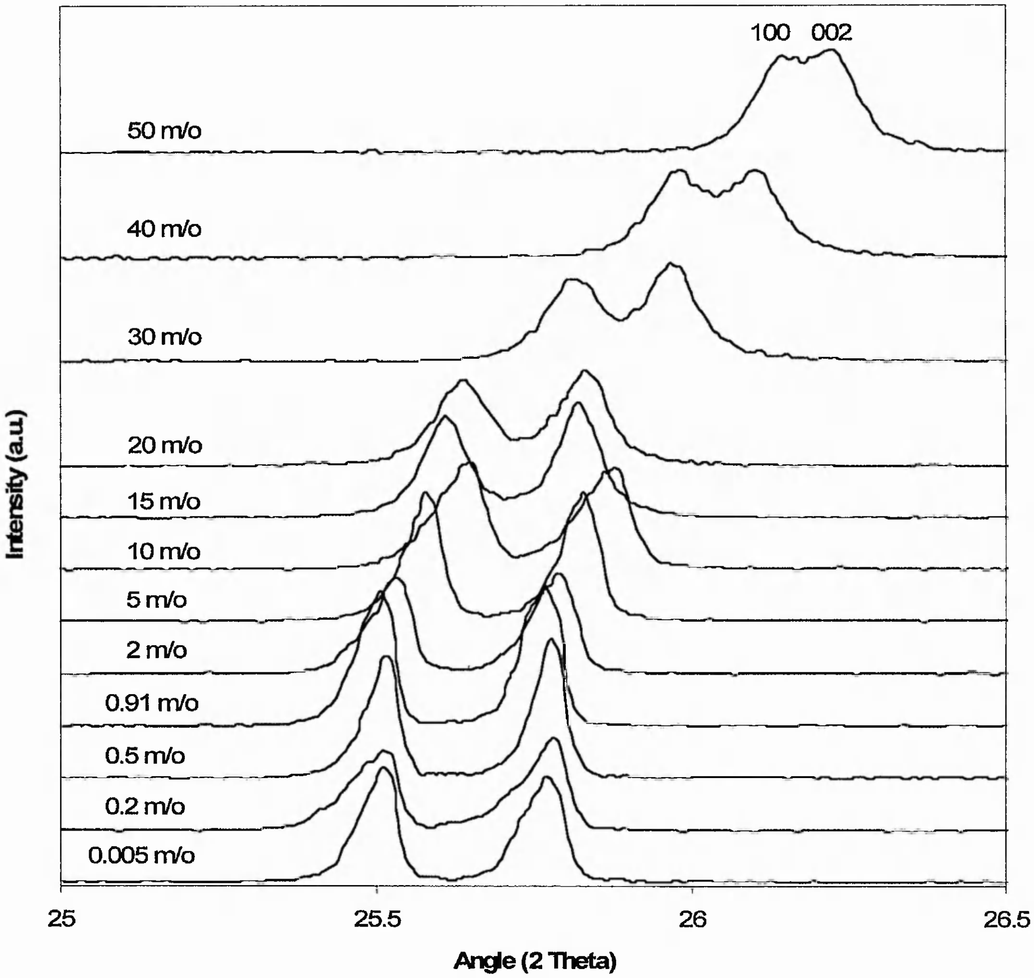

Figure 5-11 XRD patterns of various dopancy levels of La_2O_2S: Tb at (100) and (002) reflections.

In addition to the merging planes with dopant concentration, there is little change in the *c*-axis of the unit cell at low concentrations (<1 m/o) but a linear relationship was observed for dopant concentrations greater than 1 m/o Tb. There is a reduction in the *c*-axis parameter with concentration and the data fit the pseudo-linear relationship as demonstrated in Figure 5-12. In addition, the crystallite size of La_2O_2S: Tb decreases owing to a reduction in the volume of the unit cell with increasing Tb dopancy. By using the Scherrer equation, which relates the width of peaks in an X-ray powder diffraction pattern to crystal size, the crystallite size of the phosphors can be determined as tabulated in Table 5-2.

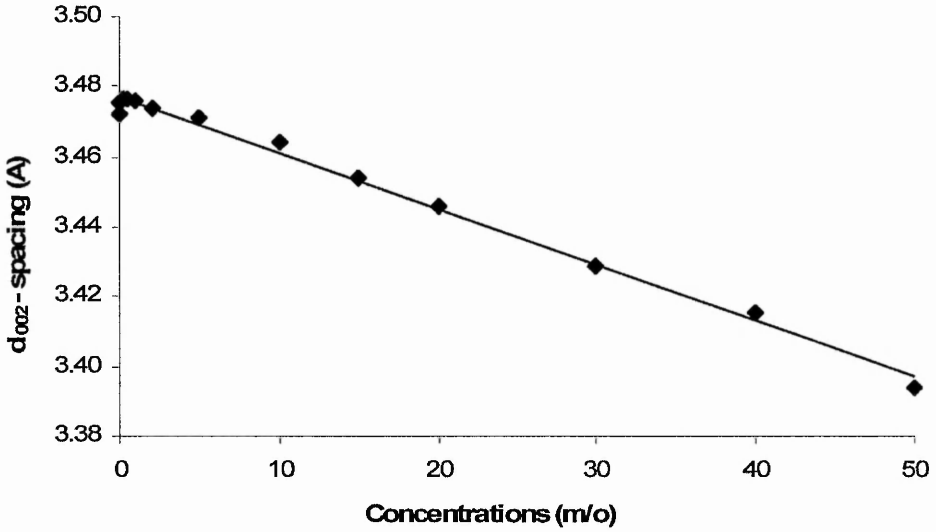

Figure 5-12: c-axis of the unit cell of La_2O_2S: Tb as a function of dopant concentration at the (002) reflection.

Table 5-2 Crystallite size of 0-50 m/o La_2O_2S: Tb.

Dopant Concentrations (m/o)	Crystallite size (Å)
0	1560
0.005	1324
0.2	1464
0.5	1416
1	1416
2	1448
5	1077
10	997
15	993
20	904
30	834
40	783
50	888

5.4 An explanation for the non-standard increase of decay time with temperature

In order to base a hypothesis to the discovery of the novel decay time characteristic, it is first necessary to relate the basis of this hypothesis back to the standard Equation 2-9. The decay time of luminescence is inversely proportional to the sum of the probability of de-excitation of radiative (W_R) and non-radiative (W_{NR}) transitions:

$$\tau_d = (W_R + W_{NR})^{-1}$$

where τ_d is the lifetime of luminescence, whereby the radiative transition is temperature independent and it is the non-radiative transition that is temperature dependent.

As can be deduced from the equation, the standard lifetime characteristic of a material typically shows a decrease in the decay time with temperature as a result of an increase in the probability of non-radiative transition. Conversely, for the novel decay time characteristic discovered in this work, the results have shown an increase in decay time against temperature for La_2O_2S: Tb above 2 m/o dopancy. For this to be true, relates to Equation 2-9, there must be a reduction in the probability of the non-radiation de-excitation, thus leading to a rise in decay time with temperature.

Referring back to the theory explained in Chapter 2, we are able to define how the decay time varies with temperature due to the energy transition required for the non-radiative transitions as follows:-

$$\tau_d(t) = \tau_0 \exp\left(\frac{\Delta E}{kT}\right)$$ **Equation 5-1**

where τ_d = decay time at any given time (t), τ_0 = initial decay time at 0 K, E = energy difference, K= Boltzmann's factor and T= ambient temperature.

The resultant graph is illustrated in Figure 5-13, with 15 m/o Tb at 544 nm as an example. A good linear relationship is indicated from which the energy transition can be calculated from the gradient. The energy transition is calculated at -4.22E-02 eV

(340.6299 cm^{-1}) for 15 m/o Tb at 544 nm, indicating that a loss of energy has occurred rather than the usual gain due to temperature increase.

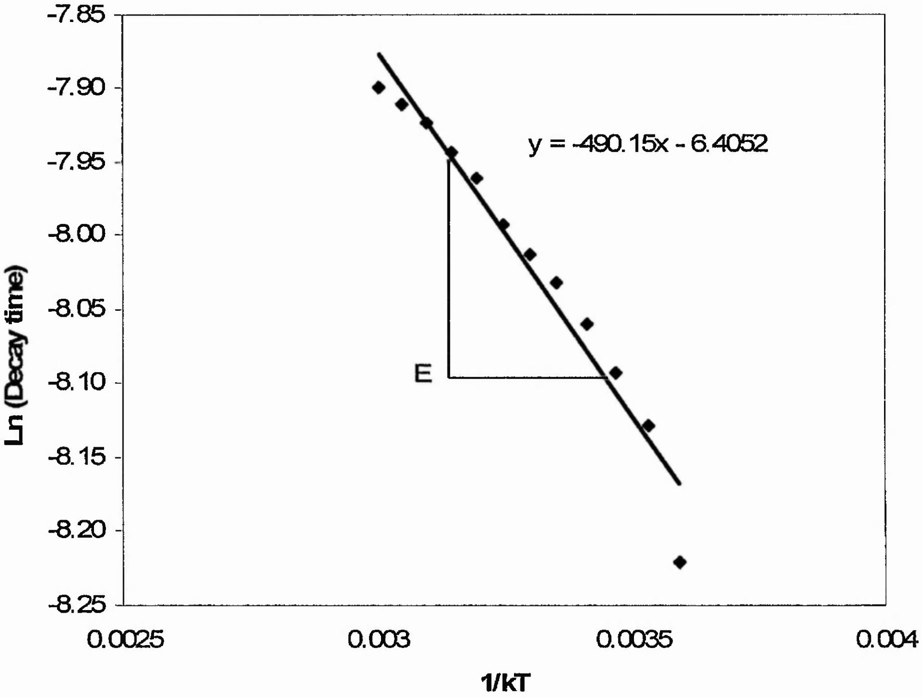

Figure 5-13: Variation of decay time of 15 m/o La_2O_2S: Tb versus temperature.

In addition, it is also believed that the resonance interaction between the neighbouring Tb ions will increase as the dopant concentration is increased, as previously illustrated by Amiryan et al[114]. Hence, it is hypothesised that the resultant energy transfer between the Tb ions will slow down the non-radiative process, resulting in a longer decay time. As stated previously, the primary non-radiative quenching in most phosphors is via vibratory motion to either a lower emitting energy state or the ground state of the ion. As the temperature of the phosphor is increased, the efficiency of these transitions increases because thermal expansion of the host lattice increases the vibratory motion necessary to dissipate the energy released by these transitions [57].

In order to assess this theory, a series of XRD experiments were carried out within a furnace (Anton Paar HTK-1200) in order to investigate the thermal expansion behaviour of various dopant concentrations of La_2O_2S: Tb over the temperature range of interest. The XRD equipment used was a X'Pert-Pro diffractometer with Cu $K\alpha_1$ radiation (45 kV and 40 mA). To fully examine the changes in the parameters of the unit cell, a plot of cell volume as a function of temperature would give a good overall picture. Hence, XRD analysis of 0.005, 0.91, 2, 15 and 50 m/o Tb was carried out over a much wider two theta range (10 - 90°) with 0.008° step size and a count time of 90 seconds per step, in 5 °C steps from the minimum operating temperature 30 °C up to 100 °C. As an example, the resultant XRD patterns of 50 m/o Tb over 30 - 100 °C are illustrated in Figure 5-14. The lattice parameters and the unit cell volume were calculated using TOPAS Academic v4.1 analysing software.

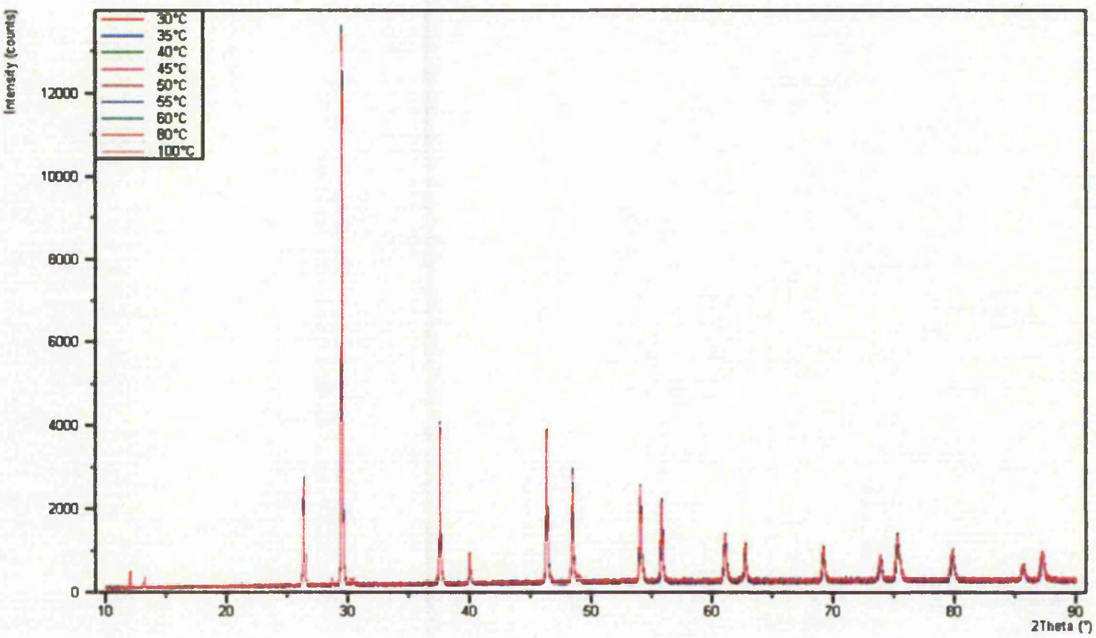

Figure 5-14: XRD patterns of 50 m/o Tb over 30 – 100 °C.

As shown in Figure 5-15 and Figure 5-16, both of the lower concentration of 0.005 m/o Tb and higher concentration 15 m/o Tb show similar positive thermal expansion characteristic whereby the a/b-axis, c-axis and the cell volume expand with temperature. This thermal expansion in cell size indicates that the Tb ions would therefore be moving further away from neighbouring Tb ions and hence would not be increasing the probability of Tb interaction as original suspected.

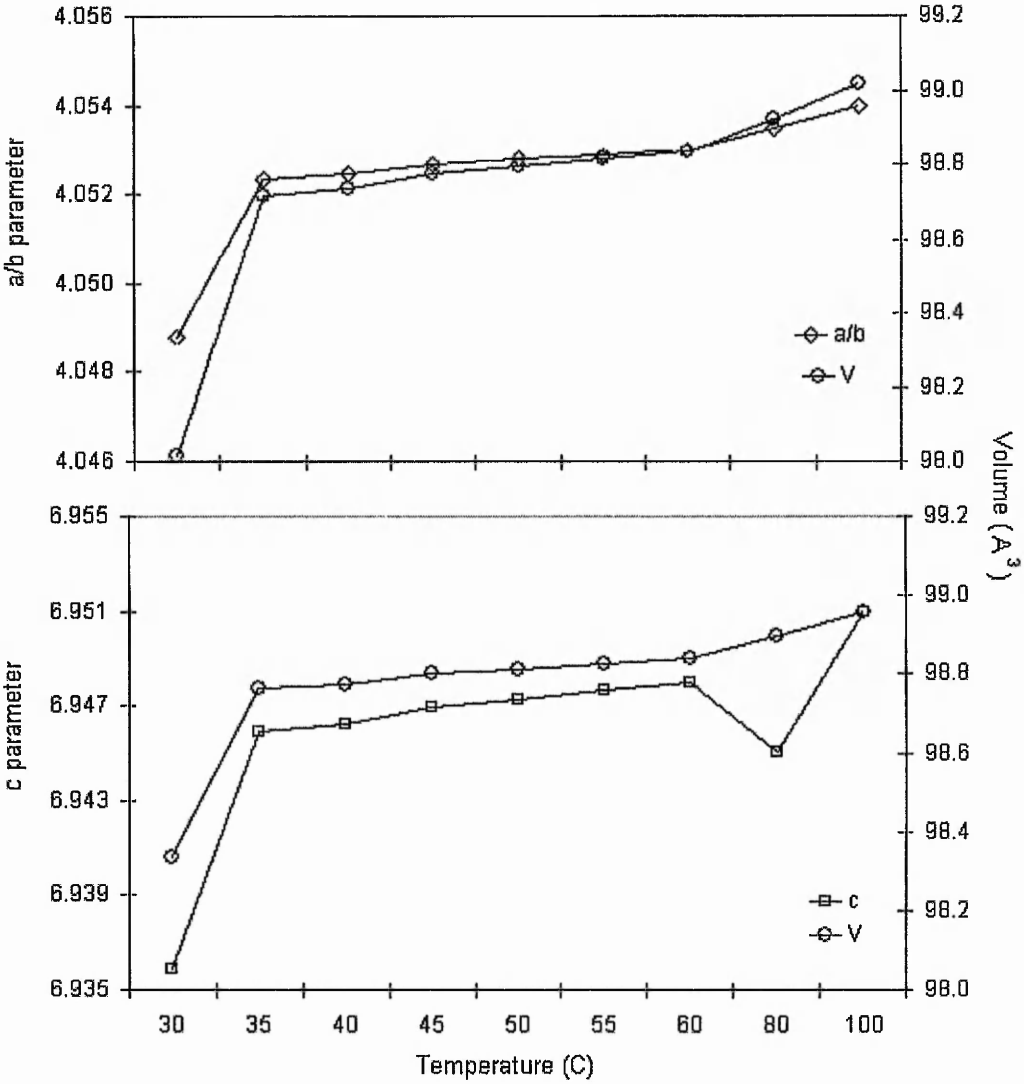

Figure 5-15: The cell volume and lattice parameters for 0.005 m/o Tb as a function of temperature.

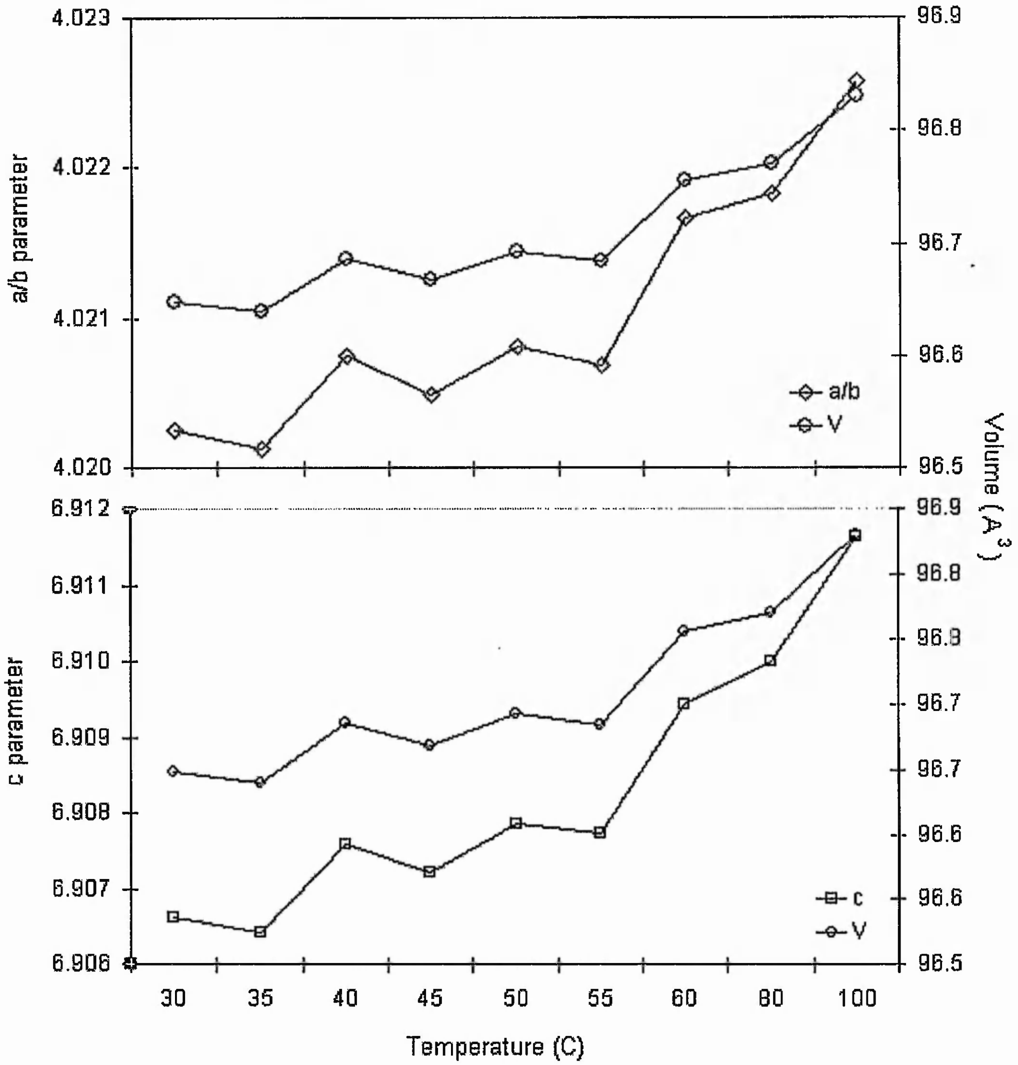

Figure 5-16: The cell volume and lattice parameters for 15 m/o Tb as a function of temperature.

5.4.1 Summary

The PL results have indicated that the optimum brightness of La_2O_2S: Tb occurred at 10 m/o and most of the emission lines of the investigated phosphors were found to be temperature dependent. In addition, the decay time results have shown that La_2O_2S: Tb is sensitive over 5-60 °C but it is less sensitive to temperature variations as compared to La_2O_2S: Eu due to its lower quenching rate of 3m $°C^{-1}$. By varying Tb concentration throughout the experimental work, an unprecedented decay time trend was discovered, a rise in decay time with increasing temperature was evident over dopant concentrations of 2-50 m/o La_2O_2S: Tb. A hypothesis based on the probability of non-radiative transition as well as the resonance interactions of the Tb ions in the excited state which is responsible for the non-radiative deactivation has been made. However, the thermal expansion behaviour of the selected phosphors (0.005 and 15 m/o) indicates the same trend of the expansion of a/b, c and volume of the unite cell with temperature. Till now, this assessment remains inconclusive and evidence to this assumption requires extensive analysis and studies for further investigation.

Chapter 6 Feasibility study of an optical sensor head

6.1 Introduction

At the final stage of this programme, investigation concentrated on the feasibility of using the optimum phosphor for producing an optical temperature sensor head for use within a MRI scanner to monitor a patient's skin temperature. Although a solution for such a sensor can be either invasive (requires an incision for internal sensing) or non-invasive (direct contact with skin surface), this research was mainly concerned with the non-invasive type. A reliable optical temperature sensing technology - the decay time system - that overcomes the drawbacks of using any metallic sensing device, has been adapted within this body of work for temperature measurement using both of the selected thermographic phosphors, La_2O_2S: Eu and La_2O_2S: Tb. Apart from the phosphor being the primary source material within the optical sensor, the optical fibre also plays an important role to allow optical access to the phosphor which will be in thermal contact with human skin via a protective membrane. Two optical fibres would be used to deliver the UV light to the phosphor and collect the visible luminescence to a detector for temperature data analysis.

As already discussed, a comprehensive investigation on the sensing capabilities of the chosen phosphors has been carried out to determine a suitable phosphor to use within an optical temperature sensor over 5-60 °C. Decay time results have indicated that 0.1 m/o La_2O_2S: Eu is the most sensitive phosphor to temperature variance due to its high quenching rate of 24 $m^{\circ}C^{-1}$. As a result, 0.1 m/o La_2O_2S: Eu is the ideal candidate to use within the desired optical sensor. This chapter discusses the practical considerations for the sensor design, photoluminescent and decay time results of the potential sensor head, and also the difficulties encountered during this feasibility study of the sensor design.

6.2 Considerations of the fabrication of a sensor head

6.2.1 Characteristics of the ideal phosphors

For a phosphor to be utilised within the desired sensor, it must have certain attributes which enable temperature variations to be detected. In an ideal scenario, the phosphor will exhibit a single emission line with strong luminance which is temperature dependent over the range of interest (5-60 °C). Of the phosphors studied, results have shown that a phosphor will emit multiple emission lines due to the numerous energy transitions that can take place. Each emission line has its own temperature dependent characteristics and at various levels of luminance.

In certain situations, the luminance emission strength must be strong enough to overcome environmental parameters, for example high level of blackbody radiation at high temperature[18]. For the desired sensor, such a problem does not exist. Therefore, we are able to be selective over the phosphor, its dopancy and the specific emission line to be monitored; and hence, we are able to choose the phosphor with the optimum temperature sensing dependency. The characteristics of the optimum phosphor 0.1 m/o La_2O_2S: Eu meet the required temperature range with a quenching rate of 24 $m°C^{-1}$ at an emission wavelength of 495 nm.

6.2.2 Bonding technique

The phosphor bonding technique (securing adhesion of a phosphor material to the surface undergoing thermography) [120] is another crucial factor that should not be overlooked when designing an optical sensor head. An ideal adhesion material must not contaminate or create chemical reactions with the phosphor[1].

In order to investigate the performance of a prototype sensor head, a few thick films have been produced using standard Araldite (a combination of hardener and resin, and the ratio of the mixture was 1:1) as a binder to adhere the powdered 0.1 m/o La_2O_2S: Eu to a substrate. The transparency of this binder allows the ultraviolet light to achieve satisfactory excitation of the phosphor. The PL results of the thick films have demonstrated no spectral shift in the emission wavelengths and their luminescent brightness compared favourably with the pellets as demonstrated in Figure 6-1. Most importantly, these thick films have temperature dependent characteristics which match those of the pellets over 5-60 ^{o}C with a quenching rate of ~22 mC^{-1} as shown in Figure 6-2. This implies that Araldite is a feasible and cost effective binder to use within an optical sensor. However, the thickness of this phosphor layer needs to be minimised in order to reduce the thermal gradient across the film and also to diminish the difference between the monitored and actual temperatures. As a result, some thin microporous tapes (1.25 cm x 3 m and 2.5 cm x 5 m) have been utilised as a substrate. The tape is made of a paper-like fabric, which allows the free flow of air through it. It is hypoallergenic adhesive and it also can be torn to a desired length. Most importantly, it is permeable to air and water vapour and conforms well to highly contoured body parts.

This provides a good starting point to design a non-invasive sensor head which can be simply placed in contact with human skin. Further investigations will be discussed in the future work section in Chapter 7.

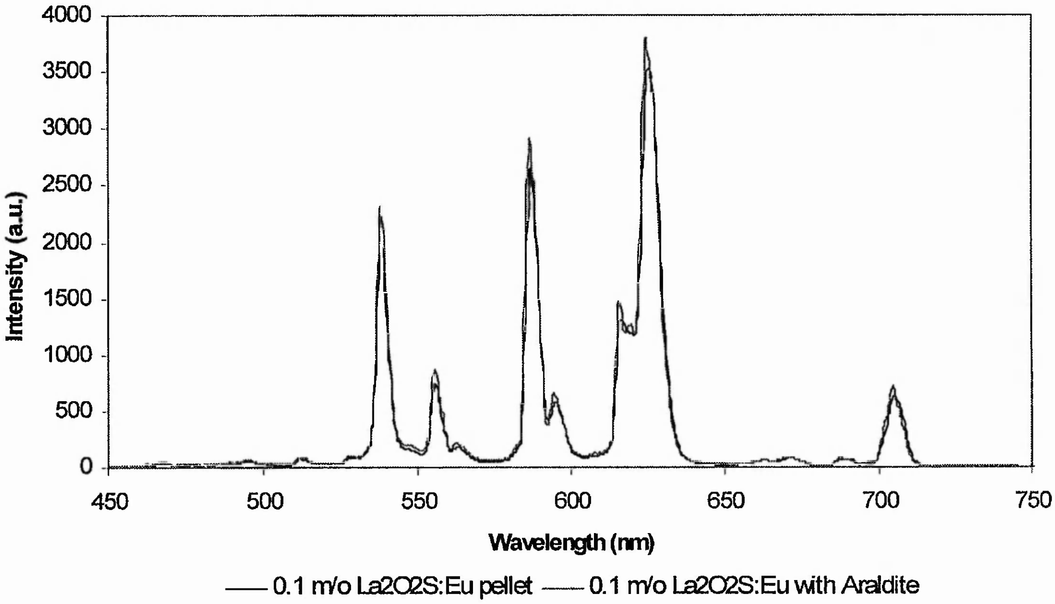

Figure 6-1: Emission spectra of 0.1 m/o Eu pellet and 0.1 m/o Eu with Araldite under 337 nm excitation.

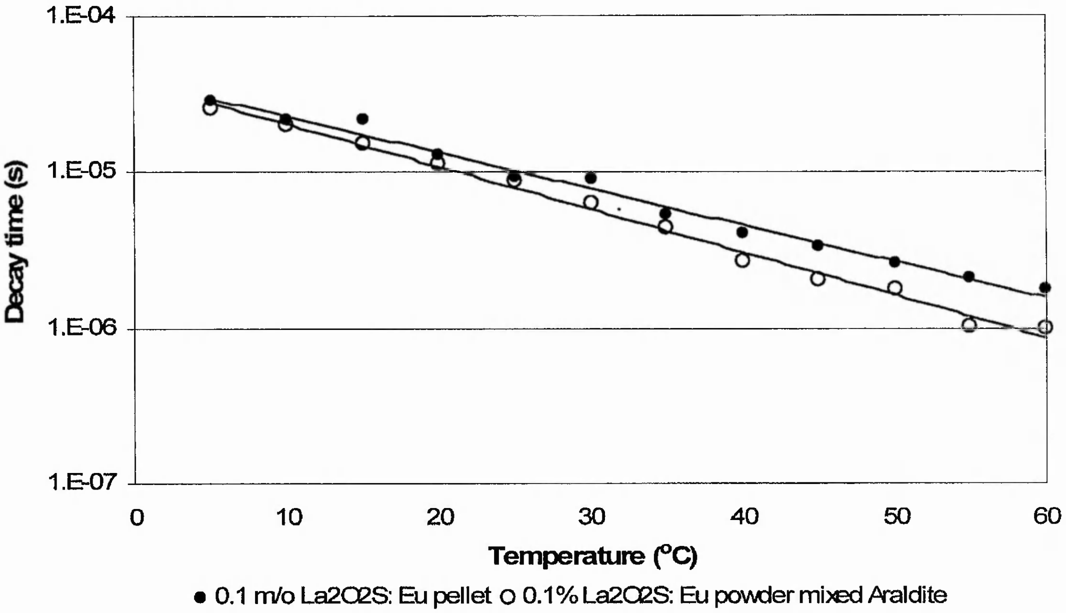

Figure 6-2: Decay time comparison of 0.1 m/o Eu pellet and 0.1 m/o Eu with Araldite under 337 nm excitation.

6.2.3 Experimental techniques

In experimentation so far, a nitrogen pulsed laser (337 nm excitation wavelength) was utilised to excite the phosphors. An alternative excitation source would be a low cost UV LED, enabling cost reduction and miniaturisation in comparison to the traditional solid-state laser system. As a consequence, three narrow-band UV LEDs (model no. TO-39 package UV TOP® with hemispherical lens for focused emission pattern, 12 nm FWHM, output power of 0.5 mW at 5.5 V) operating at 300 nm, 335 nm and 345 nm respectively were purchased from Sensor Electronic Technology, Inc. The selected emission wavelengths of the LEDs correspond to the optimum excitation wavelength of La_2O_2S: Tb at 300 nm and La_2O_2S: Eu at 345 nm, whereas 335 nm LED was selected for making a comparison with the 337 nm nitrogen laser. Each of these LEDs was incorporated into a basic electronic circuit (with a 220 ohm resistor in series) and driven by a 10 V pulse generator, providing a typical output voltage of 5.5 ± 0.1 V across the UV LED. The output pulses of the pulse generator and an UV LED were recorded using an oscilloscope as shown in Figure 6-3.

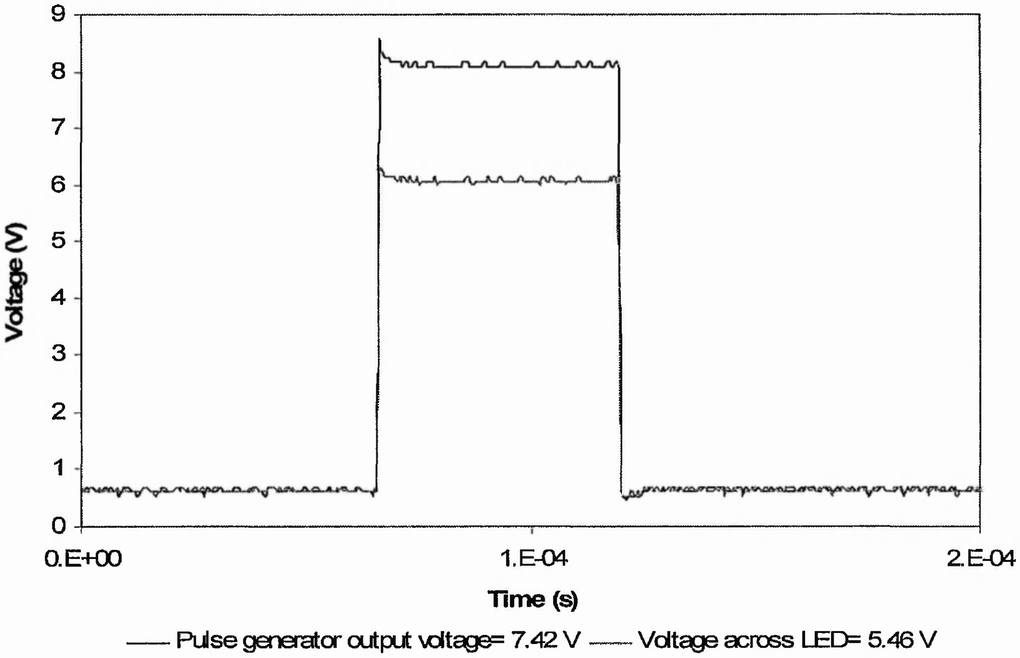

Figure 6-3: Output signals of the pulse generator and an UV LED.

6.2.3.1 Photoluminescent measurement

The experimental arrangement for photoluminescent measurement has been realigned differently to the previous set-up as mentioned in Chapter 3, due to the use of the UV LED as the excitation source. A two optical-fibre design was implemented, one for delivery of the UV excitation radiation and the other for collection of the visible phosphor emission. The PL experimental set-up is illustrated schematically in Figure 6-

4. A 84-series collimating lens (84-UV-25, Ocean Optic Inc.) was used to couple the LED excitation beam to a quartz optical fibre (1000 μm in core diameter) in order to increase the light output and a 74-UV collimating lens is attached to another end of the fibre to focus the UV light transmitted down the fibre onto the sample. The luminescence of the sample was subsequently collected by a separate quartz optical fibre (600 μm in core diameter) with a cut-on filter (wavelength > 380 nm), which subsequently transmitted the signal to a spectrometer via analogue-to-digital converter. The resultant signal is finally stored and analysed using a computer with Ocean Optics SpectraSuite software as before.

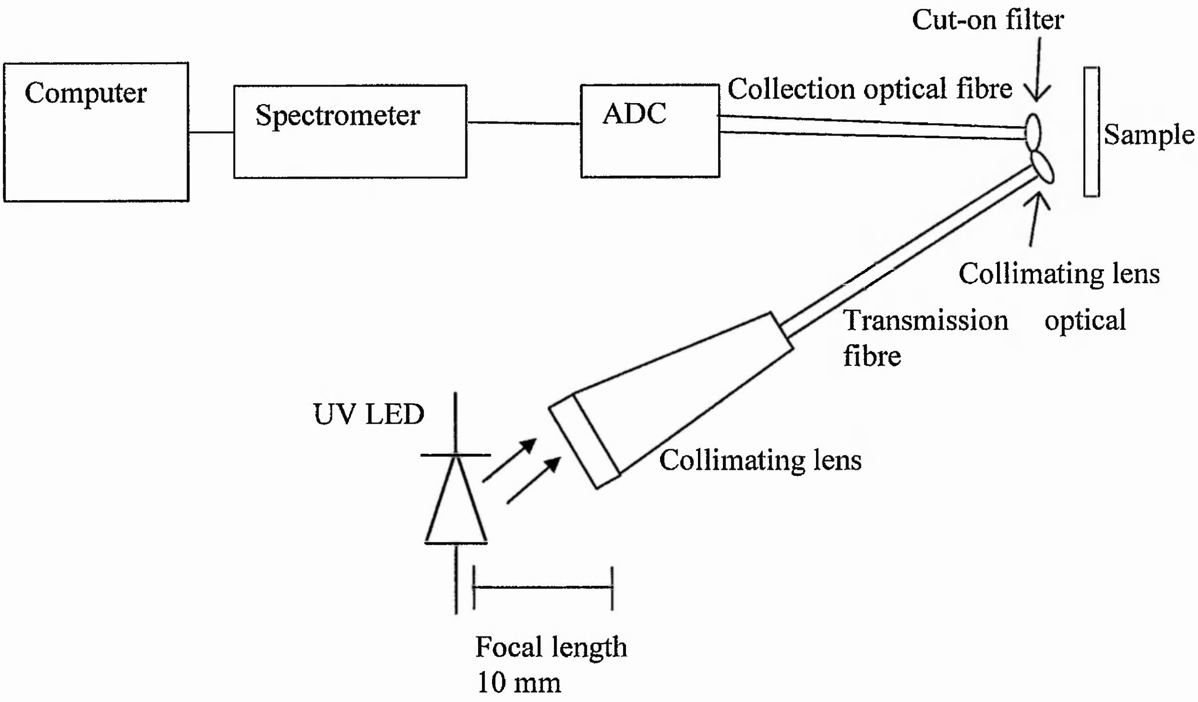

Figure 6-4: PL experimental arrangement using an UV LED as an excitation source.

To evaluate the feasibility of using the UV LED as an excitation source, the PL measurements began with the standard concentration 7.36 m/o of La_2O_2S: Eu and 10 m/o La_2O_2S: Tb as a benchmark for other dopant concentrations due to the most intense emission level at their respective dominant wavelength. These phosphors were excited by different LEDs at 300 nm, 335 nm and 345 nm excitation wavelengths. From the PL spectra of La_2O_2S: Eu and La_2O_2S: Tb shown in Figure 6-5 and Figure 6-6 respectively, it is clear that La_2O_2S: Eu at 7.36 m/o exhibited a bright red luminescence with comparable intensities and no shifts in emission wavelength when excited by the different excitation wavelength LEDs. Due to both optical losses within the quartz fibres and the lower output power of the UV source, the integration time for collecting the emission spectra had to be increased to 1500 ms (approximately 10 times longer than that utilised when using the nitrogen laser).

Unfortunately, sufficient brightness for La_2O_2S: Tb at 10 m/o could only be achieved under 300 nm excitation and its emission intensities dropped drastically by a factor of 40 when excited with the 335 nm and 345 nm LEDs. The emission peaks of La_2O_2S: Tb at other dopant concentrations less than 10 m/o were non detectable with the same integration time (1500 ms). Hence, the integration time was increased to 10,000 ms allowing more photons to be captured by the spectrometer in order to determine the emission peaks. However, the background noise increases by increasing the integration time which causes the lower emission peaks to become indistinguishable in the spectrum.

These initial results have shown that although La_2O_2S: Tb does have the required temperature sensing capabilities, excitation via an UV LED is inefficient resulting in low emission levels, with only 10 m/o showing an acceptable level of luminance. Compare to La_2O_2S: Eu, good emission levels have been achieved and thus can be studied further for its decay time characteristics.

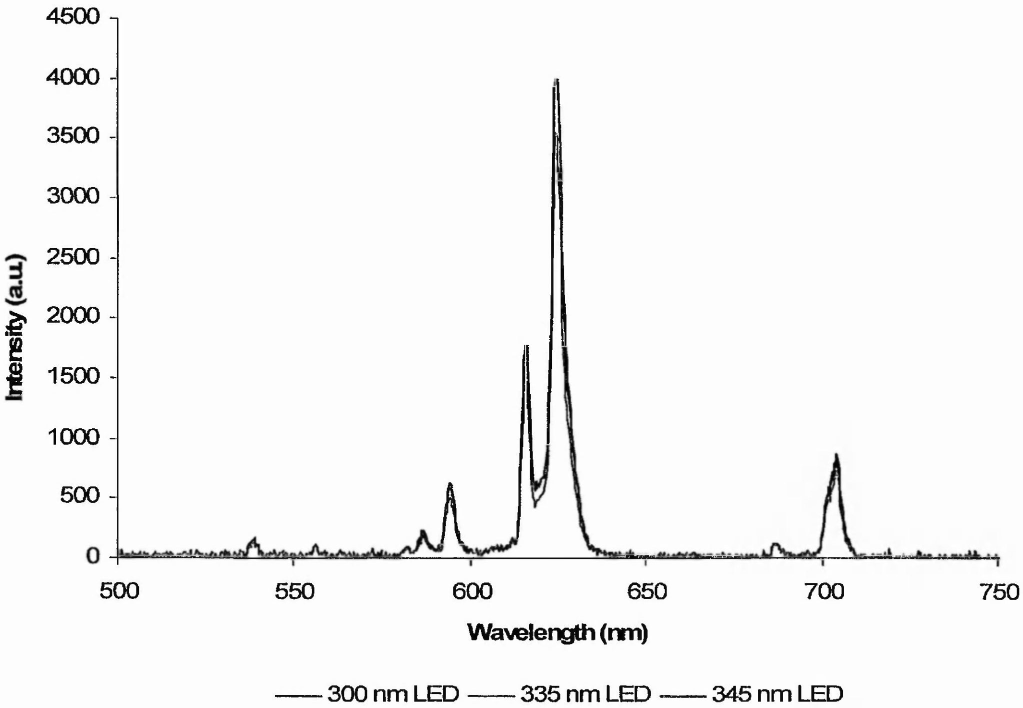

Figure 6-5: Emission spectrum of La_2O_2S: Eu at 7.36 m/o excited by different excitation wavelengths LEDs with an integration time of 1500 ms.

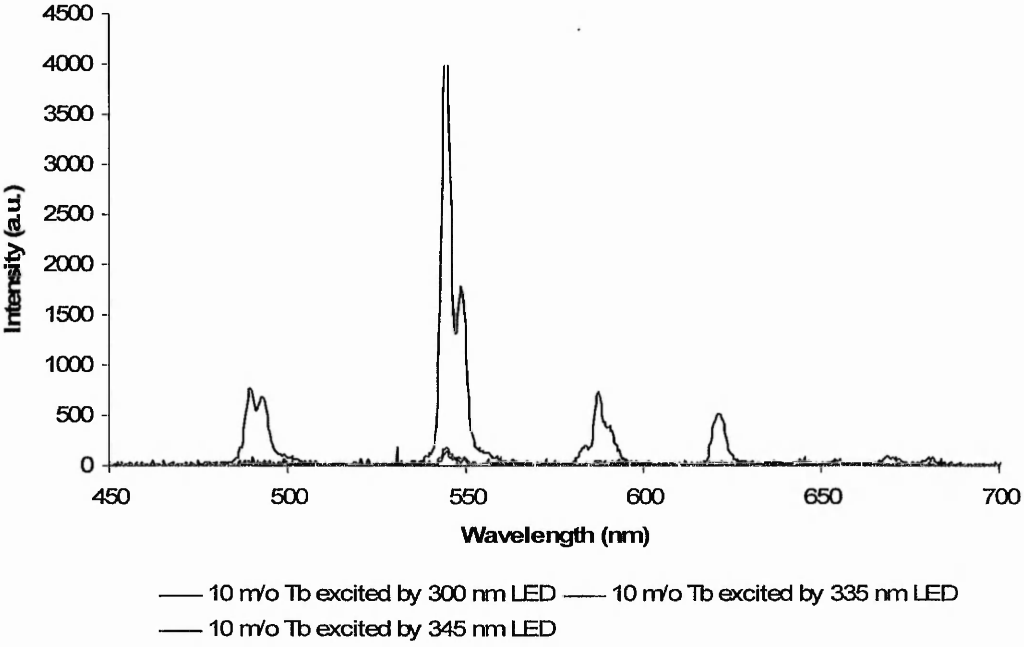

Figure 6-6: Emission spectrum of 10 m/o La_2O_2S: Tb excited by different excitation wavelengths LEDs with an integration time of 1500 ms.

The PL measurements were subsequently carried out using the optimum phosphor 0.1 m/o La_2O_2S: Eu in a form of pellet and also thick film, a mixture of phosphor with Araldite daubed on a microporous tape. These phosphor samples were excited by the excitation wavelength at 345 nm using the specific LED, their emission spectra are shown in Figure 6-7. Surprisingly, the emission spectrum of the thick film is more intense than the pellet, this may be due to the difference in the surface roughness of the samples. The overall emission intensity of 0.1 m/o La_2O_2S: Eu is weaker than the standard concentration of La_2O_2S: Eu by a factor of 8. Nevertheless, the results have proven that the UV LED operating at 345 nm is capable to excite the optimum phosphor 0.1 m/o La_2O_2S: Eu both in pellet form and the desirable thick film.

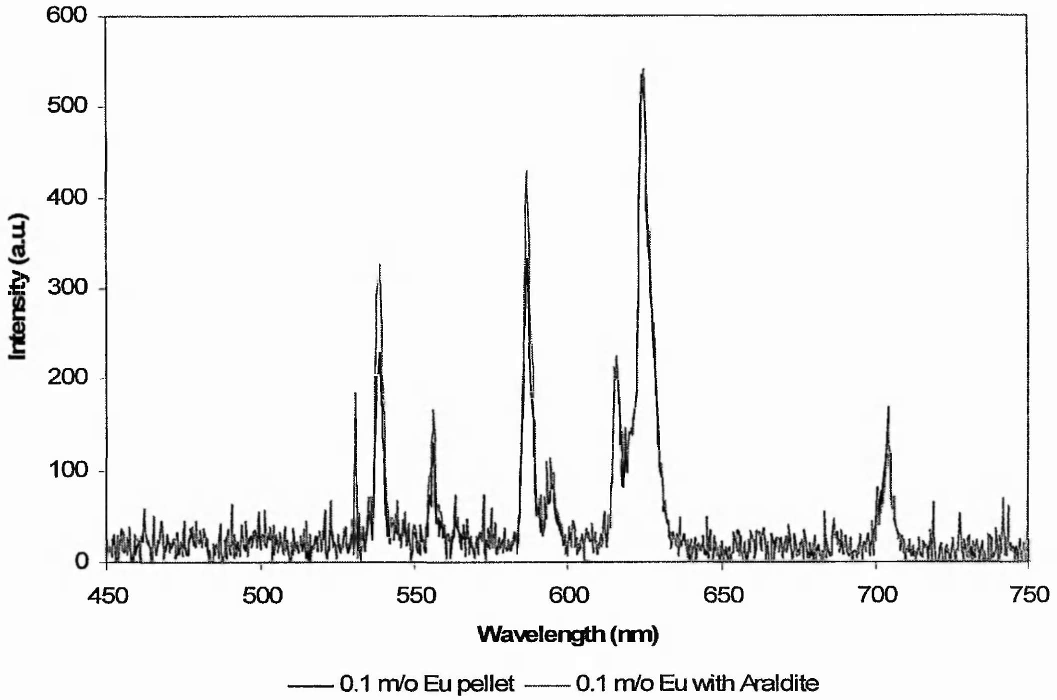

Figure 6-7: Emission spectra of 0.1 m/o La_2O_2S: Eu excited by 345 nm LED at room temperature.

6.2.3.2 Decay time measurement

The decay time experimental arrangement is similar to the set-up as described in Chapter 3, the only difference is that the nitrogen laser has been replaced by a LED source along with the optics and a transmission quartz optical fibre as illustrated previously. Although the initial PL results have proved that the excitation of LED at 345 nm is possible for 0.1 m/o La_2O_2S: Eu, the decay time measurements have induced doubts as to the possibility of using the LED source to excite the phosphor.

Similar to the PL set-up, the UV light from the LED was delivered by an optical fibre through the collimating lenses on to the sample. Since the luminescence signal from the phosphor was very weak, the quartz rod from the decay system was removed and the PMT was positioned directly in front of the sample to allow direct collection of the emission. Two filters were attached to the front of the PMT – the first was a UV cut-on filter to eliminate the UV pulsed signal from the PMT; and the second was a bandpass filter to select the 512 nm emission peak only. The decay curve of 0.1 m/o La_2O_2S: Eu at 512 nm line excited by 345 nm LED at a repetition rate of 1 kHz is shown in Figure 6-8. The decay time of this emission signal was deduced using the standard single decay exponential relationship and it is in agreement with the decay time of the same signal excited by the nitrogen laser, at approximately 10 μs. However, when the measurements were carried out over a wider temperature range of 5-60 °C with the 345 nm LED, the decay times of 0.1 m/o La_2O_2S: Eu at 512 nm showed a trend that is completely in disagreement with the results achieved using the laser excitation as demonstrated in Figure 6-9. This suggests that the decay signals excited by the LED were possibly too weak to be picked up by the detector and hence dominated by the noise.

Difficulties associated with the LED excitation have been encountered throughout the decay time measurement and various approaches such as varying the parameters of the pulse generator and realignment of the experimental set-up were attempted to overcome the problems. However, the phosphor emission signal is still difficult to be detected using the photomultiplier tube and the decay time results obtained to date remain inconclusive. Investigations into the decay time with LED excitation had to call a halt up to this point due to time constraint and this will be discussed in Chapter 7.

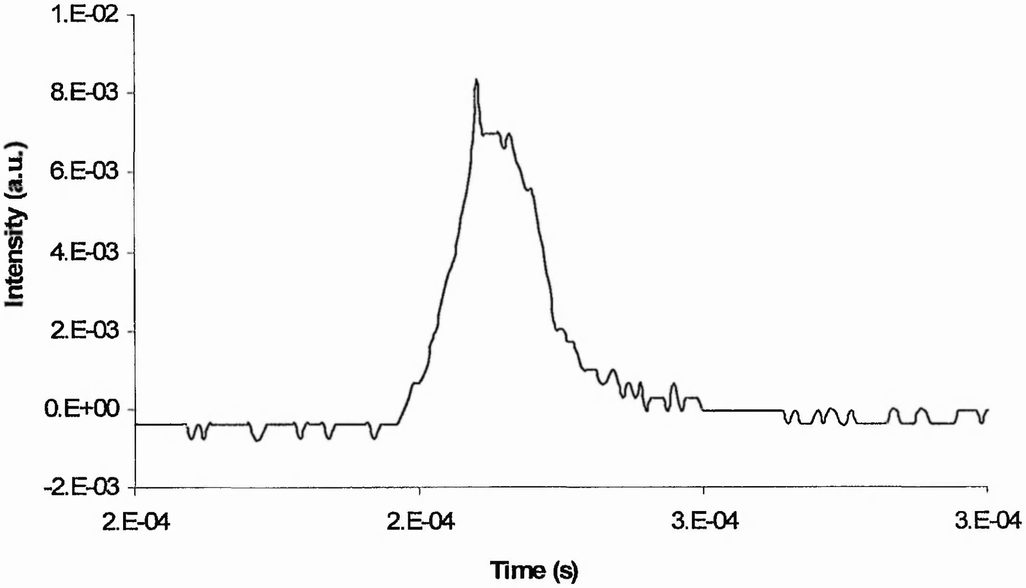

Figure 6-8: Decay signal of 0.1 m/o La_2O_2S: Eu at 512 nm line excited by 345 nm LED at room temperature.

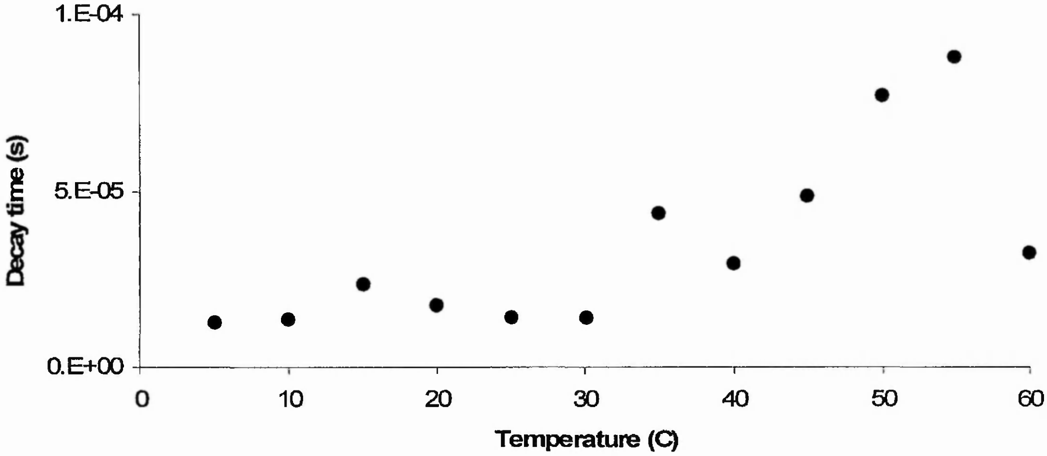

Figure 6-9: Decay times of 0.1 m/o La_2O_2S: Eu at 512 nm excited by 345 nm LED.

6.3 Summary

This feasibility study on the fabrication of an optical sensor head has clearly illustrates the need for further investigation. Although it has been proven the excitation using an UV LED is achievable, results for the decay time temperature dependent characteristics remain inconclusive. In particular, the potential issues regarding the creation of a prototype sensor head are:-

- Phosphors are widely used in optical sensing technology for various applications due to their temperature dependencies, however, long term exposure to phosphor may result in skin irritation. Particular attention must be devoted to the requisites of biocompatibility, an appropriate membrane that acts as a protective shield is therefore required to isolate the phosphor from human skin. As a consequence, thermal conductivity and the length of contact time between the human skin and the bonding of the phosphor need to be taken into account for the sensor head design.
- A simple structure of prototype sensor head was created by mixing the phosphor powder with Araldite daubed on a microporous tape. Although Araldite is compatible with the phosphor giving satisfactory results, but again it may be an irritant to human skin. A suitable binder that does not adversely affect the body is required to form a desired sensor head.
- The requisites of the excitation source such as compactness, adequate power and appropriate wavelength especially in the deep UV region, are not always fulfilled. The main problem and difficulties that arose when carrying out the decay time experiments is insufficient output power of the LEDs. The low

signal-to-noise ratio has led to the decay data analysis being susceptible to large errors.

Chapter 7 Conclusions and future work

7.1 Introduction

The main aim of this project was to investigate the temperature sensing capabilities of phosphor materials for use within an optical sensor to monitor human skin temperature, in particular within a MRI scanner. A robust and reliable optical sensor that can survive within such an electromagnetically hostile environment is desired for clinicians to offer an improvement in patient care and also to provide reassurance of a patient's physical comfort and safety. In this research, phosphor thermography has been adapted as a measurement method to determine the temperature of human skin. With a thin coated layer of thermographic phosphor placed in contact with the patient's skin, the skin temperature could then be determined by measuring the lifetimes of photoluminescence after UV pulsed excitation. The feasibility of using thermographic phosphors for the creation of an optical sensor has been carried out via a series of thermographic characterisations, including photoluminescent emission and decay time of photoluminescence at various temperatures. In addition, a full analysis of the crystal structure and crystallinity of the selected phosphors has been performed via x-ray diffraction. The results presented within this body of work have shown that the research objectives including the creation of a prototype sensor head have been achieved with reasonable success.

The work undertaken for this thesis has primarily concentrated on the thermographic characterisation of La_2O_2S: Eu and La_2O_2S: Tb over a range of dopant concentrations. The remarkable results generated from this research have resulted in the publication of two refereed journal articles (see the list of publications). From these results, it was evident that the investigated phosphors are strongly temperature dependendent, specifically over the temperature range of interest, 5-60 °C. In addition, extensive analysis of PL emission, decay time and XRD has highlighted the importance of dopant concentration in varying the optical and physical properties of these phosphors. As a consequence of that, both of the phosphors are found to have a greater sensitivity to temperature variance at lower dopant concentrations. More interestingly, the discovery of the novel decay time characteristic of La_2O_2S: Tb > 2 m/o which has an inverse manner to the conventional decay time characteristic has opened a new window for phosphor thermography applications. It is also important to note that the primary objective of this research for the identification of the most suitable phosphor for use in the fabrication of the sensor has been achieved successfully. La_2O_2S: Eu at 0.1 m/o has been identified as a highly sensitive phosphor with a quenching rate of 24 m$^\circ C^{-1}$ and thus it has been employed for the production of a prototype sensor head at the concluding level of this work.

Finally, the findings of this research and recommendations for future work are discussed below.

7.2 Achievements

The following is a summary of the achievements of this research:-

1) Experimental system to thermographic phosphor measurements

A robust analysis system has been developed for photoluminescent measurement and decay time characterisation to be carried out within a high precision controlled temperature environment from 5 to 60 °C. The limitations of the manufactured glass door have prevented the optical access to the sample. This problem has been overcome by replacing with a cost-effective polystyrene window containing apertures for the transmission and collection optics. An accuracy of ± 0.5 °C was achieved. This well designed temperature-controlled environment has offered good repeatability and high consistency with an error of less than 5% deviation for decay time measurement.

2) Characterisation of La_2O_2S: Eu

Thermographic characterisation of La_2O_2S: Eu has been carried out for a series of dopant concentrations from 0.005 to 15 m/o by using a pulsed nitrogen laser at 337 nm. The temperature sensing capability of this phosphor has been optimised by varying the dopancy levels over 5 to 60 °C. It was found that the emission intensities of the temperature dependent lines at lower dopant concentrations, notably 467, 495, 512 and 538 nm lines, appear to be an order of magnitude greater than that of higher Eu concentrations. The maximum brightness of these lines occurred at 1 m/o of La_2O_2S: Eu. Following this, the decay times of the temperature dependent lines were fitted with the single exponential decay relationship and these results have proven that lower dopant concentration has a better sensing capability. Despite the intense brightness at 1 m/o, the optimum temperature sensitivity was achieved at 0.1 m/o of La_2O_2S: Eu which has a superior quenching rate of 24.03 m°C^{-1} and an accuracy of 0.4 °C (calculated from five different pellets compacted using the same source of 0.1 m/o of La_2O_2S: Eu) at 495 nm as compared to 13.7 m°C^{-1}[113] of the well-known 512 nm line reported elsewhere. In addition, a consistent trend which indicates a reduction in decay time with increasing Eu concentration has been observed. The decay times of 15 m/o Eu are faster by an order of magnitude than that of 0.1 m/o Eu. This implies that higher Eu concentrations with shorter decay times are less sensitive to temperature fluctuations when compared to low Eu concentrations. A linear relationship between the crystallinity and dopant concentration has also been established via x-ray diffraction, it has been shown a shrink in the crystallite size and *c*-axis parameter versus Eu concentration. Correlating this observation to the temperature sensitivity of a phosphor, lower dopant concentration phosphors with larger crystallite size induced a slower decay rate but a higher quenching rate, suggesting they are more superior in temperature sensing to a higher dopant concentration phosphor (smaller crystallite size). However, further investigation is required to validate this relationship.

3) Characterisation of La_2O_2S: Tb

La_2O_2S: Tb has been characterised over an extensive dopant concentration range of 0.005 – 50 m/o. A change in the relative intensities of the different transitions is observed with varying dopant concentration and this is due to the Spark splitting effect. More emission lines can be seen for below 0.2 m/o Tb at longer wavelengths and these lines tend to be temperature dependent. Furthermore, the emission intensity of various wavelengths increases with dopant concentration and eventually the maximum brightness quenched at 10 m/o as a result of concentration quenching. An increase in the emission intensity has improved the decay time analysis in terms of a better signal-to-noise ratio in the signal and also a shorter time for the data acquisition process, as all the emission lines peaking within the visible region were found to be temperature dependent. On the other hand, the decay time measurement indicated that La_2O_2S: Tb has a lower quenching rate of 3 m $^{o}C^{-1}$ on average due to its faster decay time, implying that this phosphor is less efficient than La_2O_2S: Eu. However, it is interesting to note that a novel decay time characteristic has been discovered for La_2O_2S: Tb in this research: an unusual rise in decay time with increasing temperature was evident over dopant concentrations of 2-50 m/o and this will be further discussed below. Similar to La_2O_2S: Eu, XRD results have also shown that as the dopancy is increased, the (100) and (002) reflections merge and there is a reduction in the *c*-axis parameter as well as the crystallite size.

4) Discovery of a novel decay time characteristic

For the first time in the field of phosphor thermography, an unexpected decay time characteristic which shows an increase in decay time against temperature for > 2 m/o of La_2O_2S: Tb is introduced here as a newly discovered temperature dependent characteristic. It is hypothesised that as the dopant concentration is increased, the resonance interaction between the neighbouring terbium ions will become greater and this would potentially slow down the luminous decay process leading to a longer decay time with temperature. It was also believed that this hypothesis can be supported by determining the thermal expansion parameters of the unit cell as a function of temperature. Therefore, for comparison purposes, a series of XRD experiments was carried out for 0.005, 0.91, 2, 15 and 50 m/o within a furnace from 30 to 100 °C. The results showed a positive thermal expansion behaviour indicating an increase in the *a* and *c*-axis and cell volume with temperature. Disappointingly, >2 m/o Tb were also found to behave in the same manner. In summary, evidence for this hypothesis still remains inconclusive.

5) Feasibility of producing a prototype sensor head

While the primary objective is satisfied, a prototype sensor head has been evaluated using 0.1 m/o of La_2O_2S: Eu bonded with a commercially available binder Araldite. The resultant phosphor mixture was coated on a microporous tape which acts as a protective shield to human skin. The results of PL emission and decay time excited by a nitrogen laser at 337 nm have validated the compatibility of the binder with the phosphor. The thick films have a quenching rate of ~22 $m°C^{-1}$ which match those of the pellets over 5-60 °C. Considerably cheaper and more compact than an industrial UV laser, the use of an UV LED has provided a low cost alternative towards the sensor design. Unfortunately, the low level output energy of an UV LED has restricted the decay time characterisation to be performed adequately and hence the commercial viability of the present prototype sensor head cannot be fully assessed. This inconclusive study will consequently form a basis for future work.

7.3 Future work

The ultimate goal of this research is to produce a versatile and an efficacious optical sensor for the determination of human skin temperature within a MRI scanner. Therefore, for further assessment, a sensor head consisting of the optimum thermographic phosphor requires a full development programme for either invasive or non-invasive temperature measurement following this initial feasibility investigation. In addition, further investigation is required to gain insight into the discovery of the unprecedented decay time characteristic of La_2O_2S: Tb.

In order to aid in the progress of this ultimate objective, the following is a list of proposed future work for further research to be undertaken:

7.3.1 Development of the fabrication of the optical sensor

1) To fully utilise the luminescent properties and temperature sensitivity of 0.1 m/o La_2O_2S: Eu for use within the sensor, it is important to excite the phosphor corresponding to its optimum excitation wavelength at 350 nm. At present, characterisations of phosphors are difficult to be performed at this excitation wavelength due to a significant problem associated with inadequate output power of an UV LED. This issue could potentially be overcome by using a high power UV LED lamp which consists of multiple light emitting devices.

2) As phosphor materials and the binder candidate Araldite may cause skin irritation to a patient, a more suitable and biocompatible binder such as a silicone resin is

therefore required to adhere the powdered phosphors for use within a sensor head. Furthermore, an efficient bonding method such as using an air brush would be helpful to minimise the thickness of the phosphor layer in order to reduce the thermal gradient across the film and also to diminish the difference between the monitored and actual temperatures.

3) It has been reported by other researchers[121, 122] that certain phosphors show cross-sensitivity with regards to oxygen quenching, the luminescence signal of a material is observed to increase with decreasing oxygen concentration. As a result, it would be interesting to carry out the characterisation process within an oxygen partial pressure environment to examine if the investigated phosphors are oxygen dependent. The findings of this exercise would possibly lead to the development of a new environmental sensor for both in vitro and in vivo oxygen measurements, in particular for use in medical applications.

4) Prior to the final stage of the fabrication of the sensor, it would be beneficial to seek collaborations with hospitals in order to assess the viability and performance of the end product within a MRI scanner. Further investigations are required to look into the complexities of non-invasive temperature measurement such as determining the thermal conductivity between the bonding of the phosphor and human skin. In addition, an investigation into the potential problem associated with the Zeeman splitting within a MRI is also essential as RV Alves[123] in the 1970s reported splitting of energy levels in magnetic fields at 5 Tesla (T). However, the average

MRI scanner utilises a magnetic field strength of ≤1.5 T, and hence should not be problematic for such a sensor.

7.3.2 Investigation into the novel decay time characteristic of La_2O_2S: Tb

Firstly, an extensive study of the optical and physical properties of La_2O_2S: Tb is required to fully understand and explain the unexpected manner of the decay time characteristic. It would be interesting to carry out further investigations using dopant concentrations higher than 50 m/o up to 100 m/o Tb to explore if the trend of the novel temperature dependent characteristic continues as a result of Stark Splitting effect. In this case, XRD analysis is a crucial factor to correlate the thermal expansion parameters of a unit cell to the lifetime behaviour. In addition, an investigation into decay time characterisation over a wider temperature range may be useful to aid the justification of the discovered lifetime behaviour with relates to the crossover thermal quenching from $4f^n$ emitting states to $4f^{n-1}5d$ states. To maximise the exciting energy to be absorbed into the $4f^n$ emitting states, the use the optimum excitation wavelength at 300 nm is advantageous for the characterisations of La_2O_2S: Tb.

In summary, La_2O_2S: Eu and La_2O_2S: Tb have been identified primarily as the potential phosphors for use in the creation of an optical sensor. To pursue the objectives of this research closely, a detailed literature review of the selected thermographic phosphors and a series of phosphor characterisations in terms of photoluminescent characteristic, decay time characterisation and x-ray diffraction have been carried out using various dopant concentrations over 5-60 °C. Experimental results have demonstrated that the luminescent properties, decay time characteristics as well as the crystallinity of the phosphors are governed by dopant concentration. For instance at low Eu concentrations, the temperature dependent lines at shorter wavelengths are stronger than they are at higher concentrations. It has been observed that lower concentrations are more sensitive to temperature. With the results obtained in this work, the identification of the most ideal phosphor for use within an optical sensor has been achieved successfully, that is 0.1 m/o of La_2O_2S: Eu with a promising quenching rate of 24 m°C^{-1}. More importantly, a novel decay time characteristic of La_2O_2S: Tb > 2m/o has been discovered within this body of work and a theoretical modelling with relates to the probability of non-radiative transitions has been discussed. This unusual phenomenon has generated further interest in the field of phosphor thermography.

List of References

[1] S. W. Allison and G. T. Gillies, *'Remote thermometry with thermographic phosphors: instrumentation and applications'*, Review of Scientific Instruments, vol. 68(7), pp. 2615-2650, 1997.

[2] K. A. Wickersheim and M. H. Sun, *'Fiberoptic thermometry and its applications'*, Journal of Microwave Power and Electromagnetic Energy, vol. 22, no. 2, pp. 85-94, 1987.

[3] R. M. Ranson, *'PhD dissertation: 'Investigation into thermographic phosphors'*, Nottingham Trent University, pp. 1-6, 1999.

[4] S. Sato, N. Okubo, S. Yamashita, S. Yamamoto, M. Kumagai, S. Kihara and H. Nakayama, *'Age-related decrease in toe-thumb temperature difference with lumbar epidural anaesthesia'*, Canadian Journal of Anesthesia, vol. 41, no. 7, pp. 579-582, 1994.

[5] K. A. Wickersheim, S. O. Heinemann, H. N. Tran and M. H. Sun, *'Second generation fluoroptic thermometer'*, ISA, Research Triangle Park, USA, p. 87, 1985.

[6] L. Jansky, V. Vavra, P. Jansky, P. Kunc, I. Knizkova, D. Jandova and K. Slovacek, *'Skin temperature changes in humans induced by local peripheral cooling'*, Journal of Thermal Biology, vol. 28, no. 5, pp. 429-437, 2003.

[7] G. Wasner, J. Schattschneider and R. Baron, *'Skin temperature side differences - a diagnostic tool for CRPS?'* Journal of Pain, vol. 98, no. 1-2, pp. 19-26, 2002.

[8] R. M. Ranson, C. B. Thomas and M. R. Craven, *'A thin film coating for phosphor thermography'*, Journal of Measurement Science and Technology, vol. 9, pp. 1947-1950, 1998.

[9] R. M. Ranson, E. Evangelou and C. B. Thomas, *'Modeling the fluorescent lifetime of Y_2O_3: Eu'*, Applied Physics Letters, vol. 72, no. 21, pp. 2663-2664, 1998.

[10] D. L. Beshears, G. J. Capps, C. M. Simmons and S. W. Schwenterly, *'Laser-induced fluorescence of phosphors for remote cryogenic theromometry'*, p. 20 1990.

[11] K. A. Wickersheim, *'Fiberoptic thermometry based on measurement of fluorescent decay time and it's applications'*, Microwave Power Symposium, p. 105, 1986.

[12] Pyro-Optical, *'Classic photoscreenic wedge type pyrometer'*, The Pyrometer Instrument Company, Inc., pp. 903-904, 2007.

[13] B. G. Lipták, *'Instrument Engineers' Handbook: Process measurement and analysis '*, CRC Press, pp. 637-639, 2003.

[14] C. B. Carter and M. G. Norton, *'Ceramic materials: Science and engineering'*, Springer, p. 150, 2007.

[15] K. A. Wickersheim, *'Optical temperature measurement technique utilizing phosphors'*, US patent no. '4075493', 1978.

[16] R. Chang, *'Physical chemistry for the biosciences '*, University Science Books, p. 150, 2005.

[17] R. Ranson, *'Phosphors for biomedical and environmental sensing technology'*, EPSRC grant proposal (GR/T27792/01), 2003.

[18] R. M. Ranson, *'PhD dissertation: 'Investigation into thermographic phosphors'*, Nottingham Trent University, 1999.

[19] A. Farzana, *'Temperature of a healthy human (skin temperature)'*, The Physics Factbook, 2001.

[20] C. R. Nave, '*HyperPhysics: Cooling of the Human Body* ', Georgia State University, 2006.

[21] K. Agarwal, A. Lange and H. Beck, '*Thermal imaging in healthy humans- What is "normal" skin temperature?*' InfraMation 2007 Proceedings, ICT 121A, 2007.

[22] C. M. Tipton, M. N. Sawka, R. L. Terjung and C. A. Tate, '*Physiological systems and their responses to conditions of heat and cold*', ACSM's Advanced Exercise Physiology, pp. 535-563, 2005.

[23] R. D. Watson and K. S. Chapman, '*Radiant heating and cooling handbook* ', McGraw-Hill Professional, pp. 3.3-10, 2002.

[24] T. Togawa, '*Body temperature measurement*', Clin. Phys. Physiol. Meas., vol. 6, no. 2, pp. 83-108, 1985.

[25] T. D. McGee, '*Principles and methods of temperature measurement*', Wiley-IEEE, pp. 2-4, 1988.

[26] H. C. Bolton, '*Evolution of the thermometer* ', The Chemical publishing co., pp. 1592-1743, 1900.

[27] S. Shionoya and W. M. Yen, '*Phosphor handbook*', CRC Press LLC, pp. 5-8, 1998.

[28] B. M. Wagenaar and R. Meijer, '*Novel method for non-contact measurement of particle temperatures*', AIChE Journal, vol. 41, no. 4, pp. 773-781, 1995.

[29] P. C. Lauterbur, '*Image formation by induced local interactions: examples of employing nuclear magnetic resonance*', Nature, vol. 242, pp. 190-191, 1973.

[30] L. C. Bradley, '*A temperature sensitive phosphor used to measure surface temperatures in aerodynamics*', Review of Scientific Instruments, vol. 24, no. 3, p. 219, 1953.

[31] F. Urbach, *'Measurement of temperature distribution on the surface of solid bodies '*, US patent no. 2551650, 1951.

[32] K. A. Wickersheim, R. V. Alves and R. A. Buchanan, *'Rare earth oxysulfide x-ray phosphors'*, Nuclear Science, IEEE Transactions, vol. 17, no. 1, pp. 57-60, 1970.

[33] G. Webster and H. G. Drickamer, *'High pressure studies of luminescence efficiency and lifetime in* La_2O_2S*:Eu and* Y_2O_2S*:Eu'*, Journal of Chemical Physics, vol. 72, no. 6, p. 3740, 1980.

[34] G. Blasse and B. C. Grabmaier, *'Luminescent materials'*, Springer-Verlag Berlin Heidelberg, p. 1, 1994.

[35] S. Shionoya and W. M. Yen, *'Phosphor handbook'*, CRC Press LLC, pp. 4-5, 1998.

[36] H. W. Leverenz, *'An introduction to luminescence of solids'*, John Wiley and Sons, New York, 1950.

[37] R. C. Ropp, *'Luminescence and the solid state'*, Elsevier, vol. 12, pp. 252-253, 1991.

[38] P. Neubert, *'Device for indicating the temperature distribution of hot bodies'*, US patent no. 2071471, 1937.

[39] F. Urbach, N. R. Nail and D. Pealman, *' The observation of temperature distributions and of thermal radiation by means of non-linear phosphors'*, Journal of the Optical Society of America, vol. 39, pp. 1011-1017, 1949.

[40] L. G. V. Uitert, R. C. Linares and R. R. Soden, *'Role of f-orbital electron wave function mixing in the concentration quenching of* Eu^{3+}*'*, Jn Chem. Phys, vol. 36, no. 3, pp. 702-705, 1962.

[41] J. Silver, '*Inorganic phosphors yesterday, today and tomorrow*', DisplayMasters presentation material, 2006.

[42] S. Shionoya and W. M. Yen, '*Phosphor handbook*', CRC Press LLC, p. 21, 1998.

[43] G. Blasse and B. C. Grabmaier, '*Luminescent materials*', Springer-Verlag Berlin Heidelberg, pp. 2-3, 1994.

[44] G. Blasse and B. C. Grabmaier, '*Luminescent materials*', Springer-Verlag Berlin Heidelberg, pp. 10-11, 1994.

[45] T. S. Kuhn, '*Energy conservation as an example of simultaneous discovery*', in M. Clagett (ed.) Critical problems in the history of science, pp. 321-356, 1957.

[46] G. Sarton, '*The discovery of the law of conservation of energy*', Isis, vol. 13, pp. 18-49, 1929.

[47] R. M. Ranson, '*PhD dissertation: 'Investigation into thermographic phosphors*', Nottingham Trent University, p. 15, 1999.

[48] M. J. Weber, '*The handbook on the physics and chemistry of rare-earths*', no. 35, pp. 275-315, 1979.

[49] M. Fox, '*Optical properties of solids* ', Oxford University Press, pp. 192-195, 2006.

[50] R. M. Ranson, '*PhD dissertation: 'Investigation into thermographic phosphors*', Nottingham Trent University, pp. 148-150, 1999.

[51] J. L. Sommerdijk and A. Bril, '*Efficiency of* Dy^{3+} *activated phosphors*', vol. 122, p. 952, 1975.

[52] L. P. Goss and A. A. Smith, '*Surface thermometry by laser induced fluorescence*', Review of Scientific Instruments, vol. 60, no. 12, pp. 3702-3706, 1989.

[53] R. M. Ranson, *'PhD dissertation: 'Investigation into thermographic phosphors'*, Nottingham Trent University, pp. 16-17, 1999.

[54] J. Ervin and C. Murrawski, *'Temperature measurement of a curved surface using thermographic phosphors'*, Experimental Thermal and Fluid Science, vol. 11, pp. 387-394, 1995.

[55] A. Bethell, *'PhD dissertation: Remote measurement of temperature using laser induced luminescence'*, Loughborough University, pp. 19-20, 2002.

[56] H. Kusama, O. J. Sovers and T. Yoshioka, *'Line shift method for phosphor temperature measurements'*, Japanese Journal of Applied Physics, vol. 15, pp. 2349-2358, 1976.

[57] D. J. Bizzak and M. K. Chyu, *'Rare-earth phosphor laser-induced fluorescence thermal imaging system'*, Review of Scientific Instruments, vol. 65, no. 1, pp. 102-107, 1994.

[58] S. S. Lutz, W. D. Turley and H. M. Borella, *'Remote temperature measurement instrumentation for a heated rotating turbine disk'*, ISA, no. 88-0725, pp. 217-229, 1988.

[59] B. W. Noel, H. M. Borella, L. A. Franks, B. R. Marshall, S. W. Allison, M. R. Cates and W. A. Stange, *'Proposed Laser-Induced Fluorescence Method for Remote Thermometry in Turbine Engines'*, Journal of Propulsion and Power, vol. 2, no. 6, p. 565, 1986.

[60] G. Blasse and B. C. Grabmaier, *'Luminescent materials'*, Springer-Verlag Berlin Heidelberg, pp. 33-38, 1994.

[61] S. Shionoya and W. M. Yen, *'Phosphor handbook'*, CRC Press LLC, pp. 86-88, 1998.

[62] A. J. Simons, I. P. McClean and R. Stevens, *'Phosphors for remote thermograph sensing in lower temperature '*, Electronics Letters vol. 32, no. 3, pp. 253-254, 1996.

[63] C. C. Klick and J. H. Schulman, *'Solid state physics (Advances in research and applications)'*, Academic Press Inc., New York, Vol. 5, pp. 100-104, 1957.

[64] H. Lipson and H. Steeple, *'Interpretation of x-ray powder diffraction patterns'*, Macmillan and Co Ltd., p. 51, 1970.

[65] B. D. Cullity, *'Elements of x-ray diffraction (second edition)'*, Addison-Wesley Publishing Company, Inc, pp. 84-87, 1978.

[66] Scintag, *'Chapter 7: Basics of x-ray diffraction'*, 1999.

[67] C. Hammond, *'The basics of crystallography and diffraction'*, Oxford Science Publications, pp. 128-130, 1997.

[68] *'XRD homepage at http://www.physics.pdx.edu/~pmoeck/phy381/Topic5a-XRD.pdf'*.

[69] J. C. Fister and D. Rank, *'Delayed fluorescence optical thermometry'*, Analytical Chemistry, vol. 67, no. 23, pp. 4269-4275 1995.

[70] A. T. Augousti, K. T. V. Grattan and A. W. Palmer, *'Visible-LED pumped fiber-optic temperature sensor'*, IEEE Transactions on Instrumentation and Measurement, vol. 37, no. 3, pp. 470-472, 1988.

[71] J. S. McCormark, *'Remote optical measurement of temperature using luminescent materials'*, Electronics Letters, vol. 17, no. 18, p. 630, 1981.

[72] A. G. Davidson and E. O. Fadiran, *'Effect of variation of temperature on second-derivative fluorescence spectra '*, Analyst, vol. 113, no. 537-541, 1988.

[73] B. Campbell, T. Liu and J. Sullivan, *'Temperature sensitive fluorescent paint systems'*, AIAA Paper, pp. 94-2483, 1994.

[74] T. Liu and B. T. Campbell, *'Temperature and pressure sensitive luminescent paints in aerodynamics'*, Appl. Mech. Rev., vol. 50, no. 4, p. 94, 1997.

[75] M. K. Chyu and D. J. Bizzak, *'Two dimensional imaging of OH laser induced fluorescence in a flame '*, Optics Lettters, vol. 7, pp. 382-384, 1993.

[76] S. W. Allison, M. R. Cates, B. W. Noel and G. T. Gillies, *'Monitoring permanent-magnet motor heating with phosphor thermometry'*, IEEE Transactions on Instrumentation and Measurement, vol. 37, no. 4, pp. 637-641, 1988.

[77] C. W. Struck and W. H. Fonger, *'Thermal quenching of* Tb^{+3}, Tm^{+3}, Pr^{+3}, *and* Dy^{+3} $4f^{n}$ *emitting states in* La_2O_2S*'*, Journal of Applied Physics, vol. 42, no. 11, pp. 4515-4516, 1971.

[78] B. W. Noel and S. W. Allison, *'AIAA/SAE/ASME/ASEE 23rd Joint Propulsion Conference'* (San Diego, California), p. 10, July 1987.

[79] S. W. Allison and G. T. Gilles, *'Nanoscale thermometry via the fluorescent of YAG:Ce phosphor particles: Measurements from 7 to 77oC'*, Nanotechnology, vol. 14, pp. 859-863, 2003.

[80] L. Mannik, S. K. Brown and S. R. Campbell, *'Phosphor-based thermometry of rotating surfaces'*, Journal of Applied Optics, vol. 28, no. 18, pp. 4014-4017, 1987.

[81] A. B. P. Lever, *'Inorganic electronic spectroscopy'*, Elsevier, Amsterdam, p. 863, 1984.

[82] J. A. Duffy, *'Bonding, energy levels and bands in inorganic solids'*, Longman Scientific and Technical, Harlow, Chapter 6, p. 249 1990.

[83] C. K. Jorgensen, *'Absorption spectra and chemical bonding in complexes'*, Pergamon, Oxford, p. 290, 1962.

[84] C. K. Jorgensen, '*Modern aspects of ligand field theory*', North Holland, Amsterdam, p. 151, 1971.

[85] G. Blasse and B. C. Grabmaier, '*Luminescent materials*', Springer-Verlag Berlin Heidelberg, pp. 16-19, 1994.

[86] J. Silver, '*Personal communication at Display Master Course* ', Nottingham Trent University, 2006.

[87] L. E. Sobon, K. A. Wickersheim, R. A. Buchanan and R. V. Alves, '*Growth and properties of lanthanum oxysulfide crystals*', vol. 42, no. 8, p. 3049, 1971.

[88] T. Nishimura, K. Nomoto, K. Yokota and M. Tamatani, '*Coloration caused by mechanical stress on rare earth oxysulfides*', Materials Research Bulletin, vol. 10, no. 7, p. 747, 1975.

[89] '*Polystyrene*', International Labour Organisation chemical safety card for polystyrene, 2003.

[90] S. A. Kane, '*Introduction to physics in modern medicine*', CRC Press, pp. 24-25, 2003.

[91] '*Ocean Optics Inc. Product Catalogue* ', Halma Group Company, 2007.

[92] '*Photomultipliers and accessories*', Electron Tubes Limited, 1996.

[93] '*Photomultiplier Handbook*', Burle Industries Inc., 1980.

[94] '*Photomultiplier tubes: basics and applications, third edition*', Hamamatsu Photonics, 2006.

[95] C. Suryanarayana and M. G. Norton, '*X-ray diffraction: A practical approach*', Kluwer Academic / Plenum Publishers, 1998.

[96] B. D. Cullity, '*Elements of x-ray diffraction (second edition)*', Addison-Wesley Publishing Company, Inc, pp. 100-103, 1978.

[97] M. Kato, H. Kominami, K. Hara, Y. Nakanishi, Y. Hatanaka and M. Mikami, '*Preparation of La2O2S:Eu thin film phosphor for NUV excitation*', Proc Int Disp Workshops, vol. 12th, pp. 531-534, 2005.

[98] L. A. Ivanchenko, Y. G. Sakharova and V. N. Perov, '*The reflectivity of powdered lanthanide oxysulfides*', Sov. Powder Metall. Met. Ceram. (USA), vol. 25, no. 12, pp. 991-993, 1986.

[99] H. Peng, S. Huang, F. You, J. Chang, S. Lu and L. Cao, '*Preparation and surface effect analysis of trivalent europium-doped nanocrystalline* La_2O_2S', Journal of Physical Chemistry B, vol. 109, no. 12, pp. 5774 -5778, 2005.

[100] M. Mikami and K. Nakamura, '*Electronic structure of rare-earth sesquioxides and oxysulfides*', Journal of Alloys and Compounds, vol. 408-412, pp. 687-692, 2006.

[101] D. Pauwels, A. Demourgues and A. Tressaud, (Boston, MA, USA), p. 321, 2003.

[102] K. Ikeue, T. Kawano, M. Eto, D. Zhang and M. Machida, '*X-ray structural study on the different redox behavior of La and Pr oxysulfates/oxysulfides*', Journal of Alloys and Compounds, vol. 451, pp. 338-340, 2008.

[103] M. B. Cates, S. W. Allison, L. A. Franks, M. A. Nelson, T. J. Davies and B. W. Noel, '*Remote thermometry of moving surfaces by laser-induced fluorescence of surface-bonded phosphor*', Laser Inst of America, Los Angeles, p. 50, 1984.

[104] W. H. Fonger and C. W. Struck, 'Eu^{+3} ^5D *resonance quenching to the charge-transfer states in* Y_2O_2S, La_2O_2S, *and LaOCl*', Journal of Chemical Physics, vol. 52, no. 12, pp. 6364-6372, 1970.

[105] C. W. Struck and W. H. Fonger, *'Role of the charge-transfer states in feeding and thermally emptying the 5D states of Eu+3 in yttrium and lanthanum oxysulfides'*, Journal of Luminescence, vol. 1-2, p. 456, 1970.

[106] M. R. Cates, S. W. Allison, L. A. Franks, H. M. Borella, B. R. Marshall and B. W. Noel, *'Laser-induced fluorescence of europium-doped yttrium oxide for remote high-temperature thermometry'*, Laser Inst. America, San Francisco, USA, p. 142, 1986.

[107] W. H. Fonger and C. W. Struck, *'Energy loss and energy storage from the Eu^{+3} charge-transfer states in Y and La oxysulfides'*, Journal of the Electrochemical Society, vol. 118, no. 2, pp. 273-280, 1971.

[108] J. S. Foster, *'Some leading features of the stark effect'*, Journal of the Franklin Institute, vol. 209, no. 5, pp. 585-588, 1930.

[109] S. Ignasiak and H. Veron, *'Line emission penetration phosphors: Preparation and cathodoluminescent properties'*, Journal of the Electrochemical Society, vol. 123, no. 10, pp. 1493-1497, 1976.

[110] M. I. P. Simons A.J., Stevens R, *'Phosphors for Remote Thermograph Sensing in Lower Temperature '*, Electronics Letters vol. 32, no. 3, pp. 253-254, 1996.

[111] P.J.Brown and J.B.Forsyth, *'The Crystal Structure of Solids'*, Edward Arnold Limited, p., 1973.

[112] K. A. Wickersheim and W. D. Hyatt, *'Commercial applications of fiberoptic temperature measurement'*, The International Society for Optical Engineering, SPIE, vol. 1267, pp. 84-96, 1990.

[113] L. M. Coyle and M. Gouterman, *'Correcting lifetime measurements for temperature'*, Sensors and Actuators B: Chemical, vol. B 61, pp. 92-99, 1999.

[114] A. M. Amiryan, A. M. Gurwich and R. V. Ktomina, *'Recombination processes and emission spectrum of terbium in oxysulphides'*, Journal of Applied Spectroscopy, vol. 27, no. 3, pp. 468-472, 1977.

[115] S. Shionoya and W. M. Yen, *'Phosphor handbook'*, CRC Press LLC, pp. 838-839, 1998.

[116] H. A. Eick, *'The preparation, lattice parameters and some chemical properties of the rare earth mono-thio oxides'*, Chermical properties of rare-earth mono-thio oxides, vol. 80, pp. 43-44, 1958.

[117] G. Blasse, *'Chemistry and physics of R-activated phosphors'*, North-Holland Publishing Company, pp. 239-247, 1979.

[118] G. Blasse and B. C. Grabmaier, *'Luminescent materials'*, Springer-Verlag Berlin Heidelberg, p. 44, 1994.

[119] J. K. Gleason, H. W. Offen and W. D. Turley, *'Pressure-induced luminescence quenching of terbium-doped oxide sulfides'*, vol. 32, no. 5, pp. 639-641, 1993.

[120] D. L. Beshears, H. M. Henderson, T. J. Henson, M. J. Bridges, R. M. Sadler and M. A. Cyr, *'Martin marietta energy systems, Inc. Report no. K/ETAC-59'*, 1988.

[121] J. P. Feist, A. L. Heyes and S. Seefeldt, *'Oxygen quenching of phosphorescence from thermographic phosphors'*, Measurement Science and Technology, vol. 14, pp. 17-20, 2003.

[122] S. W. Allison, M. R. Cates and D. L. Beshears, *'Survey of thermally sensitive phosphors for pressure sensitive paint applications'*, Instrumentation in the Aerospace Industry: Proc. Int. Symp., vol. 397, pp. 29-37, 2000.

[123] R. V. Alves, J. J. Pearson, K. A. Wickersheim and R. A. Buchanan, '*Proceedings of the 8th Rare earth research conference*' pp. 703-713, 1970.

Appendix

Publications:

1) S. V. Yap, R. M. Ranson, W. M. Cranton, and D. Koutsogeorgis, "*Decay time characteristics of* La_2O_2S*:Eu and* La_2O_2S*:Tb for use within an optical sensor for human skin temperature measurement,*" Applied Optics, Vol. 47, Issue 27, pp. 4895-4899, September 2008

2) S. V. Yap, R. M. Ranson, W. M. Cranton, D. Koutsogeorgis and G. B. Hix," *Temperature dependent characteristics of* La_2O_2S*: Ln [Ln= Eu, Tb] with various Ln concentrations over 5–60 °C,*" Journal of Luminescence, Volume 129, Issue 5, pp. 416-422, 2009

Decay time characteristics of $La_2O_2S:Eu$ and $La_2O_2S:Tb$ for use within an optical sensor for human skin temperature measurement

Sook Voon Yap,* Robert M. Ranson, Wayne M. Cranton,
and Demosthenes Koutsogeorgis

School of Science and Technology, Nottingham Trent University, Clifton Lane, Nottingham, NG11 8NS, UK

*Corresponding author: sook.yap@ntu.ac.uk

Received 31 October 2007; revised 1 August 2008; accepted 15 August 2008;
posted 18 August 2008 (Doc. ID 89095); published 15 September 2008

We focus on the development of a remote temperature sensing technology, i.e., an optical laser-based sensor, using thermographic phosphors for medical applications, particularly within an electromagnetically hostile magnetic resonance imaging (MRI) environment. A MRI scanner uses a strong magnetic field and radio waves to generate images of the inside of the body. The quality of the image improves with increasing magnetic resonance; however, the drawback of applying a greater magnetic strength is the inducement of heat into the body tissue. Therefore, monitoring the patient's temperature inside MRI is vital, but until now, a practical solution for temperature measurement did not exist. We show europium doped lanthanum oxysulphide ($La_2O_2S:Eu$) and terbium doped lanthanum oxysulphide ($La_2O_2S:Tb$) are both temperature sensitive to a low temperature range of 10–50 °C when under ultraviolet (UV) excitation. The emission spectra and decay time characteristics of these phosphors were demonstrated. The results indicate that $La_2O_2S:Eu$ has a quenching rate of $13.7\,m°C^{-1}$ and $4\,m°C^{-1}$ at 512 nm and 538 nm, respectively. In addition, $La_2O_2S:Tb$ has a lower quenching rate of $4.19\,m°C^{-1}$ at 548 nm due to its faster decay time. © 2008 Optical Society of America

OCIS codes: 120.0120, 160.5690, 280.6780, 250.5230, 170.3650, 300.2530.

1. Introduction

A growing interest in the field of optical sensors has highlighted the need for research to develop remote sensor technology with adequate sensing capabilities to meet specific needs. The increased use of this remote temperature sensing technology is mainly due to the immunity of optical signals to electromagnetic interference [1]. Numerous applications take advantage of this attribute within the fields of engineering, aerospace and security, as well as medicine. Medical examples include monitoring a patient's body temperature when within a MRI system or when suffering from hyperthermia [2,3].

In the past few years, a research program carried out at Nottingham Trent University (NTU, UK) concentrated on the development of a surface thermometry technique for high temperature sensing within a gas turbine [4–6]. The work utilized the most commonly investigated thermographic phosphor, europium doped yttrium oxide ($Y_2O_2:Eu$), via a technique referred to as phosphor thermography (PT) [4,7].

The concept of phosphor-based optical sensors is to utilize a UV pulsed laser to excite the phosphor on the end of the probe, and the resulting fluorescence is monitored. The temperature is subsequently determined by measuring the decrease of fluorescence intensity with time after the laser pulse has ceased; an example of this is illustrated in Fig. 1. The initial sharp rise in the emission is due to the dominating excitation pulse. Consequently, the decay time of the phosphorescence can be deduced according to the single exponential decay relation:

0003-6935/08/274895-05$15.00/0

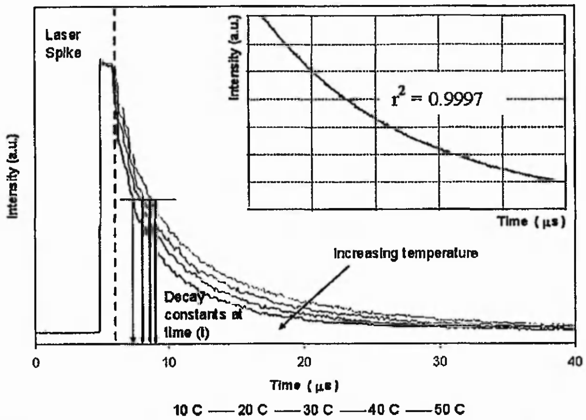

Fig. 1. Example of single exponential decay profiles of La_2O_2S:Eu at various temperatures under 337 nm excitation. The inset graph indicates a single exponential decay fitting with an accuracy of >99.9%.

$$I(t) = I_0 \times \exp\left(-\frac{t}{\tau}\right), \qquad (1)$$

where $I(t)$ is intensity at time t, I_0 is initial intensity at time 0, and τ is decay time[8].

It should be noted that a double exponential decay relationship was also fitted but resulted in a less accurate fit (<90% r^2 factor, the coefficient of determination) with both decay constants being within 5% of each other, a clear indication that the single exponential was accurate ($r^2 > 99.5\%$).

This work is aimed at investigating the sensing capabilities of various phosphor materials for use within an optical sensor to detect temperature changes associated with the human body when in electromagnetically harsh environments such as the MRI environment. Hence, the preliminary stage of this research has concentrated on the temperature sensing range around that of the human skin, namely, 27–37 °C [9,10]. In this paper, the resulting photoluminescent (PL) properties and decay time measurements of the potential candidate phosphor powders, i.e., La_2O_2S:Eu and La_2O_2S:Tb, within the temperature range of 10–50 °C are presented.

2. Experimental Procedures

Two commercially available phosphors, La_2O_2S:Eu at the standard dopant concentration of 8 at. % and La_2O_2S:Tb at 1 at. %, were investigated in this work. Both phosphors exist in the form of powders. These phosphor powders have been pressed to form a pellet (5 mm in diameter and 2 mm ± 1 mm in thickness), which can then be held on a test coupon. Five pellets of each phosphor sample were tested. These samples can be placed within a cooled incubator (IPP 200) for conducting PL and decay time measurements at various temperatures. A calibrated T-type thermocouple was attached at the back of the sample, and the temperatures over time were displayed and recorded using the Picolog software. The difference of the controlled and measured temperatures was approximately ±0.1 °C throughout the working temperature range. The PL and decay time systems are aligned on an optical table as illustrated in Fig. 2.

For decay time measurements, a nitrogen (N_2) pulsed laser (VSL-337ND, $\lambda_{\text{excitation}} = 337$ nm, <4 ns pulse width, and a repetition rate of 20 Hz at the average excitation power of 6 mW) was utilized to excite the phosphor within the incubator. The emitted luminescence was collected by a quartz rod. This is positioned perpendicular to the emitting surface in order to maximize the collection of emitted light, which is subsequently passed through a cut-on filter (wavelength > 380 nm) attached to the monochromator (DMC1-03, Optometrics LLC). Consequently, the monochromator transmitted the fluorescence to a photomultiplier tube (Electrons Tube, 9558QB) that served as a detector. A waveform processing oscilloscope (Gould DSO 4072) displayed, digitized, and stored the data for subsequent analysis. The oscilloscope was set up to average the signals received over a period of about 1 minute in order to enhance the signal-to-noise ratio, and this equates to 1200 decay rate signals. For comparison purposes, the decay constant was always calculated from the same time domain (3–5 μs after the 4 ns laser excitation pulse) with the standard form of the single exponential equation.

For PL emission spectra, the quartz rod is replaced with an optical fiber that transmits the optical signal to a spectrometer (S2000, Ocean Optics Inc. (OOI)) and conveyed to the computer by OOI software.

3. Results and Discussion

A. Europium Doped Lanthanum Oxysulphide (La_2O_2S : Eu)

Previous work [11] has reported the temperature dependent peaks of La_2O_2S:Eu occur only at 512 nm and 538 nm. However, over the temperature range of 10–50 °C, measurement of the PL spectra of La_2O_2S:Eu acquired at NTU indicate that no spectral shift occurs within this temperature range.

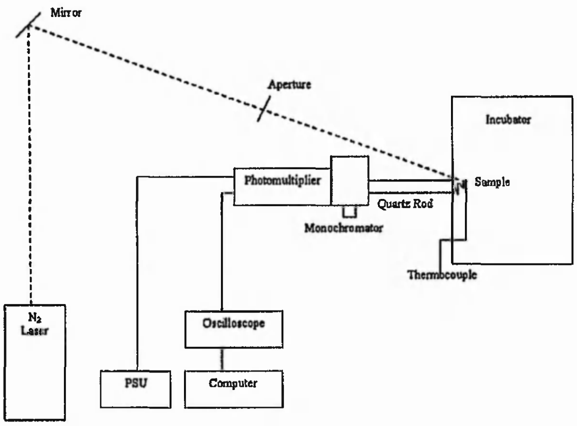

Fig. 2. Setup for photoluminescent and decay time experiment.

Figure 3 shows a typical emission spectrum for $La_2O_2S:Eu$ when excited at 337 nm with a nitrogen laser. The results of decay time measurement show temperature dependencies of 512 nm and 538 nm when excited by a nitrogen laser at 337 nm, while the other emission wavelengths are temperature independent. Temperature dependencies of emission intensity for 512 nm (corresponding to the energy levels of 5_{D_2} to 7_{F_3}) in $La_2O_2S:Eu$ and also decay times for 538 nm (the emission of $^5D1$ to 7_{F_1} transition) [12] are illustrated in Fig. 4. The decay time of a phosphor is observed to decrease with increasing temperature. These transitions that occur between the ^5D levels and charge transfer states (CTS) of $La_2O_2S:Eu$ can be described with the model developed by Fonger and Struck [12]. Their analysis suggested the Eu 5_{D_J} states quench sequentially ($J = 3, 2, 1, 0$) with increasing temperature. This is because each ^5D state empties thermally via charge transfer. Hence an empirical correlation of decay time with temperature can provide the basis for a temperature measurement. A simple model proposed by Simons *et al.* [13] is used to deduce the fluorescence decay time of a phosphor with varying temperature. The relevant expression is

$$\tau_d = \tau_q \times \exp[-Q(T - T_Q)]. \qquad (2)$$

By definition, the decay time (τ_d) is related to the component temperature (T) above the quenching point (T_Q), where τ_q is the decay time at the quenching point. The quenching rate Q is defined as the temperature change required for the decay time to decrease exponentially and is therefore a measure of the temperature sensitivity of the phosphor; the measurement sensitivity improves with increasing quenching rate. Each pellet sample showed consistency of decay constant measurement. The decay time characteristics of 512 nm from 10–50 °C, as illustrated in Fig. 4, indicate a quenching rate of 13.7 m°C^{-1} with its fast decay time of 4.97–1.91 μs. Hence this demonstrates that $La_2O_2S:Eu$ is a highly temperature-sensitive phosphor to be used within the desired optical sensor. In addition, the decay time of $La_2O_2S:Eu$ at 538 nm peak decreases consistently with a decay time of 38.8–29 μs and has a quenching rate of 4 m°C^{-1}.

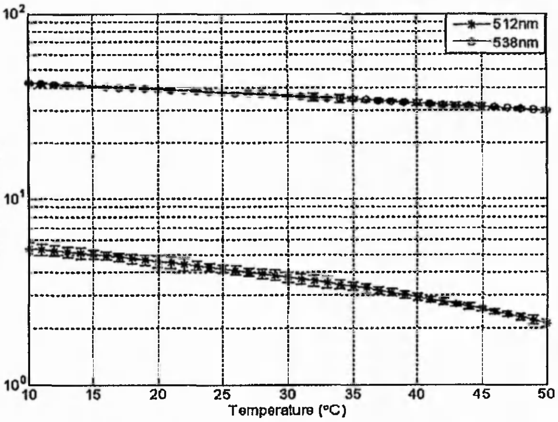

Fig. 4. Decay time characteristics of $La_2O_2S:Eu$ at 512 nm and 538 nm under 337 nm excitation.

B. Terbium Doped Lanthanum Oxysulphide ($La_2O_2S:Tb$)

The PL spectra of $La_2O_2S:Tb$ excited by a nitrogen laser (337 nm) are shown in Fig. 5, which exhibit multiple peaks. $La_2O_2S:Tb$ appears as a green emitting phosphor since the host is doped with terbium, and its dominant peak is centered at 544 nm. Again, no spectral line shifts occur with varying temperatures for this PL measurement.

Although very little work has been reported to determine the temperature sensing capabilities of $La_2O_2S:Tb$, the results obtained in this work have suggested that the decay times of this phosphor are strongly dependent upon its temperature, as indicated in Fig. 6. Of more importance, the temperature dependent characteristics occur at most of the emission intensities in $La_2O_2S:Tb$, i.e., 5_{D_4} to 7_{F_J} transitions [14] compared to only two emission lines of $La_2O_2S:Eu$. According to Struck and Fonger,

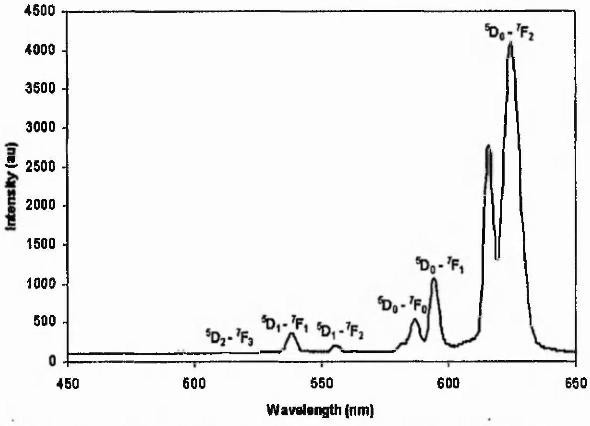

Fig. 3. Typical emission spectrum for $La_2O_2S:Eu$ excited by a nitrogen laser at room temperature.

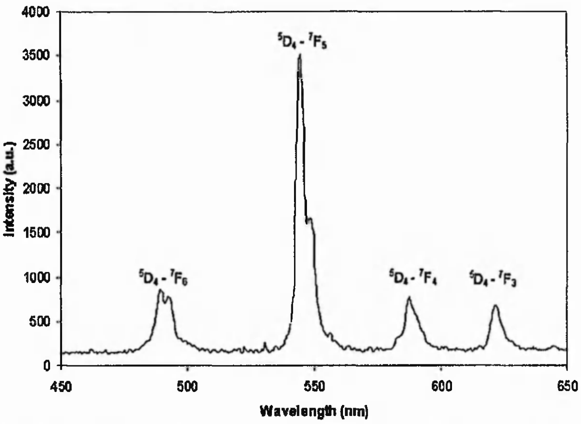

Fig. 5. Typical emission spectrum for $La_2O_2S:Tb$ excited by a nitrogen laser (337 nm) at room temperature.

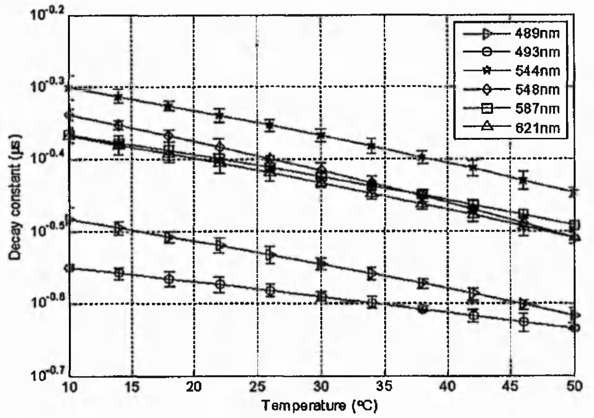

Fig. 6. Decay constant against temperature for different emission wavelengths of La_2O_2S:Tb.

again similar to La_2O_2S:Eu, the thermal quenchings of Tb in La_2O_2S are attributed to the CTS crossover relaxation to Frank–Condon shifted states.

The decay times and the quenching rates of La_2O_2S:Tb are tabulated in Table 1. The results clearly show that the 548 nm peak is more sensitive to temperature variation due to its higher quenching rate; relating this to Eq. (2), the measurement sensitivity improves with increasing quenching rate.

4. Conclusions

The results presented in this work indicate that both of the proposed thermographic phosphors, La_2O_2S:Eu and La_2O_2S:Tb, could be ideal candidates to meet the requirements of a desired optical sensor subject to their sensing capabilities within the narrow temperature range of interest, 10–50 °C. However, it is essential to adopt a robust temperature sensing technique, i.e., decay time characterization that is independent of excitation source and ambient light, allowing a greater accuracy and a better repeatability to be achieved.

In this research we are particularly interested in the temperature dependent peak 512 nm of La_2O_2S:Eu due to its impressive quenching rate of 13.7 m°C^{-1}, suggesting this phosphor is highly sensitive to temperature variations. The results obtained at NTU agree with those derived from illustrated data within the publication by Coyle *et al.* [15]: the 514 nm emission line of La_2O_2S:Eu has the quenching rate of 13.7 m°C^{-1} under 337 nm excitation. Omrane *et al.* [16] demonstrated the decay times of La_2O_2S:Eu over 30–150 °C, the quenching rate measured from the graph is 15.9 m°C^{-1} at 512 nm line with 355 nm excitation. Their results have shown a slight improvement in the quenching rate, and this may be due to the fine-tuned excitation wavelength. Nonetheless, the fast decay times of La_2O_2S:Tb with relatively low quenching rates of 2.28–4.19 m°C^{-1} at various emission wavelengths are evidently indicating it could be suitable for used in temperature measurements. To date, no relevant data for La_2O_2S:Tb has yet been reported in the public domain. We are presently analyzing various dopant concentrations of La_2O_2S:Eu and La_2O_2S:Tb attributed to their temperature dependencies. These results, plus more in depth studies of the dopant concentration quenching and temperature dependencies cited above, will be subsequently reported. In addition, the design of an optical sensor will be followed, and further investigations will be carried out within an MRI scanner in order to overcome the complexities of noninvasive temperature measurement, such as determining the thermal conductivity between the bonding of the phosphor and human skin as well as an investigation into the potential problem associated with the Zeeman splitting. The average MRI scanner utilizes a magnetic field strength of ≤1.5 Tesla, and hence should not be problematic for such a sensor.

Table 1. Decay Time of La_2O_2S:Tb Under 337 nm Excitation

Emission Wavelength (nm)	Decay Times (µs) (10–50 °C)	Quenching Rate (m°C^{-1})
489	0.39–0.25	3.40
493	0.39–0.23	2.28
544	0.48–0.37	2.94
548	0.47–0.32	4.19
587	0.36–0.28	2.61
621	0.42–0.37	3.33

The authors acknowledge financial support from The Engineering and Physics Sciences Research Council (EPSRC).

References

1. S. W. Allison and G. T. Gillies, "Remote thermometry with thermographic phosphors: instrumentation and applications," Rev. Sci. Instrum. **68**, 2615–2650 (1997).
2. A. G. Mignani and F. Baldini, "Biomedical sensors using optical fibres," Rep. Prog. Phys. **59**, 1–28 (1996).
3. K. A. Wickersheim and M. H. Sun, "Fiberoptic thermometry and its applications," J. Microwave Power Electromagn. Energy **22**, 85–94 (1987).
4. R. M. Ranson, "Investigation into thermographic phosphors," Ph.D. dissertation (The Nottingham Trent University, 1999).
5. R. M. Ranson, E. Evangelou, and C. B. Thomas, "Modeling the fluorescent lifetime of Y_2O_3:Eu," Appl. Phys. Lett. **72**, 2663–2664 (1998).
6. R. M Ranson, C. B. Thomas, and M. R. Craven, "A thin film coating for phosphor thermography," Meas. Sci. Technol. **9**, 1947–1950 (1998).
7. M. B. Cates, S. W. Allison, L. A. Franks, M. A. Nelson, T. J. Davies, and B. W. Noel, *Remote Thermometry of Moving Surfaces by Laser-Induced Fluorescence of Surface-Bonded Phosphor* (Laser Institute of America, 1984).
8. J. P. Feist and A. L. Heyes, "Development of the phosphor thermometry technique for applications in gas turbines," presented at the 10th International Symposium on Application of Laser Techniques to Fluid Mechanics, Lisbon, Spain, July 2000.
9. L. Jansky, V. Vavra, P. Jansky, P. Kunc, I. Knizkova, D. Jandova, and K. Slovacek, "Skin temperature changes in humans induced by local peripheral cooling," J. Therm. Biol. **28**, 429–437 (2003).

10. G. Wasner, J. Schattschneider, and R. Baron, "Skin temperature side differences: a diagnostic tool for CRPS?," Pain **98**, 19–26 (2002).
11. G. Webster and H. G. Drickamer, "High pressure studies of luminescence efficiency and lifetime in La_2O_2S:Eu and Y_2O_2S:Eu," J. Chem. Phys. **72**, 3740–3748 (1980).
12. W. H. Fonger and C. W. Struck, "Energy loss and energy storage from the Eu^{+3} charge-transfer states in Y and La oxysulfides," J. Electrochem. Soc. **118**, 273–280 (1971).
13. A. J. Simons, I. P. McClean, and R. Stevens, "Phosphors for remote thermograph sensing in lower temperature," Electron. Lett. **32**, 253–254 (1996).
14. C. W. Struck and W. H. Fonger, "Thermal quenching of Tb^{+3}, Tm^{+3}, Pr^{+3}, and Dy^{+3} $4f^n$ emitting states in La_2O_2S," J. Appl. Phys. **42**, 4515–4516 (1971).
15. L. M. Coyle and M. Gouterman, "Correcting lifetime measurements for temperature," Sens. Actuators B **61**, 92–99 (1999).
16. A. Omrane, G. Juhlin, F. Ossler, and M. Alden, "Temperature measurements of single droplets by use of laser-induced phosphorescence," Appl. Opt. **43**, 3523–3529 (2004).

Journal of Luminescence 129 (2009) 416–422

Contents lists available at ScienceDirect

Journal of Luminescence

journal homepage: www.elsevier.com/locate/jlumin

Temperature dependent characteristics of La_2O_2S: Ln [Ln = Eu, Tb] with various Ln concentrations over 5–60 °C

Sook Voon Yap *, Robert M. Ranson, Wayne M. Cranton, Demosthenes C. Koutsogeorgis, Gary B. Hix

School of Science and Technology, Nottingham Trent University, Clifton Lane, Nottingham NG11 8NS, UK

ARTICLE INFO

Article history:
Received 19 May 2008
Received in revised form
11 September 2008
Accepted 28 October 2008
Available online 27 November 2008

PACS:
33.50.Dq
33.50.–j
07.07.Df
78.55.–m

Keywords:
Phosphors
Photoluminescence
Decay time
Temperature sensing
Quenching rate
X-ray diffraction

ABSTRACT

This research is aimed at developing an optical sensor for remotely measuring human skin temperature in electromagnetically hostile environments, such as within a magnetic resonance imaging (MRI) scanner. In this feasibility study, various concentrations of europium-doped lanthanum oxysulphide (La_2O_2S: Eu—0.1–15 mol% (m/o)) and terbium-doped lanthanum oxysulphide (La_2O_2S: Tb—0.005–50 m/o) have been investigated in terms of crystallinity, photoluminescent (PL) spectral and decay time characteristics. For both phosphors, X-ray diffraction (XRD) has shown that as dopancy increases, the (1 0 0) and (0 0 2) reflections merge and there is a reduction in the *c*-axis parameter as well as the crystallite size. Photoluminescent characterisation (337 nm excitation) has also shown a dependency to dopant concentration through variance of peak intensity. Temperature dependent decay time measurements were carried out over a low temperature range 5–60 °C. Optimum brightness of these temperature dependent lines is achieved at concentrations of 1 and 10 m/o for La_2O_2S: Eu and La_2O_2S: Tb respectively. However, optimum temperature dependency is achieved at lower concentration for La_2O_2S: Eu, specifically at 0.1 m/o. In comparison to conventional phosphor temperature dependent characteristic, La_2O_2S: Tb showed an increase in decay time with respect to temperature for concentrations above 2 m/o.

1. Introduction

Over the last several decades, thermographic phosphors have been extensively explored for remote temperature sensing measurement. This is attributed to their accurate sensing capability over a wide range of temperatures, as well as their ability to withstand a harsh environment. For example, europium-doped yttrium oxide (Y_2O_3: Eu) has been utilised for high temperature sensing within a rotating gas turbine [1,2] and magnesium fluorogermanate doped with manganese ($Mg_4(F)GeO_6$: Mn) has been explored for thermal mapping of hot spots on the walls of a cryogenic fuel tank [3]. Problems associated with temperature monitoring within a magnetic resonance imaging (MRI) scanner, particularly to an infant or a critical-care patient, has provided an impetus for the development of a phosphor-based optical sensor for human skin temperature sensing (27–37 °C [4,5]) within such an environment. A desired optical sensor using the decay rate of luminescence from a thermographic phosphor could therefore be the ideal temperature sensing tool for this delicate application due to the fact that thermographic phosphor thermometry is independent of external triggering source and electromagnetic interference. However, the potential issues such as thermal conductivity and the length of contact time between the human skin and the bonding of the phosphor will be taken into consideration at a later stage of the sensor design. In this work, two potential phosphors have been selected for use within the desired optical sensor, namely La_2O_2S: Eu and La_2O_2S: Tb. The results indicate that both of the phosphors are temperature dependent over 5–60 °C.

The crystallite size of the phosphors plays an important role in determining the changes in decay rates. At Nottingham Trent University (NTU), the crystallite size and crystallinity of La_2O_2S: Eu (0.1–15 mol% (m/o)) and La_2O_2S: Tb (0.005–50 m/o) have been characterised by X-ray diffraction (XRD) and the measurements were concentrated on the (1 0 0) and (0 0 2) planes. As dopancy increases, the observed peaks merge and the XRD analysis has shown a reduction in the crystallite size and the *c*-axis of the (0 0 2) plane. In addition, photoluminescent (PL) results also demonstrate a change in the relative emission intensities at various dopancy levels. This is due to the electronic transitions occurring between the discrete levels of ^5D–^7F levels of the dopant ions sited in the crystal lattice in relation to the Stark effect [6]. The quenching concentrations for both phosphors are

---

* Corresponding author. Tel.: +44 0 1158483163.
E-mail address: sook.yap@ntu.ac.uk (S.V. Yap).

0022-2313/$ - see front matter © 2008 Elsevier B.V. All rights reserved.
doi:10.1016/j.jlumin.2008.10.019

encountered when the optimum brightness for the temperature dependent lines is achieved.

Typically, temperature dependent characteristics of a thermographic phosphor can be explored by decay time and two-peak intensity [7]. In this research, decay time is the preferred approach as it is independent of the excitation source and ambient light. The decay time of luminescence can be deduced according to the relation,

$$I(t) = I_0 \exp\left(-\frac{t}{\tau}\right) \qquad (1)$$

where $I(t)$ is the intensity at time t, I_0 the initial intensity at time 0 and τ the decay time [8].

It should be noted that the decay profiles presented in this paper were fitted with the standard single exponential decay equation providing goodness of fit (r^2) >99.5%. A double exponential decay relationship was also attempted but resulted in a less accurate fit (r^2 <90%) with both decay times being within 5% of each other.

Simons et al. [9] also describes the decay time of a phosphor as being strongly dependent on its temperature. The expression is

$$\tau_d = \tau_q \exp(-Q(T - T_Q)) \qquad (2)$$

where the decay constant (τ_d) is related to the component temperature (T) above the quenching point (T_Q); τ_q the decay time at the quenching point; and the quenching rate Q is the rate at which the decay time varies with temperature). Therefore, the quenching rate is directly related to the sensitivity of a phosphor; the higher the quenching rate the more sensitive a phosphor is to temperature variation. The decay time results presented in this paper indicate that both of La_2O_2S: Eu and La_2O_2S: Tb are highly sensitive with notable quenching rates over 5–60 °C. More importantly, this paper shows an unprecedented decay time characteristic, namely, the decay time for La_2O_2S: Tb at higher dopant concentrations (>2 m/o) increases as a function of temperature.

2. Experimental procedures

The powdered phosphors, La_2O_2S: Eu (SKL63/F-R1) and La_2O_2S: Tb (SKL65/N-C1) were supplied by Phosphor Technology Ltd (PTL). These polycrystalline powder phosphors at various dopant concentrations were examined using the Philips X'Pert Pro XRD system with monochromated Cu-K$_{\alpha1}$ radiation, $\lambda = 1.54056$ Å (45 kV, 40 mA operating mode). To ensure the studied data was self-consistent, XRD measurements for different concentrations of a specific phosphor were carried out on the same day and a silicon standard was used as a control sample allowing repeatability. Experiments were therefore concentrated on the $25° \leqslant 2\theta \leqslant 27°$ Bragg angles consisting of the (1 0 0) and (0 0 2) reflections which will give the variation in the c-cell parameter with dopant concentration. The data were collected with 0.008° step size and a count time of 150 s per step.

To enable decay time and PL measurements to be made, the phosphor powders have been compressed to form a pellet (5 mm diameter, 2±0.5 mm thick) so that it could be mounted within a digitally controlled incubator (IPP 200). A calibrated T-type thermocouple was attached at the back of the sample and the temperatures were measured using a PicoLog TC-08 data logger. The comparison of the controlled and measured temperatures showed an accuracy of ±0.1 °C over the working temperature range.

The excitation spectra for La_2O_2S: Tb and La_2O_2S: Eu provided by PTL indicates that the excitation wavelength at 337 nm is sufficient enough to illuminate both of the phosphors. A pulsed nitrogen (N_2) laser (VSL-337ND) was used as an UV excitation source, which emits 337 nm with a 4 ns pulse length. The laser beam is guided to the sample by a mirror. The resulting fluorescence was consequently collected by a quartz rod and transmitted to a monochromator (DMC1-03, Optometrics LLC), thus restricting the emission to a 3 nm bandwidth at the detector—a photomultiplier tube (PMT 9558QB). The PMT converted the detected decay signal into an electrical waveform via an oscilloscope (Gould DSO 4072) for subsequent analysis. In order to enhance the signal-to-noise ratio, the noise reduction was performed by digitally averaging the signals over a period of 1 min and this equates to 1200 decay rate signals. The decay time was always measured from the same time window (3–5 μs after the 4 ns laser excitation pulse) with the single exponential equation for comparison purposes. For the standard PL spectra set-up, an optical fibre is utilised to transmit the fluorescence signal to a spectrometer (S2000, Ocean Optics Inc (OOI)) and the acquired spectrum can be interpreted via OOI software.

3. Results and discussion

3.1. X- ray diffraction (XRD)

XRD patterns of La_2O_2S: Tb and La_2O_2S: Eu over the diffraction angles of $10° \leqslant 2\theta \leqslant 55°$ is shown in Fig. 1. These match the reference pattern (PDF code: 00-027-0263) of the parent compound La_2O_2S. This indicates that the hexagonal crystal structure of La_2O_2S is consistent in the doped materials and its crystal lattice parameters lie within the interval of $3.41 < a < 3.51$ Å and $6.79 < c < 6.94$ Å (the a- and c-axis of a unit cell [10]).

The shift in 2θ of the (2 0 0) reflection with an increase in the Tb dopancy level is mainly due to the variations in the crystal lattice, i.e. c-axis shrinks with increasing Tb concentration as seen in Fig. 2. This is based on the size of the ionic radius of both La (102 pm) and Tb (92 pm) in the unit cell, which decreases as the Tb concentration becomes dominant. With increasing Tb concentration, the two individual peaks at 25.52° ((1 0 0) reflection) and 25.78° ((0 0 2) reflection) merge gradually and eventually form a broad peak at 50 m/o Tb. This merging behavior alters the formation of the crystal lattice and hence produces a multitude of probability of occurrence for both radiative and non-radiative transitions. There is little change at low concentrations (<1 m/o) and the data fit the pseudo-linear relationship as demonstrated in Fig. 3. In addition, the crystallite size of La_2O_2S: Tb decreases owing to a reduction in the volume of the unit cell with increasing Tb dopancy. By using the Scherrer equation, which relates the width of peaks in an X-ray powder diffraction pattern to crystal size, the crystallite size of the phosphors can be determined as tabulated in Table 1.

Fig. 4 indicates the c-axis variations in the position of the (0 0 2) reflection peaking at 25.612° as a function of Eu concentration. This has illustrated a pseudo-linear relationship between the Eu concentration and a shift in the position of this peak to smaller values of 2θ. These data are consistent since Eu has an ionic radius of 95 pm which is smaller than La (102 pm), and hence an expected decrease in the volume of the unit cell occurs as Eu dopant concentration becomes significant.

The variation of the crystallite size of La_2O_2S: Eu is shown in Table 2. The host lattice La_2O_2S has the biggest crystallite size, which is about 0.16 μm than that of the other Eu-doped La_2O_2S. The crystallite size of La_2O_2S: Eu has reduced to 2.5 times smaller than the host lattice. In addition, results at NTU showed that the commonly investigated La_2O_2S: Eu at higher concentrations with smaller crystallite size has a faster decay rate against temperature as demonstrated in Figs. 9(a)–(d). On the other hand, Fig. 11 also

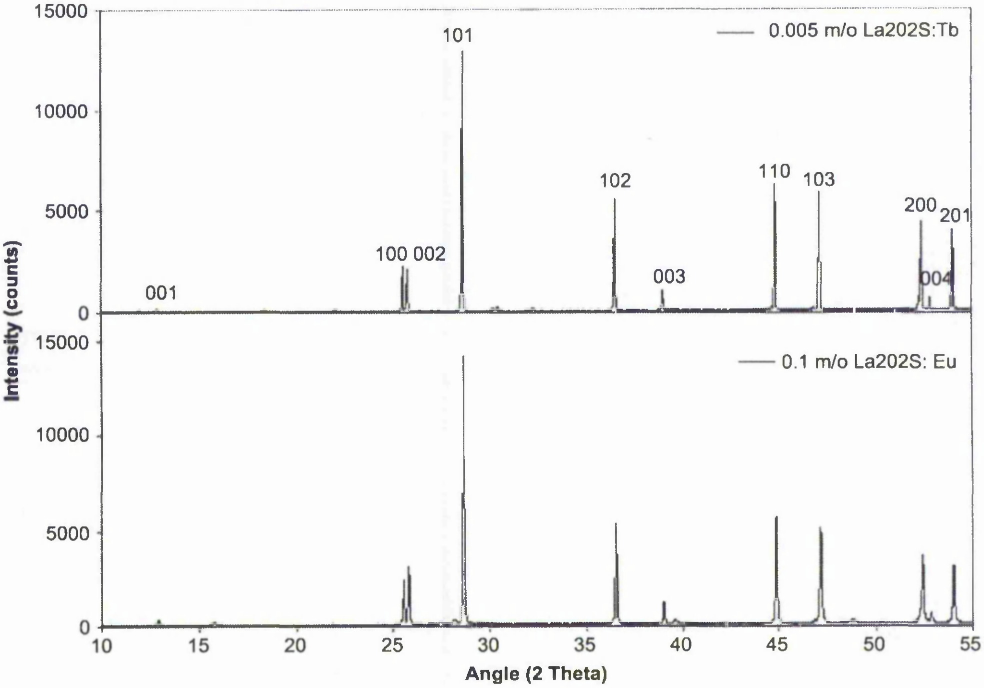

Fig. 1. XRD patterns of La_2O_2S: Tb and of La_2O_2S: Eu at room temperature.

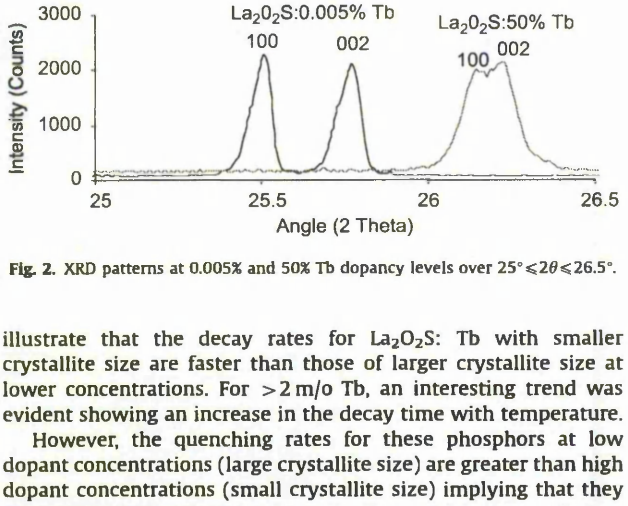

Fig. 2. XRD patterns at 0.005% and 50% Tb dopancy levels over $25° \leqslant 2\theta \leqslant 26.5°$.

illustrate that the decay rates for La_2O_2S: Tb with smaller crystallite size are faster than those of larger crystallite size at lower concentrations. For >2 m/o Tb, an interesting trend was evident showing an increase in the decay time with temperature.

However, the quenching rates for these phosphors at low dopant concentrations (large crystallite size) are greater than high dopant concentrations (small crystallite size) implying that they are more sensitive to temperature variance and hence a relationship between dopant concentration and decay time is established: a phosphor with lower concentration shows a better temperature dependency.

3.2. *Spectral data*

The emission spectrum of La_2O_2S: Tb is determined by the transitions of electrons from an upper ($^5D_3$) and a lower ($^5D_4$) excited level to the level of the multiplet term ^7F_J ($J = 0, 1, 2, 3, 4, 5, 6$) levels of the $4f^8$ configuration [11,12]. The emission of terbium-doped phosphor is mainly in the green due to transitions $^5D_4 \rightarrow {}^7F_J$ and the blue emission contributes to the emission from the higher level transitions $^5D_3 \rightarrow {}^7F_J$ [12]. At lower Tb concentrations of less than 0.5 m/o, the phosphor emits orange at 0.5 m/o, then red at 0.2 and 0.005 m/o. At low concentrations ($\leqslant$0.5 m/o), more peaks are produced in the emission spectrum due to the Stark effect [6] and the dominant peak has shifted from the green line 544 nm to the red region peaking at 624 nm as indicated in Fig. 5. The high terbium concentrations ($\geqslant$0.92 m/o) exhibit six solid emission peaks at 489, 493, 544, 548, 587 and 621 nm. These peaks showed temperature dependencies with fast decay time.

For emission wavelengths in the green region (489–548 nm), Tb concentration reached a quenching point at 10 m/o Tb as it has the optimum intensity emission as seen in Fig. 6. On the other hand, the red region ($\geqslant$587 nm) is dominated by low terbium concentrations.

The emission spectra of La_2O_2S: Eu were characterised over a dopant concentration range from 0.1 to 15 m/o of europium. Fig. 7 illustrates the intensities of the emission peaks vary with various dopant concentrations. Low dopant concentrations of Eu ($\leqslant$2 m/o) appear to have more emission lines especially at the shorter wavelengths, such as 467 and 495 nm. In addition, the shorter wavelength lines at low Eu concentrations are far more intense than they are at higher concentrations. The increased number of these emission lines in the spectrum is due to the Stark-splitting effect [6] of discrete energy levels between ^5D levels to ^7F levels [13]. It is important to note that these peaks at short wavelengths are temperature dependent and hence they could be used for remote temperature measurements.

In Fig. 8 the intensity graph of La_2O_2S: Eu over a number of dopant concentrations is shown. This clearly shows that concentrations of 1–2 m/o of Eu achieving the maximum intensity emission particularly at the temperature dependent peaks and thus they are the optimum concentrations for this phosphor. A reduction of these emission peaks occurs for 5–15 m/o Eu due to the concentration quenching [14].

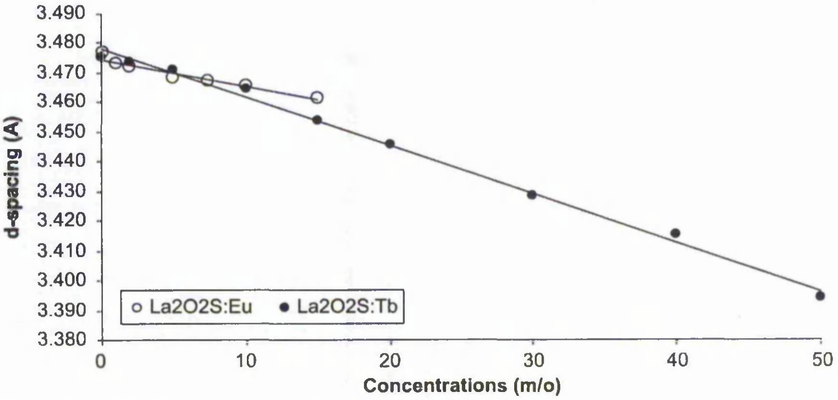

Fig. 3. C-parameter of a unit cell of La_2O_2S: Tb and La_2O_2S: Eu as a function of dopant concentration at (0 0 2) reflection.

Table 1
Crystallite size of 0–50 m/o La_2O_2S: Tb..

Dopant concentrations (m/o)	Crystallite size (Å)
0	1560
0.005	1324
0.2	1464
0.5	1416
1	1416
2	1448
5	1077
10	997
15	993
20	904
30	834
40	783
50	888

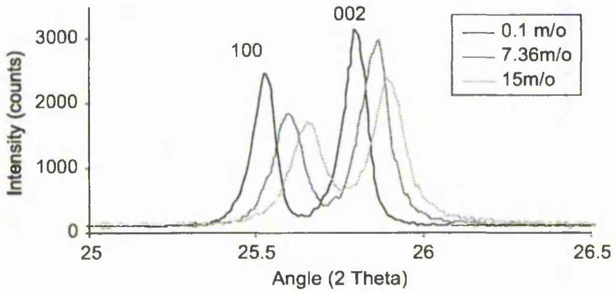

Fig. 4. XRD patterns of La_2O_2S: Eu at different dopancy levels.

Table 2
Crystallite size for various concentrations of La_2O_2S: Eu..

Dopant concentrations (m/o)	Crystallite size (Å)
0	1579
0.1	1020
1	1053
2	1015
5	891
7.36	833
10	643
15	656

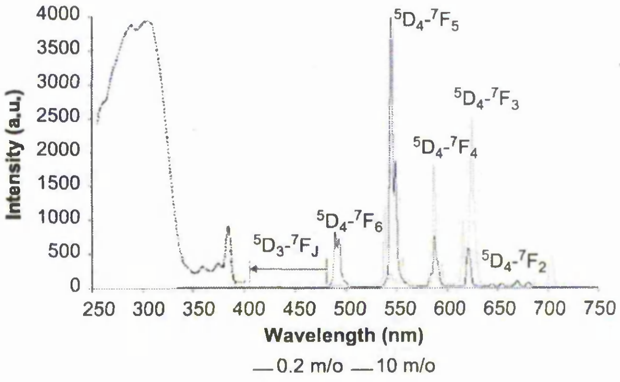

Fig. 5. Emission spectra comparison of La_2O_2S: Tb at 0.2 and 10 m/o Tb contents under 337 nm excitation at room temperature. (Excitation spectra for La_2O_2S: Tb provided by PTL.)

3.3. *Decay time characteristics*

Figs. 9(a)–(d) demonstrate the decay time characteristics of La_2O_2S: Eu 0.1–15 m/o within a temperature range of 5–60 °C. Decay time characteristics were measured at the temperature dependent wavelengths of 467, 495, 512 and 538 nm. These transitions that occur between the ^5D levels and charge transfer states (CTS) of La_2O_2S: Eu can be described with the model developed by Fonger and Struck [9,15]. Their analysis suggested the Eu ^5D_J states quench sequentially ($J = 3$, 2, 1, 0) with increasing temperature. This is because each ^5D state empties thermally via charge transfer.

Due to the constraint of the spectrometer resolution and its sensitivity, only the 467 and 495 nm are visible in lower concentrations of Eu ($\leqslant 2$ m/o) as shown in Fig. 7b (see inset). These lower emission intensity peaks could be detected at other dopant concentrations via decay time system due to the improved sensitivity of the PMT in comparison with the spectrometer's CCD array. Results presented here show the decay time of these samples decreases with an increasing temperature. At low temperatures, the decay rate for 467, 495 and 512 nm is $\sim 10^{-6}$ s whereas 538 nm has a slower decay rate of $\sim 10^{-5}$ s. For comparison, Cates and Allison [13] reported the decay time of 512 nm line was 6.2 μs.

The data summarised in Table 3 indicate that 0.1 m/o Eu has the most superior quenching rates 20.92, 24.03 and 22.23 m °C^{-1}

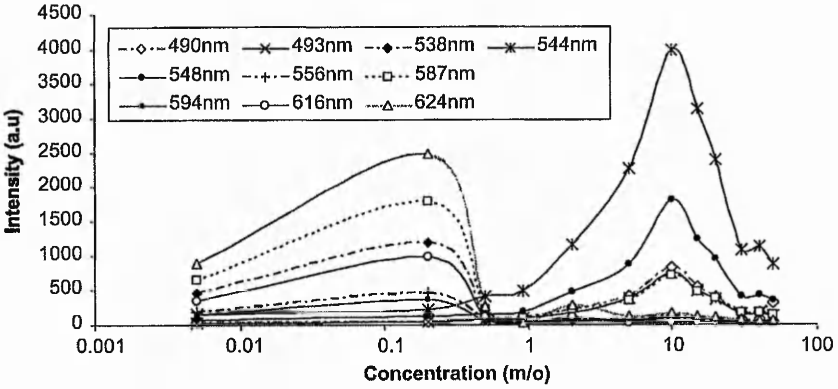

Fig. 6. Emission intensities against various dopant concentrations for La_2O_2S: Tb.

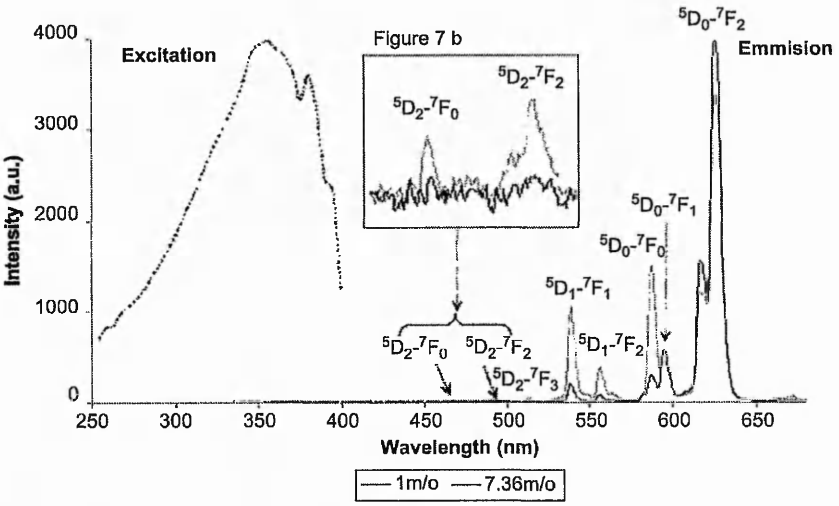

Fig. 7. Spectra emission distribution for La_2O_2S: Eu at dopant concentrations of 1 and 7.36 m/o at room temperature. (Excitation spectra for La_2O_2S: Eu provided by PTL). Fig. 7b (inset)—zoomed in on 450–500 nm to indicate 467 and 495 nm peaks at low concentration.

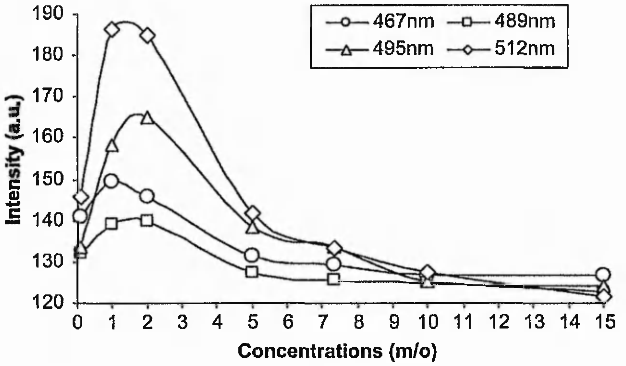

Fig. 8. Intensity levels of different dopant concentrations of La_2O_2S: Eu at short wavelengths.

at 467, 495 and 512 nm, respectively. In addition, a trend is clearly illustrated with the quenching rates decreasing as dopancy levels increase for these highly temperature-sensitive peaks. Although the emission from 1 to 2 m/o Eu are more intense, the quenching rates for these two dopancy levels are still lower than that of 0.1 m/o. It is hypothesized that the quenching rates are independent of the brightness of a phosphor but dependent on the dopant concentration as discussed earlier. As a result, 0.1 m/o Eu would be the ideal candidate for embedding within an optical temperature sensor.

Various investigations have explored the temperature sensing capabilities of La_2O_2S: Tb. The results obtained in this work have suggested that the decay times of this phosphor show strong dependency upon its temperature, as indicated in Figs. 10 and 11. Of more importance, this temperature dependent characteristic occurs at most of the emission intensities in La_2O_2S: Tb, i.e. $^5D_4$ to ^7F_J transitions [16] compared to only four emission lines of La_2O_2S: Eu. According to Struck and Fonger, again similar to La_2O_2S: Eu, the thermal quenchings of Tb in La_2O_2S are due to the CTS crossover relaxation to Frank–Condon shifted states.

Like many other cases, the decay time of La_2O_2S: Tb 0.005–0.91 m/o decreases with temperature. However, it is observed that 5–50 m/o Tb showed an unprecedented decay time characteristic: its decay time increases with temperature. A good example of this abnormal decay time behavior is shown in Fig. 10,

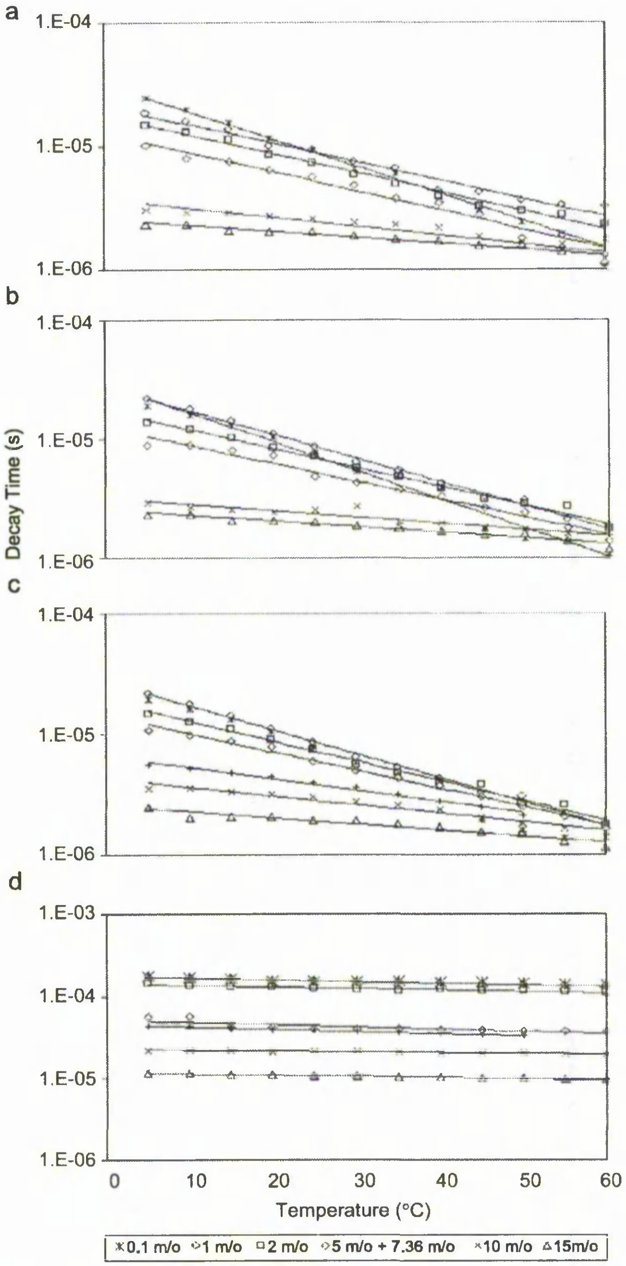

Fig. 9. Decay time against temperature for various dopant concentrations of La_2O_2S: Eu at (a) 467 nm, (b) 495 nm, (c) 512 nm and (d) 538 nm.

Table 3
Summary of quenching rates for various concentrations of La_2O_2S: Eu..

Emission wavelengths (nm)	Quenching rates (m °C^{-1}) of La_2O_2S: Eu						
	0.1 m/o	1 m/o	2 m/o	5 m/o	7.36 m/o	10 m/o	15 m/o
467	20.92	13.73	14.64	16.16	10.36	8.50	4.90
495	24.03	17.10	16.71	14.60	8.70	5.28	5.41
512	22.23	19.84	17.08	14.80	9.90	6.53	6.02
538	1.77	2.27	2.00	3.12	2.84	0.85	1.36

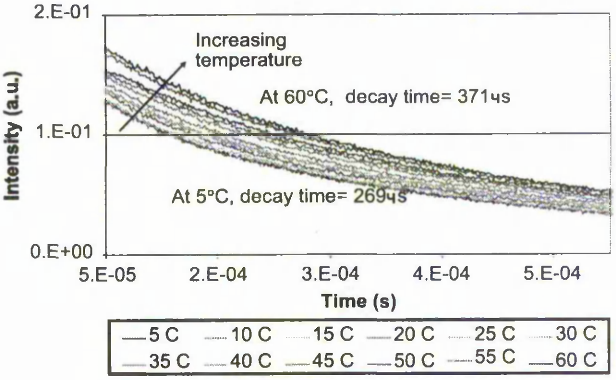

Fig. 10. Decay curves of La_2O_2S: 15% Tb at 544 nm line from 5 to 60 °C. (Refer to Fig. 11 for decay time against temperature.)

the decay time of 544 nm at 5 °C is 269 μs whilst 371 μs at 60 °C. As the dopant concentration is increased, it will result in a change of crystal structure and hence an alteration to the energy levels that exist for excited states (Stark-splitting effect). It would appear that this has induced a trapping state and/or additional energy levels, which result in phonon rather than photon emission. This would have two effects—reduction of intensity and an observed slow-down of the luminous decay process, due to the excited states now relaxing to an intermediate state before reaching the photon relaxation energy level.

The quenching rates of La_2O_2S: Tb are presented in Table 4. Unlike the steep quenching slopes of La_2O_2S: Eu, the average quenching rate of La_2O_2S: Tb is as low as ~3 m °C^{-1} with faster decay times depending on the Tb concentrations and also the emission peak.

In summary, the most superior quenching rates at those temperature dependent peaks appear to be at the lowest dopant concentration of the phosphors investigated, i.e. 0.005 m/o La_2O_2S: Tb and 0.1 m/o La_2O_2S: Eu. Further charaterisation of both phosphors at even lower dopancy level will be carried out to validate the relationship between concentration of the activators and quenching rates.

4. Conclusions

The XRD analysis, spectral data and decay time results of powdered La_2O_2S: Eu and La_2O_2S: Tb showed these phosphors to be suitable for the fabrication of the desired optical sensor. Dopant concentration is a key factor that has been taken into account for the measurements described above. The results showed significant changes in crystallinity, emission intensities and decay rates with various dopant concentrations over 5–60 °C. The most sensitive temperature sensing phosphor discovered in this work is 0.1 m/o La_2O_2S: Eu with a great quenching rate of ~20 m °C^{-1} at its temperature dependent lines.

A new decay time trend is introduced at NTU, a rise in decay time with an increasing temperature was evident over dopant concentrations of 2–50 m/o La_2O_2S: Tb. This is due to a distortion of the crystal field associated with the amount of the dopant introduced to the lattice which causes the splitting of energy levels, and thus increase the probability of occurrence for the radiative and non-radiative transitions.

In addition, a relationship between dopant concentration and decay time has been established for La_2O_2S: Eu and La_2O_2S: Tb over various dopancy levels. Lower dopant concentration

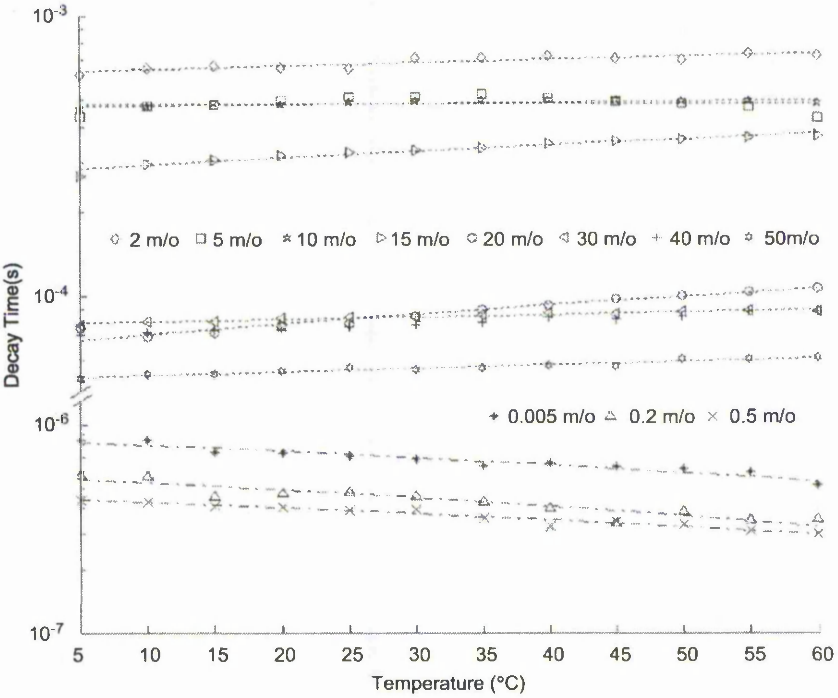

Fig. 11. Decay time of lower La_2O_2S: Tb concentrations (0.005–0.5 m/o) and higher Tb concentrations (2–50 m/o) at 544 nm as a function of temperature.

Table 4
Quenching rates of different Tb concentrations at all emission peaks..

Emission wavelengths (nm)	Quenching rates (m °C^{-1}) of La_2O_2S: Tb				
	0.005 m/o	0.91 m/o	2 m/o	10 m/o	50 m/o
467	2.79				
490	2.49	2.10	−2.97	−1.85	−1.12
493	3.29	2.39	−1.81	−2.14	−1.47
512	4.66				
531	3.36				
538	1.39				
544	3.90	3.19	−1.18	−2.01	−1.32
548		3.56	−1.10	−2.42	−0.80
555	4.19				
563	3.63				
587	2.35	4.73	−0.11	−1.58	−1.00
594	4.92				
615	3.28				
621	2.08	4.65	2.53	−1.82	−0.46

The negative sign (–) is used to denote the increase decay times with increasing temperature.

phosphors with larger crystallite size induced a slower decay rate but a higher quenching rate, suggesting they are more superior in temperature sensing to a higher dopant concentration phosphor.

Acknowledgement

The authors acknowledge the financial support from The Engineering and Physics Sciences Research Council (EPSRC).

References

[1] R.M. Ranson, C.B. Thomas, M.R. Craven, Journal of Measurement Science and Technology 9 (1998) 1947.
[2] R.M. Ranson, E. Evangelou, C.B. Thomas, Applied Physics Letters 72 (1998) 2663.
[3] D.L. Beshears, G.J. Capps, C.M. Simmons, S.W. Schwenterly, in: Laser-induced Fluorescence of Phosphors for Remote Cryogenic Theromometry, 1990.
[4] L. Jansky, V. Vavra, P. Jansky, P. Kunc, I. Knizkova, D. Jandova, K. Slovacek, Journal of Thermal Biology 28 (2003) 429.
[5] G. Wasner, J. Schattschneider, R. Baron, Journal of Pain 98 (2002) 19.
[6] J.S. Foster, Journal of the Franklin Institute 209 (1930) 585.
[7] S.W. Allison, G.T. Gillies, Review of Scientific Instruments 68 (7) (1997) 2615.
[8] S. Shionoya, W.M. Yen, Phosphor Handbook, CRC Press LLC, Boca Raton, FL, 1998.
[9] A.J. Simons, I.P. McClean, R. Stevens, Electronics Letters 32 (1996) 253.
[10] P.J. Brown, J.B. Forsyth, The Crystal Structure of Solids, Edward Arnold Limited, 1973.
[11] A.M. Amiryan, A.M. Gurwich, R.V. Ktomina, Journal of Applied Spectroscopy 27 (1977) 468.
[12] G. Blasse, B.C. Grabmaier, Luminescent Materials, Springer, Berlin, Heidelberg, 1994.
[13] M.B. Cates, S.W. Allison, L.A. Franks, M.A. Nelson, T.J. Davies, B.W. Noel, Laser Institute of America, 1984.
[14] S. Ignasiak, H. Veron, Journal of the Electrochemical Society 123 (1976) 1493.
[15] W.H. Fonger, C.W. Struck, Journal of the Electrochemical Society 118 (1971) 273.
[16] C.W. Struck, W.H. Fonger, Journal of Applied Physics 42 (1971) 4515.